Luminescent Functionalized Vesicles:
Synthesis, Characterization and Analytical Applications

Dissertation

zur Erlangung des Doktorgrades der Naturwissenschaften

(Dr. rer. nat.)

an der Fakultät Chemie und Pharmazie

der Universität Regensburg

vorgelegt von

Stefan Balk

aus Waldmünchen

Juli 2014

The experimental part of this work was carried out between November 2010 and June 2014 at the Institute of Organic Chemistry at the University of Regensburg under the supervision of Prof. Dr. Burkhard König.

Submission of thesis:	17. July 2014	
Date of colloquium:	22. August 2014	
Board of Examiners:	PD Dr. Richard Weihrich	(Chairman)
	Prof. Dr. Burkhard König	(1st Referee)
	Prof. Dr. David Diaz Diaz	(2nd Referee)
	PD Dr. Rainer Müller	(Examiner)

I, Stefan Balk, solemnly declare to have completed this work without any aid or help of any kind not mentioned in this thesis.

Regensburg, ……...

ACKNOWLEDGMENTS

I would like to express my gratitude to Prof. Dr. Burkhard König for giving me the opportunity to do my Master and PhD theses on this very interesting and versatile topic under his supervision. His helpful advises, the great motivation and the financial support were essential contributions to my work. Furthermore I am very thankful to Prof. Dr. Uday Maitra, who supervised my PhD research internship at IISc. Bangalore and provided a great collaboration. For my defense I am deeply grateful to my second referee Prof. Dr. David Diaz Diaz, my third examiner PD Dr. Rainer Müller and the chairman PD Dr. Richard Weihrich. I want to acknowledge DFG, INDIGO network and DAAD, GDCh and all other founding organizations for financial support and numerous travel grants. A very big "Thank You!" to Dr. Benjamin Gruber and Dr. Stefan Stadlbauer, who supervised my Master and Bachelor Thesis and contributed in a great part to my work in molecular recognition. Thanks are also extended to Dr. Rudolf Vasold who helped me with the time-consuming HPLC measurements and the Fraunhofer Institute for the opportunity to use their Zetasizer. Moreover, I would like to mention the permanent staff of our group Viola Rappenegger, Dr. Petra Hilgers, Susanne Schulze, Britta Badziura, Regina Hoheisel, Simone Strauss und Ernst Lautenschlager.

I want to mention my friends and (former) lab mates Dr. Benjamin Gruber, Dr. Florian Schmidt, Tobias Lang, Michal Poznik and Melanie Hacker, they helped with everyday problems in lab and we had a great working atmosphere – Thank you! It was a great time. Furthermore, I want to thank my colleagues and former members of the König's group for the wonderful community also besides chemistry, the skiing trips, Chem-Cup, PhD parties and international evenings. Very big thanks also to my friends Sayantan Chatterjee and Stefanie Jäger and all members of Prof. Dr. Uday Maitra's group for the great time we had together in India. Further thanks go to all the students who contributed to this thesis, namely: Vanessa Haas, Daniel Wutz, Simone Stark, Christian Hundshammer, David Wunderlich und Marleen Häring.

I would particularly like to mention my friends Christian Schäfer, Alen Lovric and Ines Hachani as well as my fellows from the first days at university Dr. Dennis Kühbeck, Tobias Lang, Steffen Pockes, Dr. Christian Wellner, Florian Meier, Wolfram Klosterhuber, Viktor Kais, Dr. Roland Linhardt, Florian Pielnhofer, Dr. Quirin Kainz and Paul Kohls. Thank you for the everlasting time we have had together!

Last but not least, I especially want to mention and thank Sonja Lukic for her love, our wonderful relationship and her endless support.

Finally, my biggest thanks go to my parents Ingrid and Hubert, my sisters Anja and Bettina and my whole family – Thank you so much! Without their boundless support and never-ending encouragement this thesis would not have been written.

THANKS

"Live as if you were to die tomorrow. Learn as if you were to live forever."

Mahatma Gandhi

TABLE OF CONTENTS

CHAPTER 1

DYNAMIC INTERFACE IMPRINTING: HIGH AFFINITY PEPTIDE BINDING SITES ASSEMBLED BY ANALYTE-INDUCED RECRUITING OF MEMBRANE RECEPTORS

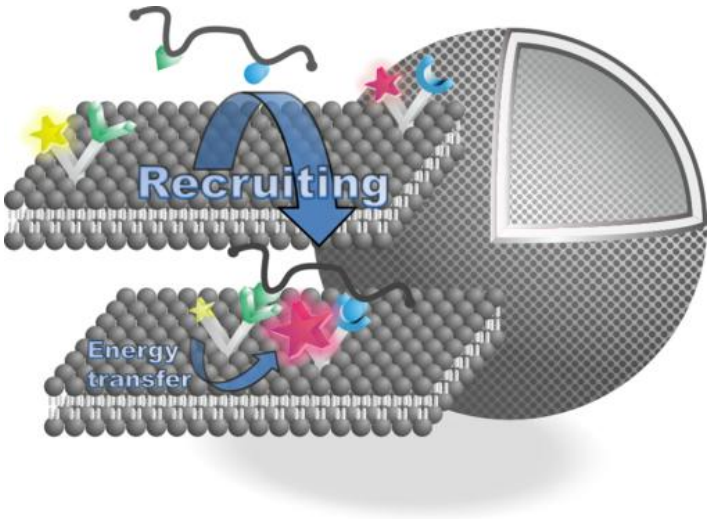

Dynamic molecular recognition events at biological membrane receptors play a key role in cell signaling. We have prepared artificial membranes with embedded synthetic receptors which dynamically arrange and selectively respond to external stimuli like small peptide ligands.

This Chapter has been published:

B. Gruber, S. Balk, S. Stadlbauer, B. König, *Angew. Chem. Int. Ed.*, **2012**, 51, 10060–10063 (Hot Paper).

Author contributions:

BG performed binding studies and wrote the manuscript; SB synthesized compound **Cu3** and performed FRET binding studies; SS synthesized compounds **Cu4**, **Zn21**, **Zn22**; BK supervised the project and is corresponding author.

Introduction

Molecular recognition between membrane-associated receptors and external ligands as stimuli is important for many biological processes.[1-3] The dynamic formation of domains and the clustering of receptors in fluid membranes play a key role e.g. in signal transduction leading to highly specific binding of competing multivalent ligands.[4-6]

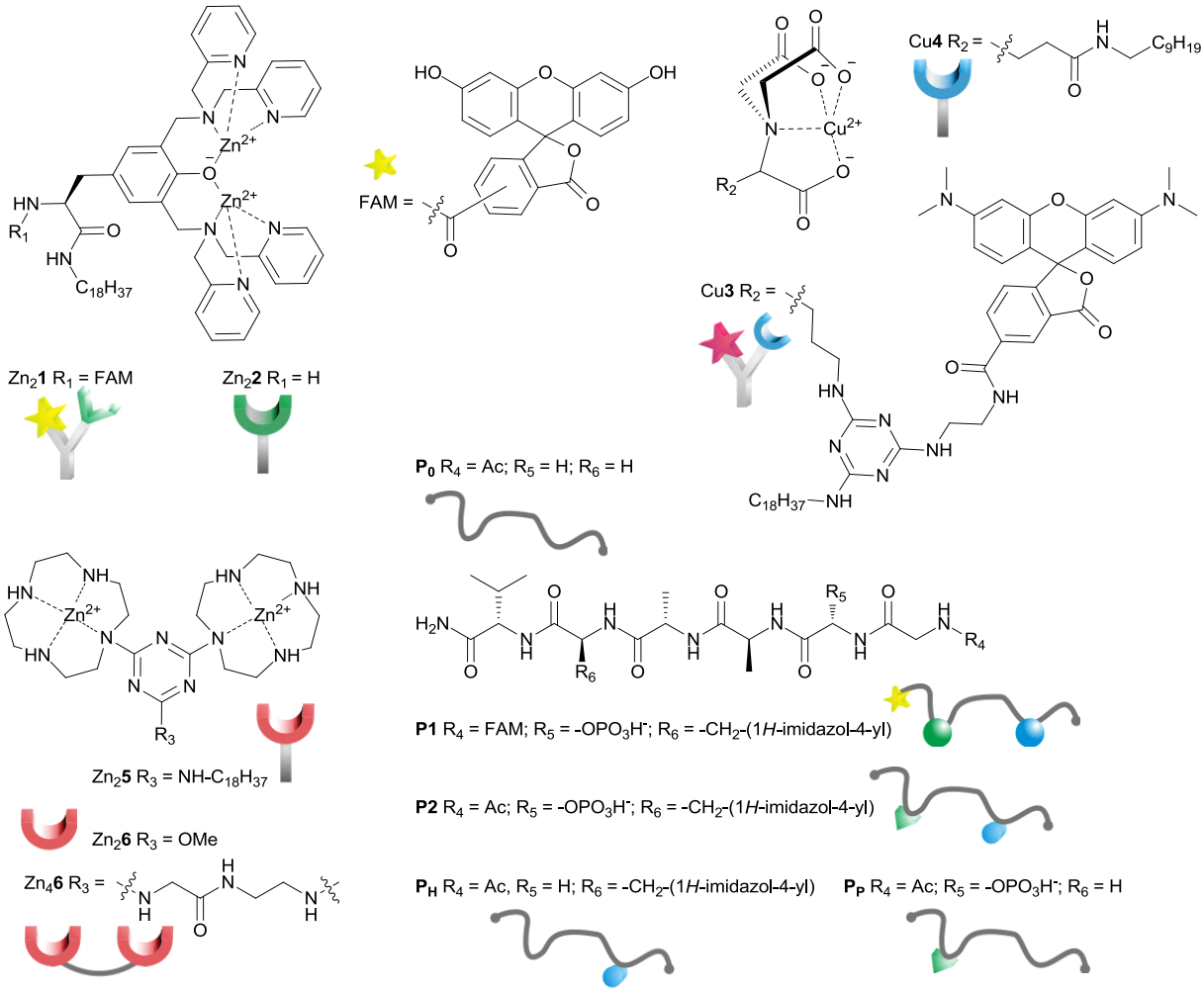

Scheme 1. Structures of synthetic receptors and ligands (counterions omitted).

Various model systems for biological membranes have been developed to understand and mimic multivalent interactions at interfaces[7-12] as well as for applications in delivery, sensing and catalysis.[13-18] The principle of template-guided assembly has also been extensively exploited in molecular imprinting,[19, 20] but the non-covalent arrangement of

binding sites in precisely defined distances still remains a challenge. We have investigated a concept that mimics immunological synapses, where receptors are recruited at a membrane interface, spatially organized by the binding partner and this orientation triggers a specific response.[21-23] Our vesicles with membrane-embedded luminescent receptors produce a characteristic optical response in the presence of small peptides as external ligands. Depending on the functional groups present in the peptide, suitable receptors with complementary binding sites are recruited and arranged in the fluid membrane, which triggers a FRET signal.

Results and Discussion

We have previously reported on the recognition of small biomolecules and phosphorylated proteins by multi-site interactions[24, 25] at the lipid-water interface using synthetic vesicle membranes with embedded artificial receptors based on transition metal complexes of 1,4,7,10-tetraazacyclododecane (cyclen) and nitrilotriacetic acid (NTA). We now expand this concept to the dynamic recruiting of synthetic receptors allowing the multivalent recognition of phosphorylated peptides. The selective recognition of phospho-serine (pSer) and histidine (His) moieties in model-peptide **P1** by metal-complex binding sites was investigated in a previous study in homogeneous solution.[26] It was found that in buffered aqueous solution Zn(II)-cyclen receptor Zn_2**6** binds peptide **P1** with log *K* = 4.8, while dimer Zn_4**6**, allowing a simultaneous two-prong interaction to pSer and His, shows an affinity of log *K* = 7.5 (see Table 1, entries 1 and 2 and Supporting Information). Instead of covalently connecting two receptor sites, as in Zn_4**6**, distinct binding sites are now simply embedded in synthetic lipid bilayers. Recruiting and self-organization by the peptide ligand allows the divalent binding of both pSer and His residues of **P1** at the membrane interface.

First we embedded Zn_2**5** (1 mol%) in vesicular lipid bilayers from 1,2-distearoyl-sn-glycero-3-phosphocholine (DSPC) using previously reported procedures (see Supporting Information). The emission intensity of peptide **P1** increases significantly upon binding to the surface receptors (see SI) and a binding constant of log *K* = 5.9 (Table 1, entry 3) at ambient temperature was derived. This value is in good agreement with the recognition of pSer by a single Zn_2**5** receptor[24] and reasonable, because DSPC's high phase transition

temperature (54 °C)[27] restricts diffusion and thus participation of more than a single metal complex binding site in the peptide recognition (cf. Figure 1, Top). Binding affinities could only be enhanced by drastically increasing the vesicle receptor loading to 10 mol% (Table 1, entry 4) resulting in the formation of tightly packed metal complex patches.[16] However, replacing the saturated DSPC lipid by unsaturated 1,2-dioleoyl-sn-glycero-3-phosphocholine (DOPC), which has a much lower transition temperature of -20 °C,[27] leads to an increase in peptide **P1** binding affinity by more than two orders of magnitude (Table 1, entry 5). The embedded receptor sites can now diffuse in the membrane at room temperature allowing complex formation of one **P1** with two Zn_2**5** units by a dynamic assembly process (Figure 1, Top). Unchanged particle sizes determined by dynamic light scattering (Supporting Information, Figure S11) confirm binding of the peptide to receptors of one vesicle (intra-membrane binding mode) and excludes peptide crosslinking of different vesicles (inter-membrane binding).

Entry	Lipid	Receptor	Mol%	log *K*
1	-	Zn_2**6**	-	4.8 [a]
2	-	Zn_4**6**	-	7.5 [a]
3	DSPC	Zn_2**5**	1	5.9
4	DSPC	Zn_2**5**	10	8.1
5	DOPC	Zn_2**5**	1	8.6
6	DSPC	Zn_2**2**	1	6.2
7	DSPC	Cu**4**	1	5.0
8	DSPC	Zn_2**2** + Cu**4**	1 (each)	6.3
9	DOPC	Zn_2**2**	1	5.5
10	DOPC	Cu**4**	1	5.8
11	DOPC	Zn_2**2** + Cu**4**	1 (each)	8.8

Table 1. Summary of apparent binding constants for peptide **P1** by synthetic receptors in homogeneous solution (entry 1 and 2) and embedded in vesicle membranes (HEPES buffer, pH 7.4, 25 °C).

The experiments show that analyte induced recruiting of binding sites in a fluid membrane leads to higher binding affinities due to multipoint interaction. Next, vesicle membranes with two different embedded receptors, which bind selectively either pSer or His of **P1,** were investigated. The synthesis of amphiphilic Cu(II)-NTA complex Cu**4** for the recognition of histidine was reported previously,[24] the synthesis of the amphiphilic Zn(II)-3,5-bis-[(bis-pyridin-2-ylmethyl-amino)-methyl]-4-hydroxy-phenyl (DPA) complex Zn_2**2** for the selective recognition of phosphate[28] is described in the Supporting Information. Stable metal complex-doped DOPC and DSPC vesicle membranes were prepared using Zn_2**2** or Cu**4** and a mixture of both (1 mol% each). For DSPC membranes with one type of receptor embedded the emission titrations with **P1** revealed monovalent binding either to Zn-DPA or to Cu-NTA coordination,[29] with log *K* = 5.0 and 6.2, resp. (Table 1, entries 6 and 7). Job's plots with **P1** as limiting reagent confirm the 1:1 stoichiometry of the binding event (Figure S18). Combining both receptors in gel-phase DSPC-membranes (Figure 1, Bottom) does not increase the binding affinity for peptide **P1** (log K = 6.3; Table 1, entries 6, 7, 8). The binding isotherm for the receptor vesicles bearing both complexes resembles the average of the binding properties of the individual receptor vesicles (see SI for data). This is explained by a random, but fixed position of lipid bilayer embedded metal complex receptors, which prevents the formation of a ternary Zn_2**2**-**P1**-Cu**4** complex (see SI for Job´s plots). DOPC membranes, in contrast, show a completely different behaviour: Whereas vesicles with either Zn_2**2** or Cu**4** as embedded receptors give similar binding isotherms and affinity constants (log *K* = 5.5 and 5.8, resp.; Table 1, entries 9, 10), the liquid-crystalline membrane containing both receptor binding sites shows a significantly higher affinity for peptide **P1** in the nanomolar range (log *K* = 8.8, Table 1, entry 11 and Figure 1, Bottom). We explain this by the divalent binding of **P1** by a heterodimeric Zn_2- and Cu-receptor assembly in the fluid lipid bilayer (cf. Figure 1, Bottom) resulting from peptide induced self-organization of the membrane receptors. The Job's plot analysis (Figure S19) supports this conclusion.

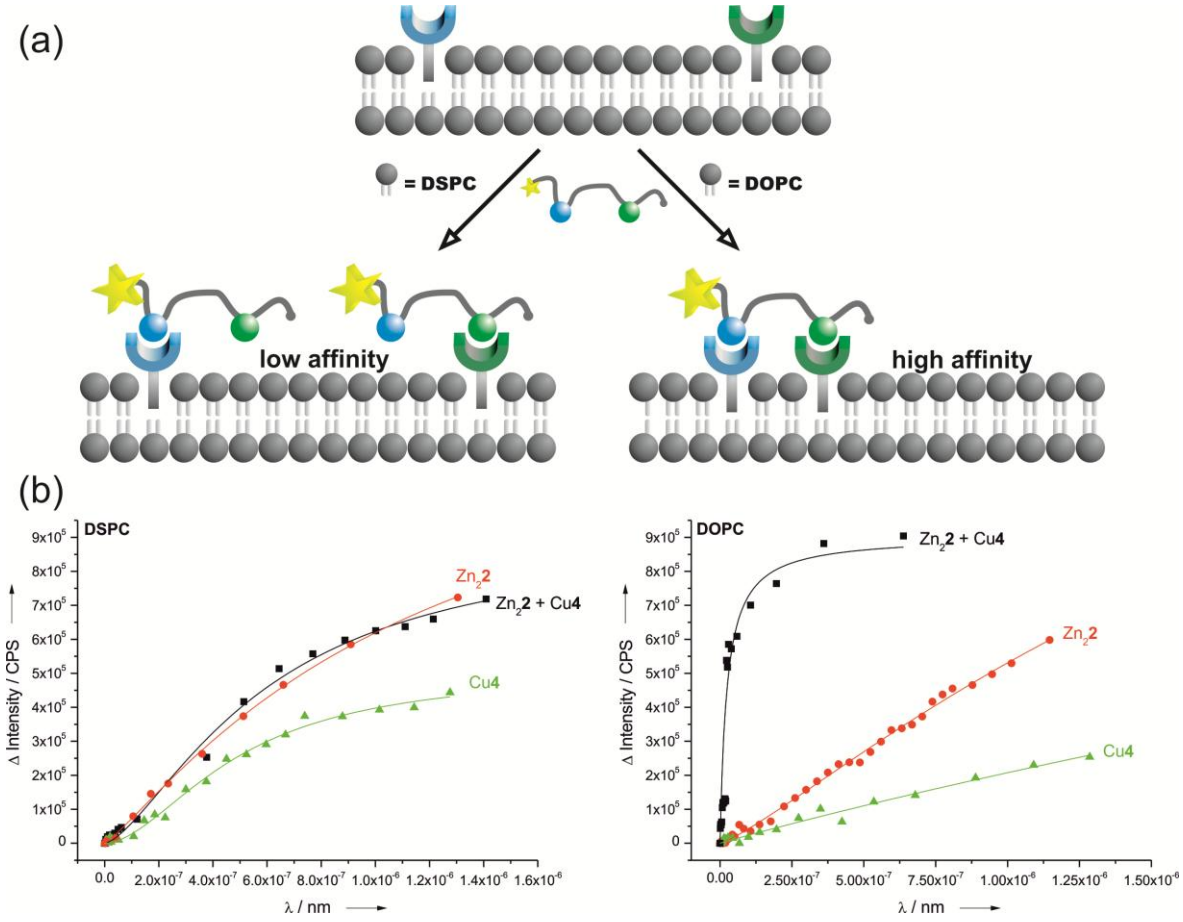

Figure 1. (Top) Schematic receptor assembly in vesicle membranes: Fixed receptors in gel-phase DSPC-membranes vs. analyte-induced clustering in fluid DOPC-membranes; (Bottom) Emission titrations of **P1** vs. DSPC and DOPC- membranes containing Zn_2**1**, Cu**3** or both receptors.

For bioanalytical applications, the labeling of the peptide analyte must be avoided. Therefore amphiphilic receptor binding sites that signal the presence of the target analyte by induced FRET were developed: Zn(II)-DPA complex (Zn_2**1**) is labeled with carboxyfluorescein (FAM) and Cu(II)-NTA complex Cu**3** is rhodamine (TMR) labeled. FRET techniques are widely used in molecular biology to measure distances within bio-molecules or to explore membrane structures.[30] We use the FRET signal, which is induced by the close distance of the membrane-embedded luminescent binding sites to signal the presence of peptide **P2**, which in contrast to **P1**, does not carry a fluorescent label. Divalent binding of **P2** to the membrane embedded binding sites recruits Zn_2**1** and Cu**3** into close proximity and therefore within the Förster distance of 5.5 nm[31] resulting in a FRET signal as optical output (Figure 2, Top).[32]

The vesicles responded to the presence of the target peptide **P2** with a significant FRET-signature. Formation of a Zn_2**1**-**P2**-Cu**3** ternary complex leads to energy transfer of the donor label FAM at 490 nm to the acceptor label TMR at 580 nm (Figures 2, Bottom and S22). However, an excess of the target peptide is necessary to reach the maximum energy transfer. Control experiments with monovalent ligands ($\mathbf{P_P}$, $\mathbf{P_H}$ and $\mathbf{P_0}$) did not change the observed emission spectra significantly (Figure S23). We exclude inter-vesicular FRET via crosslinking of distinct vesicles as the solution particle size remains unchanged in the presence of **P2** (Figures S24, 25). Additionally, vesicles were purified by size exclusion chromatography before binding experiments to remove traces of amphiphilic receptors or micellar aggregates from the solution and the concentrations of the embedded receptors were verified by Zn- and Cu-element analysis using ICP-AES (see SI).[33]

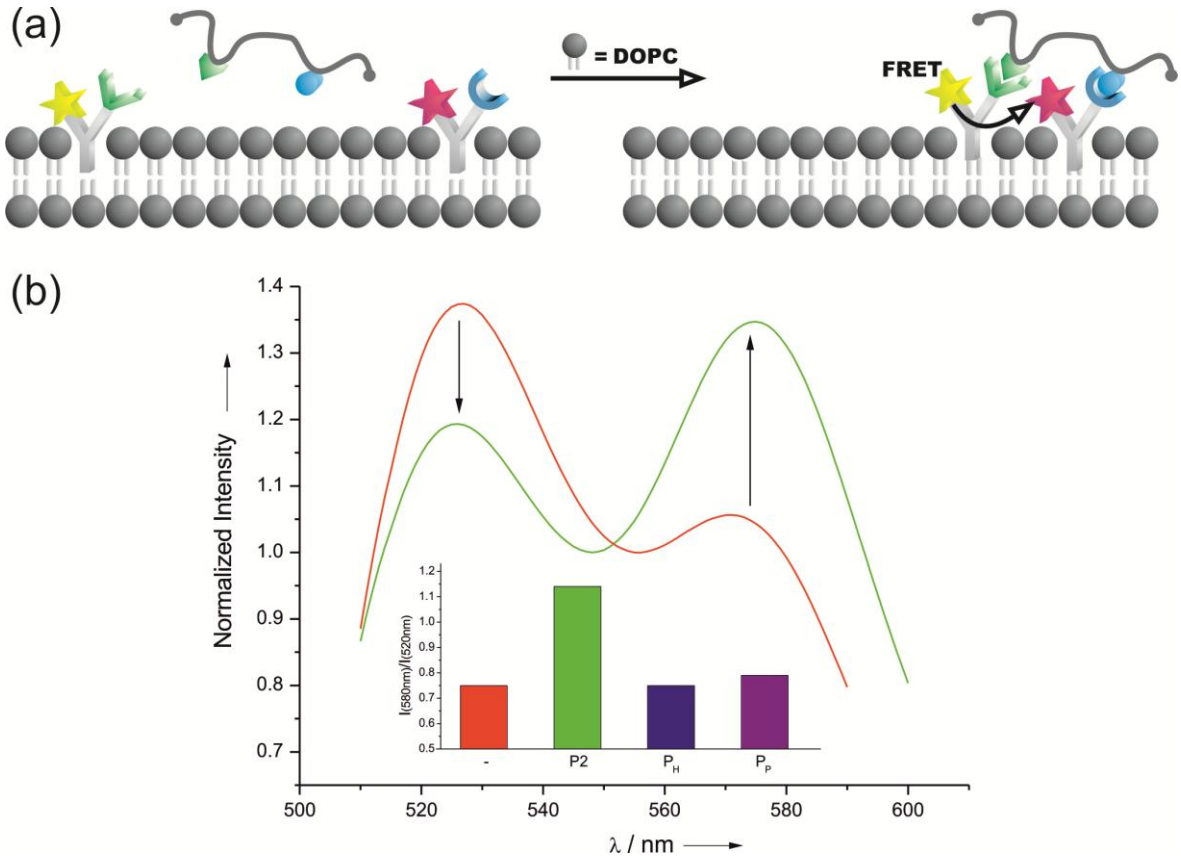

Figure 2. (Top) Schematic recruiting of labeled membrane receptors by a peptide ligand resulting in a FRET signal; (Bottom) Fluorescence spectra of DOPC vesicles containing labeled receptors Zn_2**1** + Cu**3** (1 mol% each) in the absence (red) and presence (green) of peptide **P2**. Relative FRET emission ratio (I_{580nm}/I_{520nm}) of $\mathbf{P_2}$ and monovalent $\mathbf{P_H}$ and $\mathbf{P_P}$ as control (inset).

As additional control experiments, DOPC and DSPC vesicles with only one of the two binding sites were prepared and used for emission titrations with increasing amounts of corresponding ligands (pSer/$\mathbf{P_P}$ for Zn_2**1** and His/$\mathbf{P_H}$ for Cu**3**). As expected, no significant change in the optical properties of the fluorescent receptor-vesicles was observed (Figure S21). DSPC vesicles with both co-embedded receptors Zn_2**1** and Cu**3** (0.1 mol% each) show a small energy transfer between the FAM- and TMR-labels in the absence of the peptide ligand (Figure S20), which might be explained by the partial formation of Zn_2**1**/Cu**3** heterodynes. Upon addition of any mono- or divalent ligand no change in emission was detected, as the gel-phase state of the DSPC membranes at room temperature limits the diffusion of the embedded metal complexes (Figure S22).

Conclusion

In conclusion, we demonstrated the specific recognition of peptides by dynamic interface imprinting of synthetic binding sites embedded in vesicle membranes. The amphiphilic metal complex binding sites are recruited in the membrane by the target peptide resulting in multivalent interactions and nanomolar binding affinity. The use of amphiphilic binding sites with FRET pair chromophores, leads to self-organization of a specific analyte epitope at the lipid-water interface and a FRET signal indicating the presence of the target analyte.

The experimental data proof that dynamic binding site recruitment in fluid membranes by analytes (dynamic interface imprinting, DII) leads to the formation of high affinity epitopes. The process allows the specific detection of functional groups in peptides with nanomolar affinity. To further improve the sensitivity and selectivity of functionalized luminescent vesicles in chemical bioanalysis the number and nature of simultaneously embedded binding sites may be increased, including peptides or nucleotides as recognition moieties. The combined use of several chromophores in the membrane gives a specific spectroscopic output depending on their spatial arrangement. Such functionalized luminescent vesicles may in some applications replace antibody based assays.

Experimental Part and Supporting Information

General methods and material

Fluorescence measurements were performed with UV-grade solvents (Baker or Merck) in 1 cm quartz cuvettes (Hellma) and recorded on a Varian 'Cary Eclipse' fluorescence spectrophotometer with temperature control. Absorption was recorded on a Varian Cary BIO 50 UV/VIS/NIR Spectrometer with temperature control by use of a 1 cm quartz cuvettes (Hellma) and Uvasol solvents (Merck or Baker). PCS measurements were performed on a Malvern Zetasizer Nano at 25 °C using 1 cm disposable polystyrene cuvettes (VWR). NMR spectra were recorded on Bruker Avance 600 (1H: 600.1 MHz, 13C: 150.1 MHz, T = 300 K), Bruker Avance 400 (^{1}H: 400.1 MHz, ^{13}C: 100.6 MHz, T = 300 K), Bruker Avance 300 (^{1}H: 300.1 MHz, ^{13}C: 75.5 MHz, T = 300 K). The chemical shifts are reported in δ [ppm] relative to external standards (solvent residual peak). The spectra were analyzed by first order, the coupling constants are given in Hertz [Hz]. Characterization of the signals: s = singlet, d = doublet, t = triplet, q = quartet, m = multiplet, bs = broad singlet, psq = pseudo quintet, dd = double doublet, dt = double triplet, ddd = double double doublet. Integration is determined as the relative number of atoms. Assignment of signals in ^{13}C-spectra was determined with DEPT-technique (pulse angle: 135 °) and given as (+) for CH_3 or CH, (–) for CH_2 and (C_q) for quaternary C. Error of reported values: chemical shift: 0.01 ppm for ^{1}H-NMR, 0.1 ppm for ^{13}C-NMR and 0.1 Hz for coupling constants. The solvent used is reported for each spectrum. Mass spectra were measured on Varian CH-5 (EI), Finnigan MAT 95 (CI; FAB and FD), Finnigan MAT TSQ 7000 (ESI) with Xenon as ionization gas for FAB. IR spectra were recorded on Bio-Rad FTS 2000 MX FT-IR and Bio-Rad FT-IR FTS 155. Melting Points were determined on Büchi SMP or a Lambda Photometrics OptiMelt MPA 100. Thin layer chromatography (TLC) analyses were performed on silica gel 60 F-254 with a 0.2 mm layer thickness. Detection via UV light at 254 nm / 326 nm or through staining with ninhydrin in EtOH. Column chromatography was performed on silica gel (70–230 mesh) from Merck. Commercially available solvents of standard quality were used. Starting materials were used without any further purification. Phospholipids were purchased from Avanti Polar Lipids Inc. Commercially available solvents of standard quality were used. If not otherwise stated, purification and drying was done according to accepted general procedures.[34]

Elemental analyses were carried out by the Centre for Chemical Analysis of the Faculty of Chemistry and Pharmacy of the University of Regensburg.

Synthesis of amphiphilic bis-Zn(II)-DPA complexes $Zn_2$1 and $Zn_2$2

Receptor Zn_2**1** and Zn_2**2** were prepared from a tyrosine based bis-DPA metal chelating lipid which was synthesized according to a modified protocol of the procedure for the binuclear tyrosine based bis-DPA reported by Hamachi *et al*.[35] Derivatization of the tyrosine scaffold on large scale was possible by standard peptide solution chemistry.

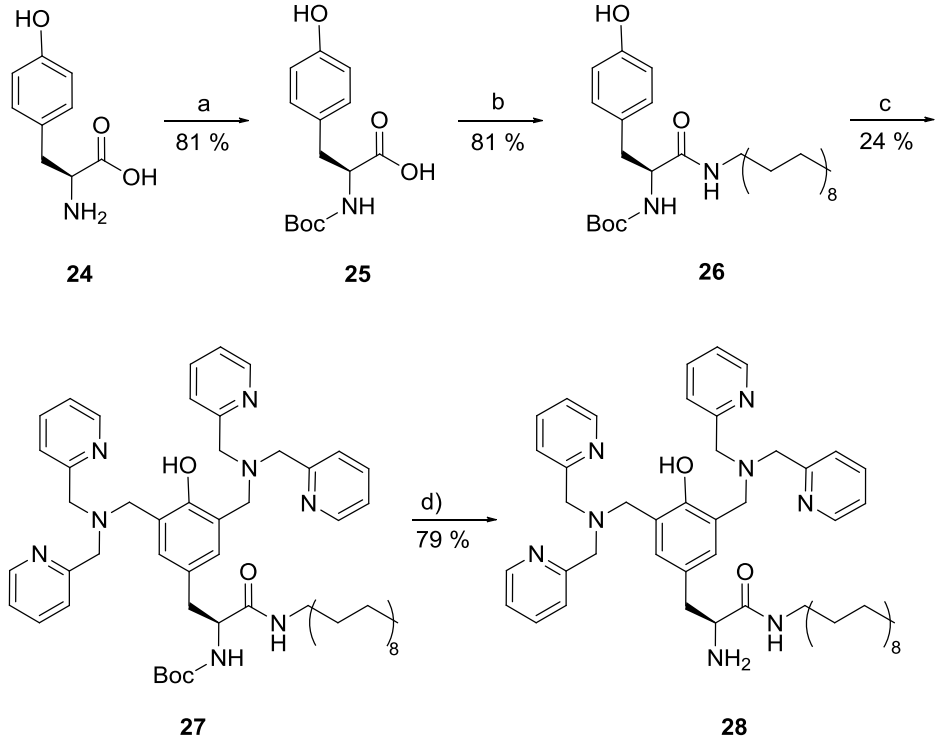

Scheme S1a. Synthesis of amphiphilic tyrosine based bis-dpa zinc complexes. (a) Boc_2O, DCM, RT, 20 h; (b) EDC, HOBt, DIPEA, DMF, toluene, 60 °C, 22h; (c) 2,2`-dipicoloylamine, paraformaldehyde, H_2O, ^{i}PrOH, 80 °C, 30 min, reflux, 17 h; (d) HCl / ether, DCM, RT, 16 h.

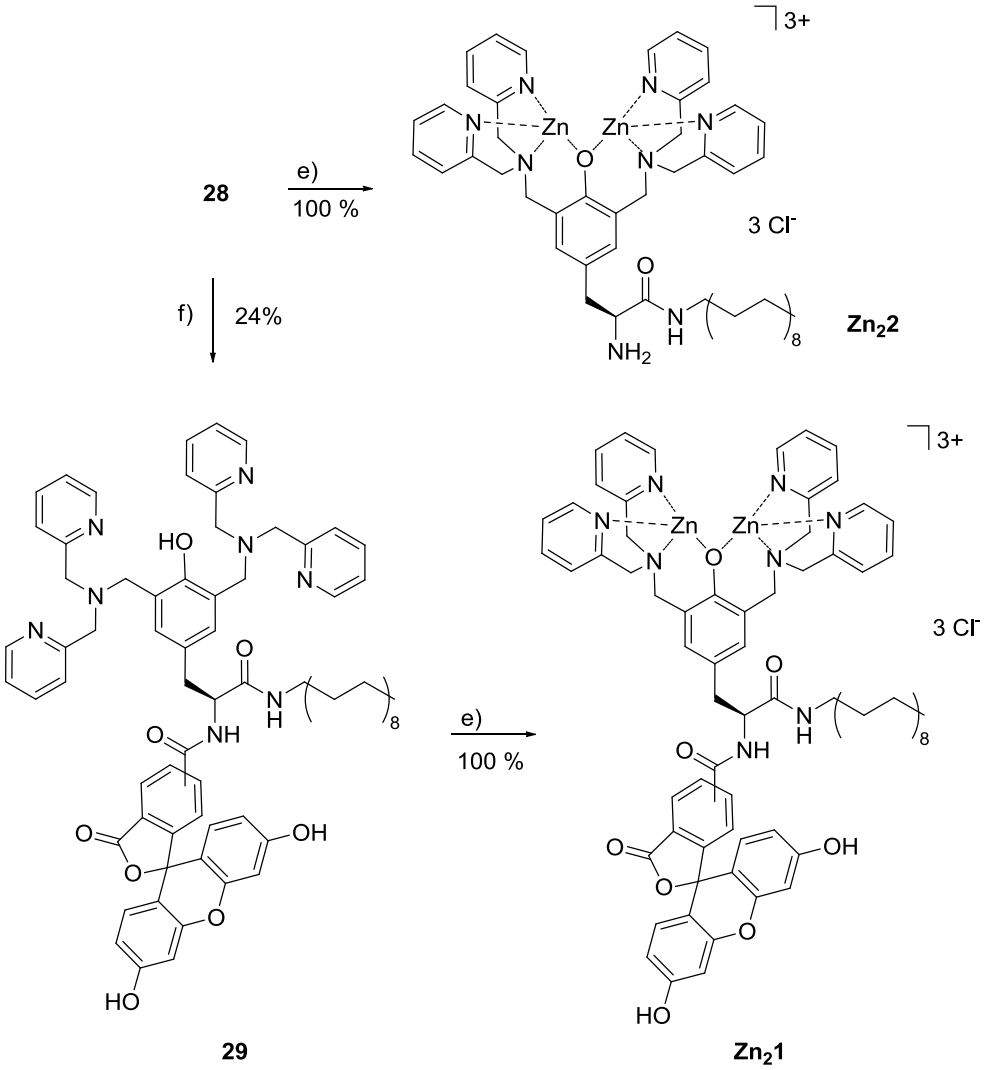

Scheme S1b. Synthesis of amphiphilic tyrosine based bis-dpa zinc complexes. (e) $ZnCl_2$, MeOH, RT, 2 - 3 h; (f) 5/6-carboxyfluorescein, DIPEA, TBTU, HOBt, DMF, 40 °C, 22 h.

Amide formation of **25**[36] with octadecylamine gave amphiphilic tyrosine derivative **26** in good yields. *Mannich* type reaction using 2,2`-dipycolylamine and paraformaldehyde according to literature known procedure gave the protected metal chelating lipid **27**.[35] Removal of the Boc group in acidic conditions (HCl/ether) yielded compound **28** which was finally treated with two equivalents of $ZnCl_2$ to give **$Zn_2$2**.

A fluorescein label was introduced by amide formation of **28** with an isomeric mixture of 5/6-carboxy fluorescein. Subsequent treatment with $ZnCl_2$ gave the fluorescent amphiphilic binuclear tyrosine based metal complex **$Zn_2$1**.

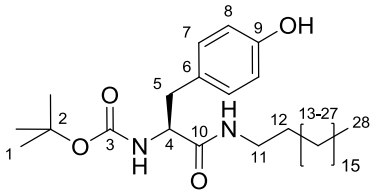

[2-(4-Hydroxy-phenyl)-1-octadecylcarbamoyl-ethyl]-carbamic acid tert-butyl ester (**26**)

Boc-Tyr-OH **25** (2.50 g, 8.9 mmol), DIPEA (5.0 mL, 29.3 mmol), EDC (1.73 mL, 9.8 mmol), and HOBt (1.32 g, 9.8 mmol) were dissolved in DMF (4 mL) under ice cooling and stirred for 45 min. Subsequently a solution of octadecylamine (2.89 g, 9.8 mmol) in 25 mL DMF was added slowly. The reaction was allowed to warm to room temp. and was stirred over night (22 h) at 60 °C. The reaction progress was monitored by TLC ($CHCl_3$ / MeOH 9:1). After completion of the reaction the solvent was removed and the crude product was loaded on flash silica gel and purified by flash column chromatography ($CHCl_3$ / MeOH 95:5, R_f = 0.40) yielding **26** (3.82 g, 7.2 mmol, 81 %) as a colourless solid. **MP:** 115 °C. – **^{1}H-NMR** (600 MHz; $CDCl_3$): δ (ppm) = 0.87 (t, ^3J = 7.0 Hz, 3 H, $C^{28}H_3$), 1.25 (s, 30 H, $C^{13}H_2$ – $C^{27}H_2$), 1.36 (bs, 2 H, COSY: $C^{12}H_2$), 1.42 (s, 9 H, COSY: C^1H_3), 2.83-3.02 (m, 2 H, COSY: C^5H_2), 3.07-3.24 (m, 2 H, COSY: $C^{11}H_2$), 4.21 (m, 1 H, HMBC, COSY: C^4H), 5.17 (bs, 1 H, COSY: NH^a), 5.91 (bs, 1 H, COSY: NH^b), 6.74 (d, ^2J = 8.5 Hz, 2 H, HMBC: C^8H), 7.02 (d, ^2J = 7.7 Hz, 2 H, HMBC: C^7H). – **^{13}C-NMR** (150 MHz; $CDCl_3$): δ (ppm) = 14.1 (+, 1 C, $C^{28}H_3$), 22.7 (–, 1 C, alkyl-CH_2), 26.8 (–, 1 C, alkyl-CH_2), 28.3 (+, 3 C, C^1H_3), 29.2 (–, 1 C, alkyl-CH_2), 29.3 (–, 1 C, alkyl-CH_2), 29.5 (–, 1 C, $C^{12}H_2$), 29.60, 29.65, 29.69 (–, 10 C, alkyl-CH_2), 31.9 (–, 1 C, alkyl-CH_2), 37.9 (–, 1 C, C^5H_2), 39.6 (–, 1 C, $C^{11}H_2$), 56.2 (+, 1 C, HMBC: C^4H_3), 80.3 (C_q, 1 C, C^2), 115.6 (+, 2 C, HMBC: C^7H), 130.4 (+, 2 C, HMBC: C^8H), 128.1 (C_q, 1 C, HMBC: C^6), 155.2 (C_q, 1 C, HMBC: C^9), 155.6 (C_q, 1 C, HMBC: C^3), 171.3 (C_q, 1 C, HMBC: C^{10}). – **IR** (ATR) [cm^{-1}]: $\tilde{\nu}$ [cm] = 3335, 3306, 2959, 2917, 1682, 1655, 1523, 1468, 1367, 1295, 1236, 1168, 1046, 896, 799. – **MS** (ESI(+), DCM/MeOH + 10 mmol/L NH_4Ac): m/z (%) = 533.6 (100) [MH^+], 477.4 (19) [MH^+ - C_4H_8]$^+$, 555.5 (36) [MNa^+]. – **Elemental analysis** calcd. (%) for $C_{32}H_{56}N_2O_4$: C 72.14, H 10.59, N 5.26; found C 72.13, H 10.63, N 5.00. – **MF**: $C_{32}H_{56}N_2O_4$ – **FW**: 532.81 g/mol.

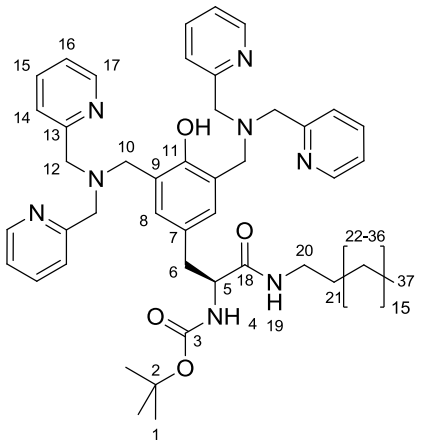

(2-{3,5-Bis-[(bis-pyridin-2-ylmethyl-amino)-methyl]-4-hydroxy-phenyl}-1-octadecyl carbamoyl-ethyl)- carbamic acid tert-butyl ester (**27**)

2,2'-Dipicolylamine (2.35 g, 11.8 mmol) and paraformaldehyde (0.56 g, 18.9 mmol) were dissolved in 30 mL water / isopropanol (5:3) and the pH was adjusted to 8 by adding 1 M NaOH. After stirring at 80 °C for 35 min, compound **26** (2.51 g, 4.7 mmol) was added, and the reaction mixture was refluxed for 17 h. After cooling to room temperature the solvent was evaporated and the residue was dissolved in ethyl acetate. The solution subsequently was washed with saturated $NaHCO_3$ (3x) and brine (3x) followed by drying over $MgSO_4$. After removal of the solvent in vacuo the crude product was purified by flash column chromatography on flash silica gel (ethyl acetate / MeOH 2:1, R_f = 0.1) obtaining **27** (1.1 g, 1.15 mmol, 24 %) as a colourless oil. **^{1}H-NMR** (400 MHz; acetone-d6): δ (ppm) = 0.86 (t, ^3J = 6.9 Hz, 3 H, $C^{37}H_3$), 1.14-1.28 (m, 30 H, $C^{22}H_2$ – $C^{36}H_2$), 1.29 (s, 11 H, HSQC: C^1H_3, $C^{21}H_2$), 2.87 (dd, ^3J = 13.5 Hz, ^2J = 6.5 Hz, 1 H, HSQC, COSY: C^6H_2), 2.94 (dd, ^3J = 13.5 Hz, ^2J = 7.4 Hz, 1 H, HSQC, COSY: C^6H_2), 3.02 (dd, ^3J = 12.9 Hz, ^2J = 6.6 Hz, 2 H, HSQC: $C^{20}H_2$), 3.74 (d, ^2J = 13.7 Hz, 2 H, HMBC, COSY: $C^{10}H_2$), 3.80 (d, ^2J = 13.7 Hz, 2 H, HMBC, COSY: $C^{10}H_2$), 3.85 (s, 8 H, COSY: $C^{12}H_2$), 3.34 (dd, ^3J = 14.4 Hz, ^2J = 7.1Hz, 1 H, COSY: $C^{20}H_2$), 5.98 (d, ^3J = 8.2 Hz, 1 H, HSQC, COSY: N^4H), 7.10 (s, 2 H, HMBC, COSY: C^8H), 7.20 (ddd, ^3J = 7.4 Hz, 4.9 Hz, 1.1 Hz, 4 H, HMBC: $C^{16}H$), 7.29 (bs, 1 H, HSQC, COSY: $N^{19}H$), 7.55 (d, ^3J = 7.8 Hz, 4 H, HMBC: $C^{14}H$), 7.69 (dt, ^3J = 7.7 Hz, ^2J = 1.9 Hz, 4 H, HMBC: $C^{15}H$), 8.52 (m, 4 H, HMBC: $C^{17}H$), 10.96 (bs, 1 H, HSQC: OH). – **^{13}C-NMR** (100 MHz; acetone-d6): δ (ppm) = 14.3 (+, 1 C, $C^{37}H_3$), 23.3 (–, 1 C, alkyl-CH_2), 27.5 (–, 1 C, alkyl-CH_2), 28.5 (+, 3 C, C^1H_3), 29.9 (–, 1 C, alkyl-CH_2), 30.22 (–, 1 C, alkyl-CH_2), 30.27 (–, 1 C, alkyl-CH_2), 30.4 (–, 9 C, alkyl-CH_2,

solvent peak), 32.6 (–, 1 C, alkyl-CH_2), 38.8 (–, 1 C, COSY: C^6H_2), 39.7 (–, 1 C, HSQC: $C^{20}H_2$), 55.3 (–, 2 C, HMBC, COSY: $C^{10}H_2$), 60.1 (–, 4 C, HMBC, COSY: $C^{12}H_2$), 56.9 (+, 1 C, HMBC: C^5H_3), 79.0 (C_q, 1 C, HMBC, HSQC, C^2), 122.8 (+, 4 C, HMBC: $C^{16}H$), 123.8 (+, 4 C, HMBC: $C^{14}H$), 124.6 (C_q, 2 C, HMBC: C^9), 127.7 (C_q, 1 C, HMBC: C^7), 131.3 (+, 2 C, HMBC, COSY: C^8H), 137.3 (+, 4 C, HMBC, COSY: $C^{15}H$), 149.7 (+, 4 C, HMBC, COSY: $C^{17}H$), 155.8 (C_q, 1 C, HMBC: C^{11}), 155.8 (C_q, 1 C, HMBC: C^{11}), 159.9 (C_q, 1 C, HMBC: C^3), 160.2 (C_q, 4 C, HMBC: C^{13}), 171.9 (C_q, 1 C, HMBC: C^{18}). – **IR** (ATR) [cm^{-1}]: $\tilde{\nu}$ [cm] = 3383, 2922, 2852, 1706, 1656, 1590, 1569, 1433, 1364, 1288, 1245, 1167, 1048, 995, 791. – **MS** (ESI(+), DCM/MeOH + 10 mmol/L NH_4Ac): m/z (%) = 478.5 (100) $[M + 2\ H^+]^{2+}$, 955.8 (85) $[MH^+]$. – **Elemental analysis** calcd. (%) for $C_{58}H_{82}N_8O_4$: C 72.92, H 8.65, N 11.73; found C 72.38, H 8.34, N 11.63 – **MF**: $C_{58}H_{82}N_8O_4$ – **FW**: 955.35 g/mol.

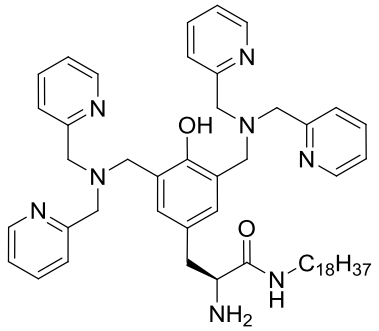

2-Amino-3-{3,5-bis-[(bis-pyridin-2-ylmethyl-amino)-methyl]-4-hydroxy-phenyl}-N-octadecyl-propionamide (**28**)

Boc protected **27** (700 mg, 0.73 mmol) was dissolved in DCM under ice cooling and mixed with HCl/ether (3.7 mL; 1 mL / 0.2 mmol Boc group). The reaction was allowed to warm to room temp. and was stirred for additional 16 hours. After completion the reaction mixture was evaporated to dryness, the residue was suspended in saturated $NaHCO_3$ and extracted with ethyl acetate (4x). Subsequently the organic phase was dried over $MgSO_4$ and the solvent was removed in vacuo yielding **28**·(497 mg, 0.58 mmol, 79 %) as a pale yellow oil. **^{1}H-NMR** (300 MHz; DMSO-d6): δ (ppm) = 0.82 (t, ^3J = 6.9 Hz, 3 H, CH_3), 1.04 (bs, 4 H, alkyl-CH_2), 1.19 (s, 28 H, alkyl-CH_2), 2.57 (dd, ^3J = 13.5 Hz, ^2J = 7.1 Hz, 1 H, Tyr-CH_2), 2.73 (dd, ^3J = 13.5 Hz, ^2J = 7.1 Hz, 1 H, Tyr-CH_2), 2.91 (m, 2 H, CH_2), 3.29 (t, ^3J = 6.4 Hz, 1 H, C□H), 3.65 (s, 4 H, Ar-CH_2-pyr), 3.74 (s, 8 H, N-CH_2-pyr), 6.98 (s, 2 H, Ar-CH), 7.21 (m, 4 H, Pyr-CH), 7.46 (d, ^3J = 8.0 Hz, 4 H, Pyr-CH), 7.70 (dt, ^3J = 7.6 Hz,

1.7 Hz, 4 H, pyr-CH), 8.47 (dd, ^{3}J = 4.4 Hz, 0.3 Hz, 4 H, pyr-CH). – **^{13}C-NMR** (75 MHz; DMSO-d6): δ (ppm) = 13.8 (+, 1 C, CH_3), 22.0 (–, 1 C, alkyl-CH_2), 26.1 (–, 1 C, alkyl-CH_2), 28.52 (–, 1 C, alkyl-CH_2), 28.57 (–, 1 C, alkyl-CH_2), 28.78, 28.81, 28.89 (–, 11 C, alkyl-CH_2), 31.4 (–, 1 C, alkyl-CH_2), 38.0 (–, 1 C, CH_2), 40.2 (–, 1 C, CH_2), 53.9 (–, 2 C, CH_2), 55.9 (+, 1 C, CH), 58.8 (–, 4 C, CH_2), 122.1 (+, 4 C, CH), 122.5 (+, 4 C, CH), 123.1 (C_q, 1 C), 127.4 (C_q, 1 C), 129.8 (+, 2 C, CH), 136.5 (+, 4 C, CH), 148.5 (+, 4 C, CH), 153.7 (C_q, 1 C), 158.5 (C_q, 4 C), 173.5 (C_q, 1 C). – **IR** (ATR) [cm^{-1}]: $\tilde{\nu}$ [cm] = 2921, 2852, 1658, 1590, 1522, 1474, 1433, 1372, 1233, 1149, 1048, 996, 754. – **MS** (ESI(+), DCM/MeCN/TFA): m/z (%) = 428.4 (100) $[M + 2\ H^+]^{2+}$, 299.6 (16) $[M + 3\ H^+ + MeCN]^{3+}$, 855.8 (14) $[MH^+]$, 286 (12) $[M + 3\ H^+]$. – **HRMS** Calcd for $C_{53}H_{75}N_8O_2$ 855.6013; Found: 855.6000. – **MF**: $C_{53}H_{74}N_8O_2$ – **FW**: 855.23 g/mol.

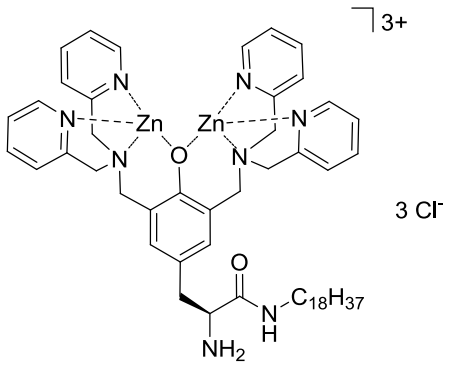

Amphiphilic binuclear Zn(II)-Dpa complex (**$Zn_2$2**)

To a solution of compound **28** (36.5 mg, 43 µmol) in MeOH (2 mL) was added dropwise a methanolic solution of $ZnCl_2$ (100 mM, 858 µL, 86 µmol). After stirring the reaction mixture for 2 h at room temperature, the methanol was removed in vacuo. The residue was dissolved in water and was lyophilized yielding complex **12** as a colourless solid in quantitative yield. **MP**: 147 °C. – **IR** (ATR) [cm^{-1}]: $\tilde{\nu}$ = 2924, 2852, 1676, 1608, 1573, 1477, 1440, 1303, 1270, 1156, 1100, 1053, 1023, 763. – **UV** (MeOH): λ_{max} (log ε) = 261 (4.076), 296 (3.436). – **MS** (ESI(+), H_2O/MeOH + 10 mmol/L NH_4Ac): m/z (%) = 1099.7 (100) $[M^{3+} + 2\ CH_3COO^-]^+$, 520.4 (69) $[M^{3+} + CH_3COO^-]^{2+}$. – **MF**: $C_{53}H_{74}N_8O_2Zn_2Cl_4$ – **FW**: 1127.79 g/mol.

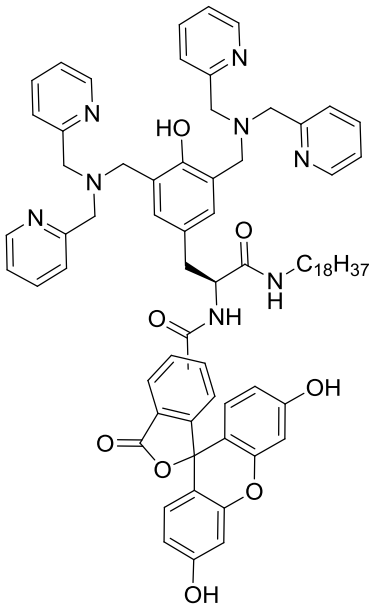

Isomeric mixture of amphiphilic, fluorescein labeled Dpa ligand (**29**)

An isomeric mixture of 5/6-carboxyfluorescein (246 mg, 0.65 mmol), DIPEA (323 µL, 1.87 mmol), TBTU (315 mg, 0.98 mmol), and HOBt (133 mg, 0.98 mmol) were dissolved under nitrogen atmosphere in dry DMF (4 mL) under ice cooling and stirred for 1 h. Subsequently **28** (400 mg, 0.47 mmol) in 4 mL DMF was added slowly. The reaction was allowed to warm to room temperature and was stirred 22 h at 40 °C. The reaction progress was monitored by TLC ($CHCl_3$ / MeOH 9:1). After completion of the reaction the solvent was removed and the crude product was purified by preparative HPLC yielding the isomers **29** as an orange-yellow solid. **MP**: 97 – 99 °C. – **UV** (MeOH): λ_{max} (log ε) = 224 (4.629), 260 (4.158), 454 (3.500), 481 (3.481). – **IR** (ATR) [cm^{-1}]: $\tilde{\nu}$ [cm] = 2924, 2853, 1757, 1670, 1609, 1438, 1377, 1246, 1178, 1126, 955, 837, 798, 755, 719. – **MS** (ESI(+), DCM/MeCN/TFA): m/z (%) = 607.6 (100) $[M + 2\ H^+]^{2+}$, 405.3 (65) $[M + 3\ H^+]^{2+}$, 1213.9 (11) $[MH^+]$. – **LC-MS** (+ p ESI Q1MS ; RT 40 min): m/z (%) = 607.6 (100) $[M + 2\ H^+]^{2+}$, 1213.9 (65) $[MH^+]^+$, 405.3 (38) $[M + 3\ H^+]^{2+}$. – **MF**: $C_{74}H_{84}N_8O_8$ – **FW**: 1213.53 g/mol.

Purification by preparative HPLC:

Column: LabID75 Phenomenex Luna 250 x 21.2 mm 10 um / Ser.Nr. 453159-3

Flow: 21 mL / min

Concentration 10 mg / mL

Injection volume: 500 µL

Detection wavelength: 220 nm

Gradient: 0 min – 5 % MeCN / H_2O (+ 0.0059 % TFA)

43 min – 72 % MeCN / H_2O (+ 0.0059 % TFA)

45 min – 98 % MeCN / H_2O (+ 0.0059 % TFA)

55 min – 98 % MeCN / H_2O (+ 0.0059 % TFA)

Retention time: ca. 42 min

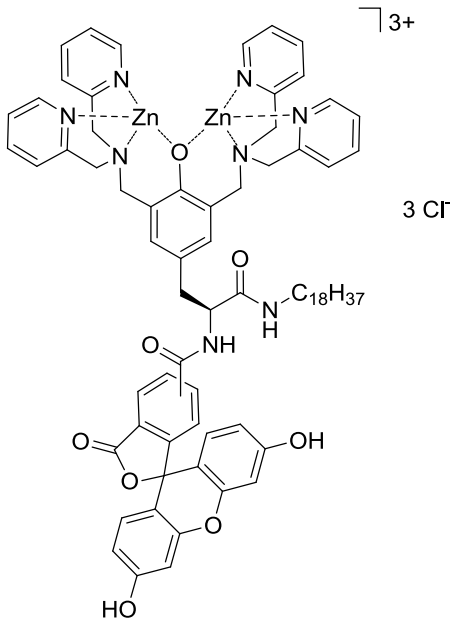

Fluorescent binuclear Zn(II)-Dpa complex (**$Zn_2$1**)

To a solution of compound **29** (10.5 mg, 8.7 µmol) in MeOH (2 mL) was added dropwise a methanolic solution of $MnCl_2$ (100 mM, 174 µL, 17.4 µmol). After stirring the reaction mixture for 2.5 h at room temperature, the methanol was removed in vacuo. The residue was dissolved in water and was lyophilized yielding complex **14** as an orange solid in quantitative yield (13 mg, 8.7 µmol). **MS** (ESI(+), H_2O/MeOH + 10 mmol/L NH_4Ac):

m/z (%) = 701.7 (100) $[M^{3+} + CH_3COO^-]^+$, 1398.0 (8) $[M^{3+} - H^+ + CH_3COO^-]^+$, 1458.0 (7) $[M^{3+} + 2\ CH_3COO^-]^+$. – **MF**: $C_{74}H_{84}N_8O_8Zn_2Cl_4$ – **FW**: 1486.10g/mol.

Synthesis of amphiphilic Cu(II)-NTA complex Cu3

Receptor **Cu3** was prepared by connecting a carboxytetramethylrhodamine label, an ornithine based NTA binding site and a hydrophobic anchor via a central cyanuric chloride linker and complexation of the amphiphilic ligand with Cu(II).

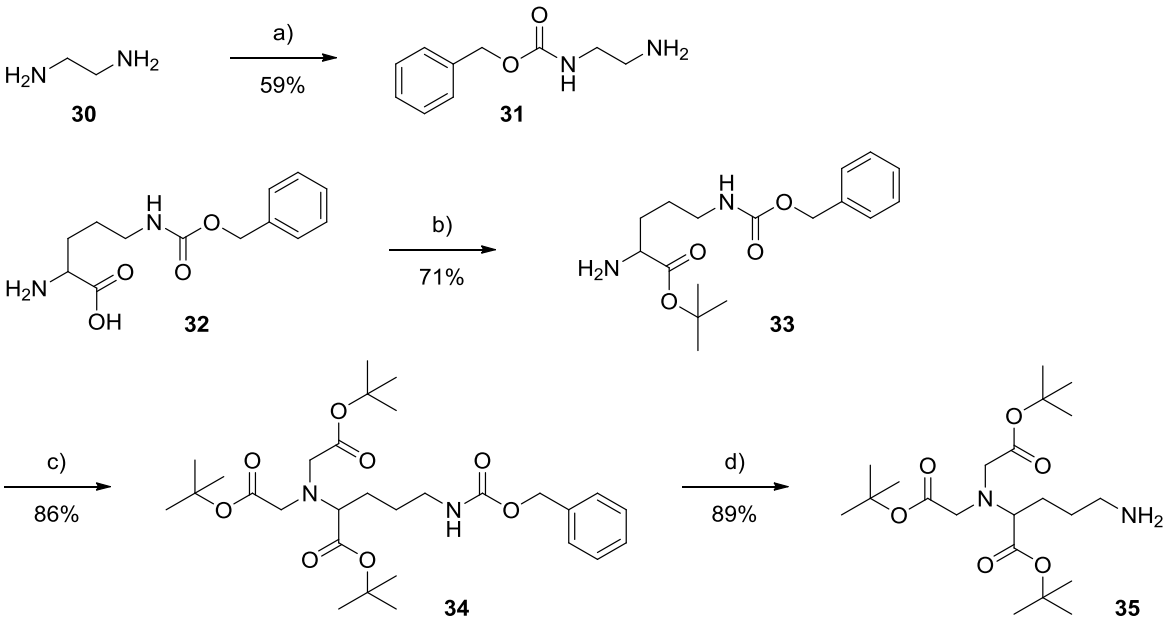

Scheme S2. Synthesis of an amphiphilic, fluorescent copper complex: (a) Cbz chloride, DCM, 0°C, 3 h; (b) tert butyl acetate, $HClO_4$, RT, 72 h; (c) bromo tert butyl acetate, DMF, 55°C, 20 h; (d) Pd/C.H_2, EtOH, RT, 72 h.

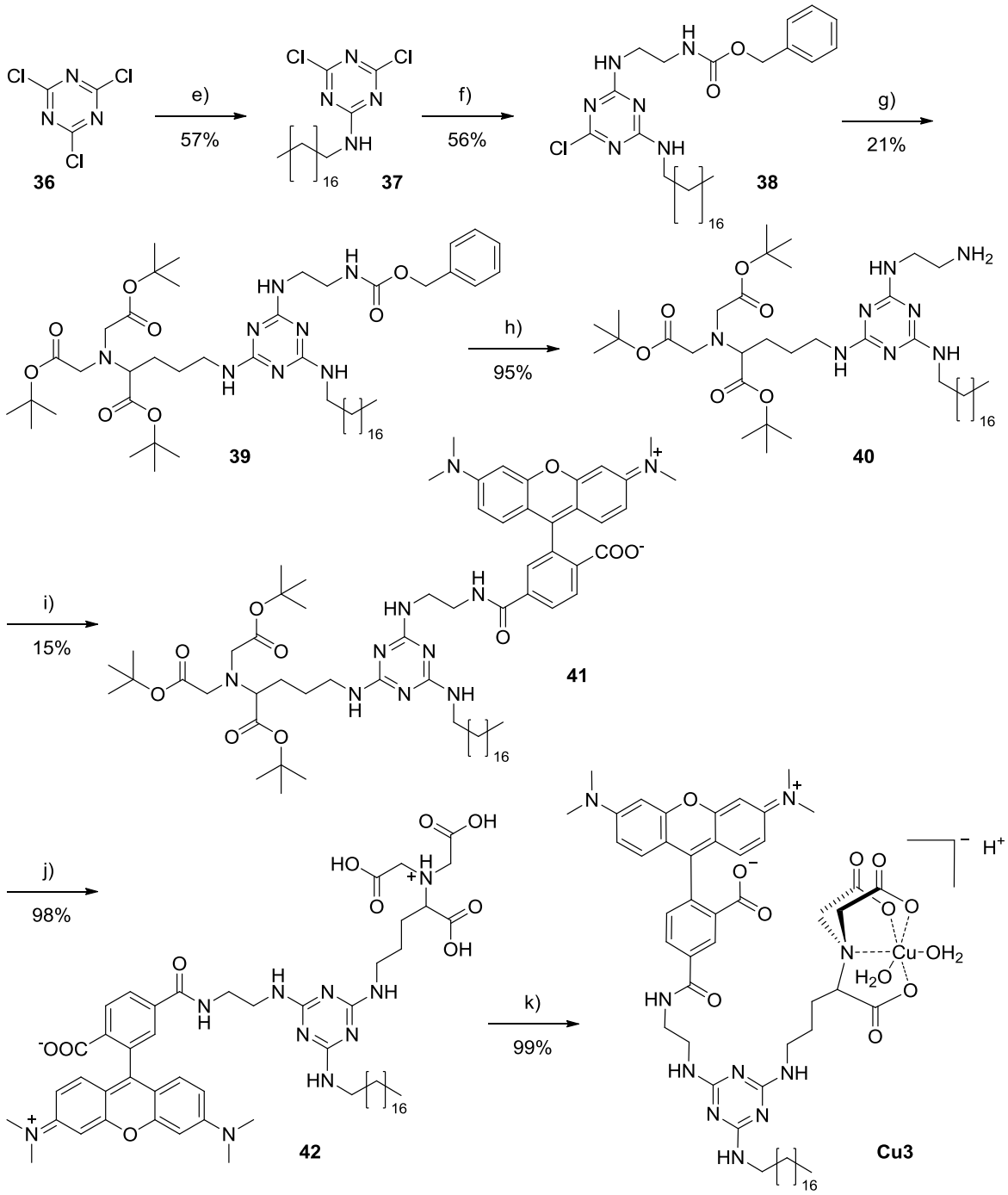

Scheme S3. Synthesis of an amphiphilic, fluorescent copper complex: (e) octadecylamine, K_2CO_3, acetone, RT, 20 h; (f) Cbz-diamine **31**, K_2CO_3, acetone, 50°C, 48 h; (g) NTA-precursor **35**, collidine, dioxane, 140°C (MW), 1.5 h; (h) Pd/C, H_2, EtOH, RT, 48 h; (i) carboxytetramethylrhodamine, TBTU, HOBt, DIPEA, DMF, 0°C, 1 h / 40°C, 24 h; (j) TFA, RT, 24 h; (k) $Cu_2(OH)_2CO_3$, MeOH, 60°C, 4 h.

Ethylenediamine **30** is Cbz-protected to give mono-amine **31**. Cbz-protected L-ornithine **32** is converted into the butyl acetate ester **33**. The amine group of **33** reacts in a nucleophilic substitution with bromo-tert-butyl-acetate to give **34** and yields after deprotection the free amine **35**. To introduce the hydrophobic anchor octadodecanylamine **13** is tethered by nucleophilic substitution to cyanuric chloride **36** yielding compound **37**. Subsequently Cbz-protected ethylenediamine **31** is attached to **37** yielding **38** to connect carboxytetramethylrhodamine as fluorescent label. Next, the NTA-precursor **35** is coupled to the unprotected functional group of the linker **38** via nucleophilic substitution yielding **39.** Hydrogenolytic Cbz-deprotection gives compound **40**, which is tethered to an *in situ* formed active ester of carboxytetramethylrhodamine. Treatment of **41** with TFA leads to the free acid **42**. In a last step copper is chelated by the acid groups of the NTA-complex **42** yielding the target receptor **Cu3**.

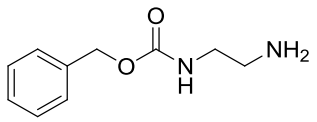

Synthesis of benzyl (2-aminoethyl)carbamate (**31**)

Ethylenediamine **30** (12.1 mL, 180 mmol) was dissolved in DCM (240 mL) and a solution of benzyl chloroformate (2.5 mL, 18 mmol) in DCM (60 mL) was added dropwise over 1.5 h at 0 °C. The reaction mixture was stirred at this temperature for further 1.5 h and at room temperature overnight. The formed precipitate was filtered off, the filtrate was washed three times with brine (150 mL) and the organic phase was dried over $MgSO_4$. Evaporation of the solvent leads to a pale-yellow, crystalline raw product which was purified via column chromatography (silica gel, $CHCl_3$/MeOH/Et_3N 70:29:1; R_f = 0.09). The product **31** (2.07 g, 10.7 mmol, 59 %) was obtained as pale-yellow oil which crystallizes at 0 °C. **^{1}H-NMR** (400 MHz, $CDCl_3$), δ [ppm]: 1.70 (2 H, bs, N*H*$_2$-CH_2), 2.73 (2 H, pt, H_2N-C*H*$_2$-CH_2), 3.17 (2 H, dd, CH_2-C*H*$_2$-NH), 5.05 (2 H, s, O-C*H*$_2$-C), 5.65 (1 H, bs, CH_2-N*H*-C), 7.29 (5 H, m, *CH*$_{arom}$). – **^{13}C-NMR** (100 MHz, $CDCl_3$), δ [ppm]: 156.84 (NH-*C*O_2), 136.64 (CH_2-*C*-C_5H_5), 128.51, 128.48, 128.02v (C-*C*$_5$*H*$_5$), 66.60 (O-*CH*$_2$-C), 43.71 (CH_2-*CH*$_2$-NH), 41.62 (H_2N-*CH*$_2$-CH_2). **– MS** (ESI(+), H_2O + 0.1% FA/MeCN + 0.1% FA): m/z (%) = 195.1 (100) [MH^+].

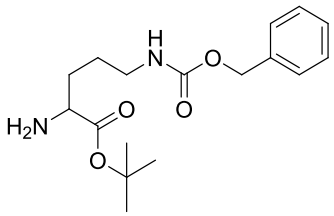

Synthesis of tertbutyl protected 2-amino-5-(((benzyloxy)carbonyl)amino) pentanoic acid (**33**)

Benzyloxycarbonyl ornithine **32** (10.00 g, 37.55 mmol) was dissolved in tert butyl acetate (471 mL, 3.47 mol), perchloric acid (70 %, 5.64 mL, 67.59 mmol) was added and the solution was stirred at RT for 72 h. The reaction mixture was cooled to 0°C and four times extracted with 0.5 M hydrochloric acid (300 mL). 2 M sodium hydroxide solution was added to the aqueous phase and the target molecule was extracted from the basic solution with diethyl ether (three times, 200 mL), dried over Na_2SO_4 and the solvent was removed in vacuo. **33** was obtained as yellow oil (8.61 g, 26.71 mmol, 71 %). – **^{1}H-NMR** (400 MHz, $CDCl_3$): δ [ppm] = 1.43 (s, 9H, *CH_3*), 1.55 – 1.70 (m, 4H, 2x *CH_2*), 3.18 (m, 2H, *CH_2*-NH), 3.30 (m, 1H, *CH*), 5.05 (s, 2H, *CH_2*-Cbz), 5.25 (s, 1H, *NH*), 7.25 – 7.36 (m, 5H, *$CH_{aromat.}$*). – **^{13}C-NMR** (100 MHz, $CDCl_3$): δ [ppm] = 26.0 (*CH_3*), 28.2 (*CH_2*), 40.9 (*CH_2*), 54.4 (*CH*), 66.6 (*CH_2*), 81.3 (*$CH_{quart.}$*), 128.6 (*$CH_{arom.}$*), 137.0 (*$C_{quart,arom.}$*), 156,5 (*$C_{carbonyl}$*), 175,0 (*$C_{carbonyl}$*). – **MS** (ESI(+), H_2O + 0.1% FA/MeCN + 0.1% FA): m/z (%) = 323.0 (100) [MH^+], 645.4 (36) [$2MH^+$].

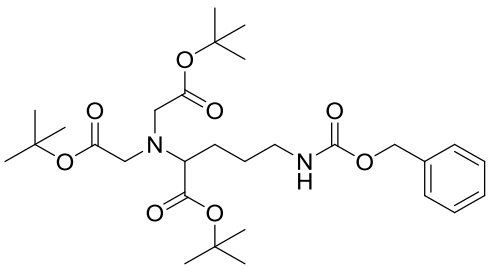

Synthesis of di-tert-butyl 2,2'-((5-(((benzyloxy)carbonyl)amino)-1-(tert-butoxy)-1-oxopentan-2-yl)azanediyl)diacetate (**34**)

Two-fold protected ornithine **33** (8.61 g, 26.71 mmol), tert butyl bromoacetate (15.50 mL, 106.82 mmol) and DIPEA (22.71 mL, 133.53 mmol) were dissolved in dry DMF (100 mL) under nitrogen atmosphere and the mixture was stirred at 55 °C for 20 h. Subsequently

the solvent was removed under vacuo yielding a dark brown solid which was suspended in ethyl acetate (60 mL) and filtered off. The residue was washed three times with hexane/ethyl acetate (3:1, 120 mL). After evaporation a brown oil (17.54 g) was obtained. The crude product was purified via column chromatography (flash silical gel, hexanes/EA 3:1; R_f = 0.27) to give **34** as pale yellow solid (12.74 g, 23.mmol, 86 %). – **^{1}H-NMR** (400 MHz, $CDCl_3$): δ [ppm] = 1.38 (s, 27H, *CH_3*), 1.55 – 1.70 (m, 4H, 2x *CH_2*), 3.16 – 3.25 (m, 3H, *CH* and *CH_2*-NH), 3.30 – 3.44 (m, 4H, 2x *CH_2*-Ntert.), 5.00 (s, 2H, *CH_2*-Cbz), 5.22 (s, 1H, *NH*), 7.21 – 7.27 (m, 5H, *$CH_{aromat.}$*). – **^{13}C-NMR** (100 MHz, $CDCl_3$): δ [ppm] = 26.0 (*CH_3*), 28.2 (*CH_2*), 40.6 (*CH_2*), 54.0 (*CH*), 65.1 (*CH_2*), 66.4 (*CH_2*), 81.2 (*$CH_{quart.}$*), 128.0 (*$CH_{arom.}$*), 136.8 (*$C_{quart,arom.}$*), 156.5 (*$CH_{carbonyl}$*), 175.1 (*$CH_{carbonyl}$*). – **MS** (ESI(+), H_2O + 0.1% FA/MeCN + 0.1% FA): m/z (%) = 551.2 (100) [MH^+].

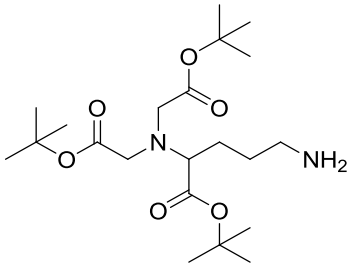

Synthesis of di-tert-butyl 2,2'-((5-amino-1-(tert-butoxy)-1-oxopentan-2-yl)azanediyl)diacetate (**35**)

Cbz-protected NTA-precursor **34** (484 mg, 0.51 mmol) was dissolved in ethanol (15 mL) and Pd/C (500 mg) was added. The reaction mixture was stirred at RT and under hydrogen atmosphere (30 bar) for 72 h. Subsequently Pd/C was filtered off via celite and the solvent was evaporated yielding the yellow oil **35** (372 mg, 0.45 mmol, 89%). **^{1}H-NMR** (300 MHz, $CDCl_3$) δ [ppm] = 5.00 (bs, 1 H, *NH*), 3.41 (s, 2 H, *CH_2*-N), 3.38 (s, 2 H, *CH_2*-N), 3.31 (m, 1 H, *CH*-N), 2.85 (m, 2H, *CH_2*-NH_2), 1.52- 1.87 (m, 4 H, 2x *CH_{2alkyl}*), 1.41 - 1.38 (m, 27 H, *CH_3*). – **^{13}C-NMR** (100 MHz, $CDCl_3$) δ [ppm] = 171.82 (*COO*), 170.68 (*COO*), 81.40 (*$CO_{quart.}$*), 81.03 (*$CO_{quart.}$*), 65.21 (*CH*-N), 57.79 (*CH_2*-N), 40.36 (*CH_2*-NH_2), 28.13 (*CH_{2alkyl}*), 28.04 (*CH_3*), 27.04 (*CH_2*-CH), 18.30 (*CH_3*). – **MS** (ESI(+), H_2O + 0.1% FA/MeCN + 0.1% FA): m/z (%) = 417.3 (100) [MH^+].

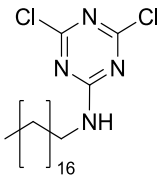

Synthesis of 4,6-dichloro-N-propyl-1,3,5 triazin-2-amine (**37**)

Octadecylamine (1.02 g, 5.50 mmol) was dissolved in acetone (40 mL) and a solution of 2,4,6-trichloro-1,3,5-triazine **36** (1.47 g, 5.44 mmol) in acetone (25 mL) and water (5 mL) was added at 0 °C, followed by the addition of K_2CO_3 (2.25 g, 16.28 mmol) in water (10 mL). The reaction mixture was stirred at 0 °C for further 30 min and at RT for 20 h. After the solvent was removed in vacuo the residue was washed with brine (5 mL) and extracted three times with $CHCl_3$ (25 mL). The organic phases were dried over $MgSO_4$ and the solvent was evaporated to give a white powder (2.20 g). The crude product was purified via silica column chromatography (hexanes/EA 10:1; R_f = 0.37) yielding the white solid **37** (1.30 g, 3.11 mmol, 57 %). – **^{1}H-NMR** (300 MHz, $CDCl_3$) δ [ppm] = 3.47 (q, 2H, *CH_2*-NH), 1.59 (m, 2H, *CH_{2alkyl}*), 1.25 -1.32 (m, 30H, 15 x *CH_{2alkyl}*), 0.88 (t, 3H, *CH_3*). – **^{13}C-NMR** (100 MHz, $CDCl_3$) δ [ppm] = 171.01 (*$C_{arom.}$*-NH), 165.83 (*$C_{arom.}$*-Cl), 41.58 (*CH_{2alkyl}*), 31.94 (*CH_{2alkyl}*), 29.48 (*CH_{2alkyl}*), 26.64 (*CH_{2alkyl}*), 22.71 (*CH_{2alkyl}*), 14.14 (*CH_3*). – **MS** (ESI(+), H_2O + 0.1% FA/MeCN + 0.1% FA): m/z (%) = 417.2 (100) [MH^+].

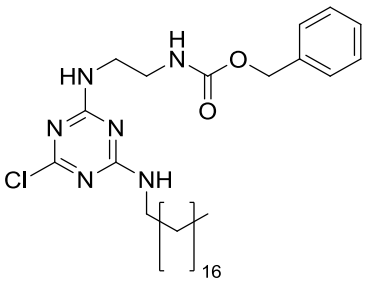

Synthesis of benzyl (2-((4-chloro-6-(propylamino)-1,3,5-triazin-2-yl) amino)ethyl)carbamate (**38**)

Amphiphilic triazine **37** (4.50 g, 10.80 mmol) was dissolved in acetone (50 mL) followed by the addition of Cbz-protected ethylendiamine **31** (2.10 g, 10.80 mmol) and K_2CO_3 (7.46 g, 54.00 mmol). The mixture was stirred at 50 °C for 40 h before the solvent was removed in vacuo. The residue was redissolved in $CHCl_3$ (100 mL) and washed three times with a

water/brine solution (2:1, 100 mL). The organic phases were dried over $MgSO_4$ and the solvent was evaporated. The obtained crude product was recrystallized from EA yielding **38** as a light brown solid (3.46 g, 6.01 mmol, 56 %). **^{1}H-NMR** (300 MHz, $CDCl_3$) δ [ppm] = 7.29 (m, 5 H, *CH_{arom}*), 5.08 (s, 2 H, *CH_2*-Cbz.), 3.56 (m, 2 H, *CH_{2alkyl}*), 3.27- 3.45 (m, 4 H, *CH_2-CH_2*), 1.53 (t, 2 H, *CH_{2alkyl}*), 1.25 (bs, 30 H, 15 x *CH_{2alkyl}*), 0.88 (t, 3 H, CH_3). – **^{13}C-NMR** (100 MHz, $CDCl_3$) δ [ppm] = 136.53 (*C_{arom}*), 128.07- 128.54 (*CH_{arom}*.), 66.72 (*CH_2-CH_2*), 41.05 (*CH_{2alkyl}*), 31.94 (*CH_{2alkyl}*), 29.38 - 29.72 (*CH_{2alkyl}*), 22.71 (*CH_{2alkyl}*), 14.14 (*CH_3*). – **MS** (ESI(+), H_2O + 0.1% FA/MeCN + 0.1% FA): m/z (%) = 574.4 (100) [MH^+].

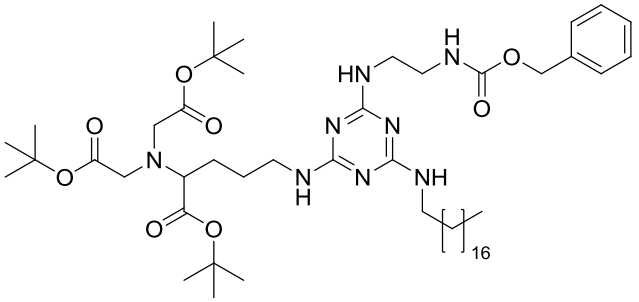

Synthesis of di-tert-butyl 2,2'-((5-((4-((2-(((benzyloxy)carbonyl)amino) ethyl)amino)-6-(octadecylamino)-1,3,5-triazin-2-yl)amino)-1-(tert-butoxy)-1-oxopentan-2-yl)azanediyl)diacetate (**39**)

Amine **35** (1.00 g, 2.47 mmol) was suspended in dioxane (10 mL) followed by the addition of the two-fold substituted triazine **38** (1.42 g, 2.47 mmol) and collidine (1.63 µl, 12.37 mmol). The reaction was carried out in a microwave (150 W, 1.7 bar) at 140 °C for 1.5 h. After evaporation a brown oil was obtained. The crude product was purified via column chromatography (flash silica gel, EA/hexanes/Et_3N 75:20:5; R_f = 0.43) to give product **39** as a dark yellow oil (0.48 g, 0.51 mmol, 21 %). **^{1}H-NMR** (300 MHz, $CDCl_3$) δ [ppm] = 7.29 - 7.33 (m, 5 H, *CH_{arom}*), 5.07 (s, 2 H, *CH_2*-Cbz), 3.26 - 3,50 (m, 13 H, *CH* and 6 x *CH_{2alkyl}*), 1.70 (m, 2 H, *CH_{2alkyl}*), 1.64 (m, 2 H, *CH_{2alkyl}*), 1.50 (t, 2 H, *CH_{2alkyl}*), 1.43 (bs, 30 H, *CH_{2alkyl}*), 1.24 (bs, 27 H, *CH_3*), 0.88 (t, 3 H, *CH_3*). – **^{13}C-NMR** (100 MHz, $CDCl_3$) δ [ppm] =172.22 (*COO*), 170.66 (*COO*), 136.73 (*CH_{arom}*)), 128.45 (*CH_{arom}*)), 127.96 (*CH_{arom}*), 81.11 (*CO_{quart}*), 80.67 (*CO_{quart}*), 66.49 (*CH*COO), 65.1, (*CH_2*O), 53.82 (*CH_2*-N), 40.68 (*CH_2*-NH), 40.39 (*CH_2*-NH), 31.92 - 26.22 (*CH_{2alkyl}*), 26.97 (*CH_3*), 22.69 (*CH_2*-CH_3), 14.12 (*CH_3*). – **MS** (ESI(+), H2O + 0.1% FA/MeCN + 0.1% FA): m/z (%) = 478.4 (100) [M + 2 H^+]2+, 955.8 (64) [MH^+].

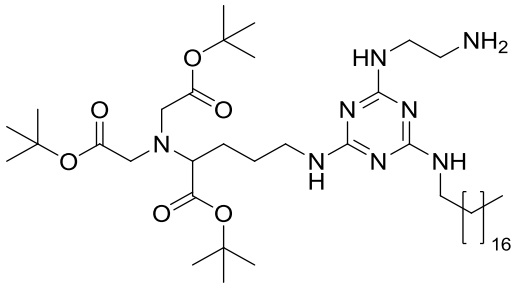

Synthesis of di-tert-butyl 2,2'-(5-((4-((2-aminoethyl)amino)-6-(octodecylamino)-1,3,5-triazin-2-yl)amino)1-(tert-butoxy)-1-oxopentan-2-yl)azanediyl)diacetate (**40**)

Cbz-protected spacer moiety **39** (190 mg, 0.20 mmol) was dissolved in ethanol (15 mL) and Pd/C (500 mg) was added. The reaction mixture was stirred at RT and under hydrogen atmosphere (30 bar) for 48 h. Subsequently Pd/C was filtered off via celite and the solvent was evaporated yielding **40** as light-yellow oil (156 mg, 0.19 mmol, 95%). **^{1}H-NMR** (300 MHz, $CDCl_3$) δ [ppm] = 3.26 – 3.58 (m, 13 H, *CH* and 6 x CH_{2alkyl}), 1.71 (m, 2 H, CH_{2alkyl}), 1.64 (m, 2 H, CH_{2alkyl}), 1.55 (t, 2 H, CH_{2alkyl}), 1.42 (bs, 30 H, CH_{2alkyl}), 1.24 (bs, 27 H, CH_3), 0.88 (t, 3 H, CH_3). – **^{13}C-NMR** (100 MHz, $CDCl_3$) δ [ppm] =172.22 (*COO*), 170.66 (*COO*), 136.73 (CH_{arom})), 128.45 (CH_{arom})), 127.96 (CH_{arom}), 81.11 (CO_{quart}), 80.67 (CO_{quart}), 66.49 (*CH*COO), 65.1. (CH_2O), 53.82 (CH_2-N), 40.68 (CH_2-NH), 40.39 (CH_2-NH), 31.93 - 26.22 (CH_{2alkyl}), 26.97 (CH_3), 22.69 (CH_2-CH_3), 14.13 (CH_3). – **MS** (ESI(+), H2O + 0.1% FA/MeCN + 0.1% FA): m/z (%) = 411.2 (70) $[M + 2\ H^+]^{2+}$, 431.8 (100) $[M + 2\ H^+ + MeCN]^{2+}$, 821.7 (30) $[MH^+]$.

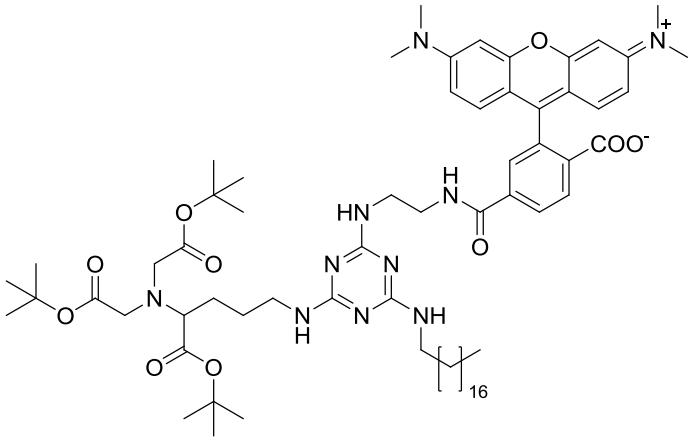

Synthesis of 4-((2-((4-((4-(bis(2-(tert-butoxy)-2-oxoethyl)amino)-5-(tert-butoxy)-5-oxopentyl)amino)-6-(octadecylamino)-1,3,5-triazin-2-yl)amino) ethyl)carbamoyl)-2-(6-(dimethylamino)-3-(dimethyliminio)-3H-xanthen-9-yl)benzoate (**41**)

Carboxytetramethylrhodamine (180 mg, 0.42 mmol), TBTU (148 mg, 0.46 mmol), HOBt (62 mg, 0.46 mmol) and DIPEA (284 µL, 1.67 mmol) were dissolved in dry DMF (4.5 mL) under nitrogen atmosphere at 0°C and the reaction mixture was stirred at RT. After 1 h a solution of the receptor-precursor **40** (343 mg, 0.42 mmol) in dry DMF (3 mL) was added dropwise over 35 min. The reaction mixture was warmed to 45 °C and stirred for another 40 h. Subsequently the solvent was removed and the pink residue was purified via column chromatography (flash silica gel, EA/MeOH/Et_3N 75:20:5) to give **41** as magenta oil. (76 mg, 0.06 mmol, 15 %). **^{1}H-NMR** (300 MHz, $CDCl_3$) δ [ppm] = 0.80 (t, 3 H, CH_3), 1.11 (m, 2 H, $CH_{2\ alkyl}$), 1.17 (m, 28 H, $CH_{2\ alkyl}$), 1.27 (m, 2 H, $CH_{2\ alkyl}$), 1.35 (s, 27 H, $CH_{3\ Boc}$), 1.45 – 1.73 (m, 4 H, $CH_{2\ alkyl}$), 3,00 (m, 12 H, CH_3-N), 3.16-3.55 (m,13 H, CH_2 and CH), 7.22 (s, 1H, arom.), 7.34 – 7.49 (m, 4 H, arom), 7.64 – 7.67 (m, 4H, arom.). – **^{13}C-NMR** (100 MHz, $CDCl_3$) δ [ppm] = 8.7, 14.1, 22.7, 28.0, 28.3, 29.7, 31.9, 45.7, 53.4, 110.7, 110.9, 118.5, 124.0, 125.1, 127.8. – **MS** (ESI(+), H_2O + 0.1% FA/MeCN + 0.1% FA): m/z (%) = 1234.0 (100) [MH^+].

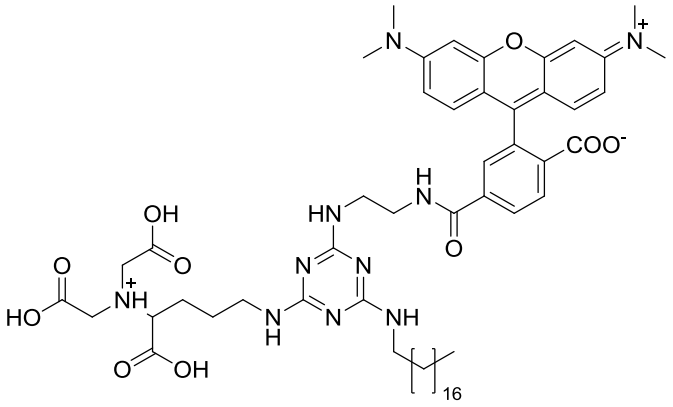

Synthesis of 4-((2-((4-((4-(bis(carboxymethyl)ammonio)-4-carboxybutyl) amino)-6-(octadecylamino)-1,3,5-triazin-2-yl)amino)ethyl)carbamoyl)-2-(6-(dimethylamino)-3-(dimethyliminio)-3H-xanthen-9-yl)benzoate (**42**)

41 (92 mg, 0.08 mmol) was dissolved in TFA (1.6 mL, 20.77 mmol) and stirred at RT for 30 h. TFA was evaporated in vacuo, the residue was suspended in water (3 mL) and lyophilized giving product **42** (83 mg, 0.08 mmol, 98 %) as a magenta solid. **^{1}H-NMR** (600 MHz, $CDCl_3$) δ [ppm] = 0.86 (t, 3 H, CH_3), 1.15 – 1.28 (m, 28 H, $CH_{2\ alkyl}$), 1.36-1.38 (m, 4 H, $CH_{2\ alkyl}$), 1.39 – 1.42 (m, 12 H, CH_3), 3.09 – 3.15 (m, 5 H, CH-$(CH_2)_2$), 3.16 – 3.20 (m, 8 H, CH_2-NH), 3.69 – 3.71 (m, 4 H, CH_2-COOH), 6.61 (bs,1 H, NH), 6.74 (bs,1 H, NH), 6.98 (bs,1 H, NH), 7.39 (t, 1H, $CH_{arom.}$), 7.41 – 7.53 (m, 4 H, $CH_{arom.}$), 7.56 (d, 1H, $CH_{arom.}$), 7.75 – 7.83 (m, 2H, $CH_{arom.}$), 8.02 (d, 1H, $CH_{arom.}$), 8.61 (bs,1 H, NH), 9.12 (bs,1 H, NH). – **^{13}C-NMR** (150 MHz, $CDCl_3$) δ [ppm] = 14.1 (+, 1 C, CH_3), 17.3 (+, 2 C, CH_3), 18.5 (+, 2 C, CH_3), 22.6 (-, 1 C, $CH_{2\ alkyl}$), 28.8 – 29.7 (-, 16 C, $CH_{2\ alkyl}$), 31.9 (-,1 C, $CH_{2\ alkyl}$), 40.6 (+, 1 C, CH), 41.0 (-, 1 C, CH-$(CH_2)_2$), 42.5 (-, 1 C, CH-$(CH_2)_2$), 46.3 (-, 4C, CH_2-NH), 54.4 (-, 2 C, CH_2-COOH), 109.8 (+, 1 C, $CH_{arom.}$), 112.6 (+, 1 C, $CH_{arom.}$), 114.1 (+, 1 C, $CH_{arom.}$), 114.7 (-, 1 C, C_q), 114.8 (-, 1 C, C_q), 116.7 (-, 1 C, C_q), 118.6 (-, 1 C, C_q), 119.7 (+, 1 C, $CH_{arom.}$), 124.8 (+, 1 C, $CH_{arom.}$), 127.0 (+, 1 C, $CH_{arom.}$), 128.1 (+, 1 C, $CH_{arom.}$), 128.6 (+, 1 C, $CH_{arom.}$), 128.9 (+, 1 C, $CH_{arom.}$), 130.4 (-, 1 C, C_q), 130.9 (-, 1 C, C_q), 136.6 (-, 1 C, C_q), 142.5 (-, 1 C, C_q), 157.0 (-, 1 C, C_q), 157.3 (-, 1 C, C_q), 160.6 (-, 1 C, C_q), 160.9 (-, 1 C, C_q), 161.1 (-, 1 C, C_q), 161.4 (-, 1 C, C_q). – **MS** (ESI(+), DCM/MeOH + 0.1% FA): m/z (%) = 533.5 (100) $[M + 2\ H^+]^{2+}$, 1065.7 (26) $[MH^+]$.

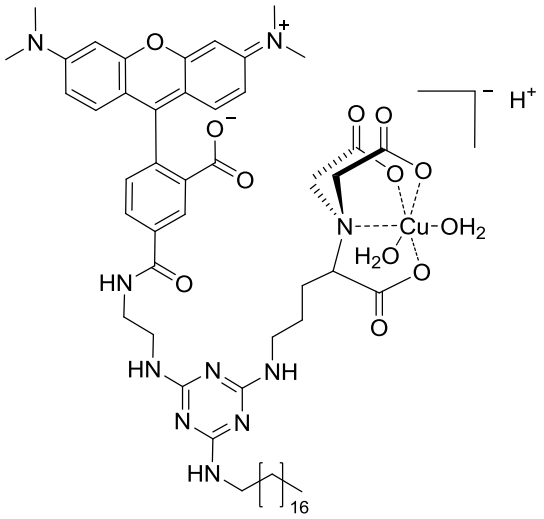

Synthesis of the amphiphilic, labeled Cu(II)-NTA-complex (**Cu3**)

Deprotected **42** (83.0 mg, 0.08 mmol) was dissolved in MeOH (1.5 mL) and a suspension of $Cu(OH)_2CO_3$ and a very small amount of MeOH was added. The reaction was completed by stirring the mixture at RT for 20 h and at 60°C for 3 h. Subsequently the warm solution was filtered immediately and the solvent was evaporated. The residue was suspended in water (2 mL) and lyophilized yielding **Cu3** (89.0 mg, 0.08 mmol, 99 %) as a dark magenta solid. **MS** (ESI(-), H_2O/MeOH + 10 mmol/L NH_4Ac): m/z (%) = 1124.4 (100) $[M - H - 2\ H_2O]^-$.

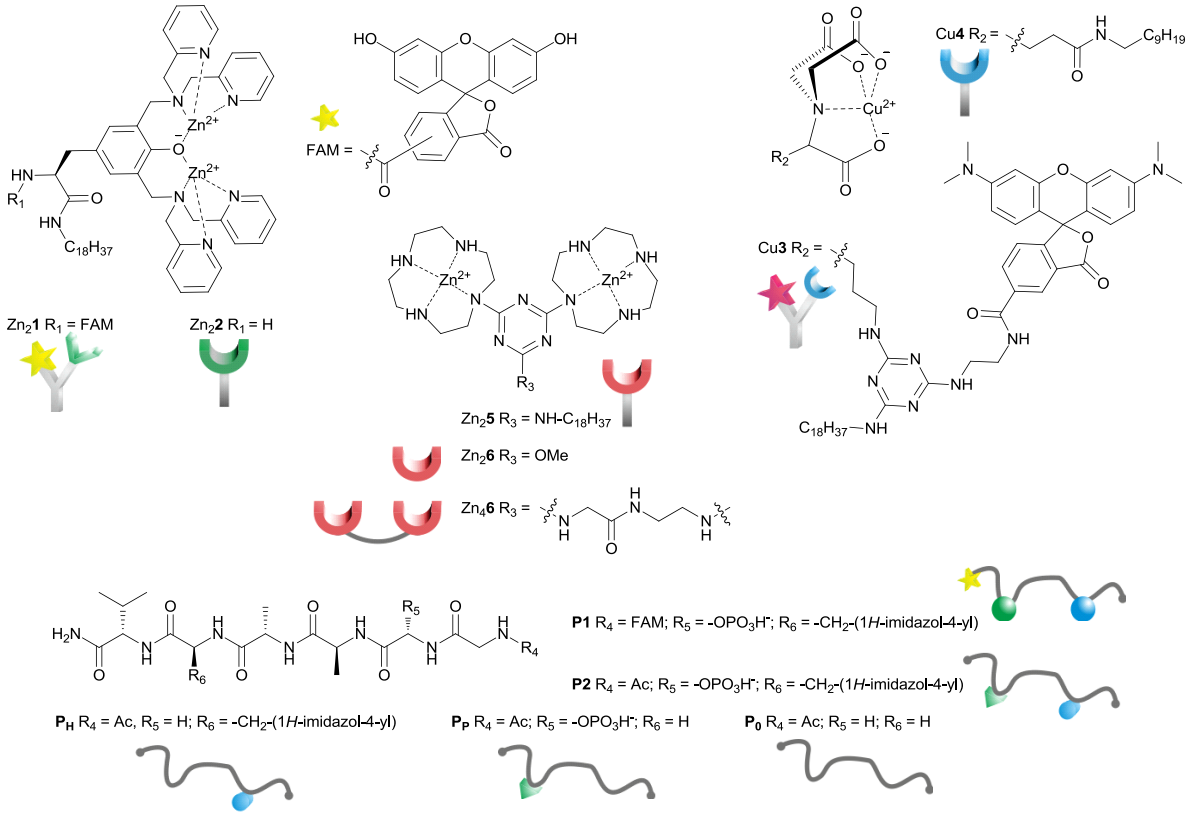

Scheme S4. Structures and symbols of (non-)amphiphilic receptors and ligands (counterions omitted).

Receptor-ligand binding in homogeneous (Zn_2**6**, Zn_4**6**) and vesicular (Zn_2**5**) solution

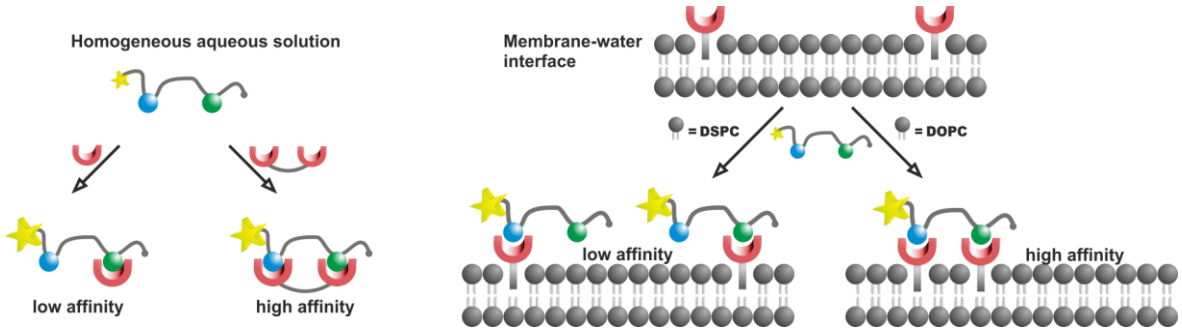

Figure S1. (a) Schematic recognition of **P1** in homogeneous aqueous solution by previously developed receptors[26] Zn_2**6** and Zn_4**6**; (b) Schematic recognition of **P1** by membrane-embedded receptor Zn_2**5** in DSPC and DOPC vesicles.

Vesicles

Preparation

In small glass reaction vessels 1 - 5 µmol of DOPC or DSPC were dissolved in chloroform and optionally 0.1-10 mol% of dissolved metal complexes were added and mixed. The solvent was completely removed under reduced pressure at 25 °C (DOPC) or 75°C (DSPC) and an appropriate amount of buffer (HEPES 10 mM, pH 7.4) was added to obtain lipid concentrations of 1 - 2 mM. Vigorous shaking at 25 °C (DOPC) or 75 °C (DSPC) for 5 - 10 minutes yielded a turbid multi-lamellar vesicle suspension. Small uni-lamellar dispersions were obtained by extrusion through 100 nm-pore size polycarbonate membranes with a LiposoFast liposome extruder from Avestin.[37]

Metal complex concentration

For all vesicles the receptor concentration refers to the outer surface exposed binding sites, as only these should be reactive, with the assumption that embedded compounds distribute equally in both layers of the vesicle membrane and the bilayer thickness for the prepared vesicles amounts to 5 nm.[11, 38-40]

Dynamic light scattering (DLS)

Vesicle size distributions were determined using Dynamic light scattering (DLS). The standard size distribution of species obtained after extrusion is the following:

			Diam. (nm)	% Intensity	Width (nm)
Z-Average (d.nm):	92,99	Peak 1:	98,42	100,0	24,62
PdI:	0,039	Peak 2:	0,000	0,0	0,000
Intercept:	0,922	Peak 3:	0,000	0,0	0,000
Result quality	Good				

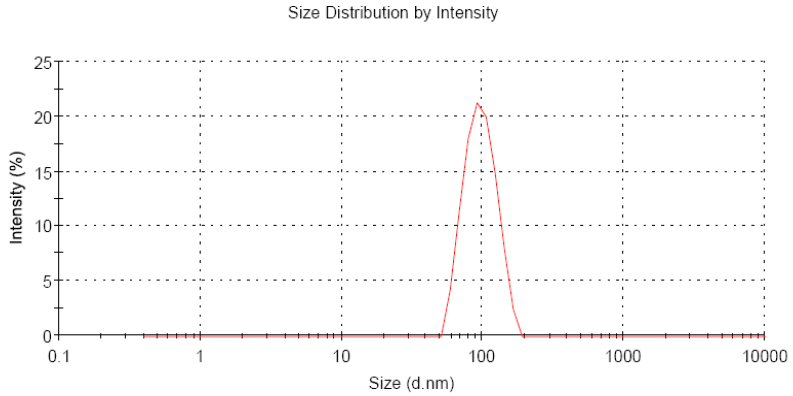

Figure S2. Typical size distribution of 100 nm-sized vesicles.

In order to remove low molecular weight solutes vesicles can be purified by size exclusion chromatography via small spin columns.[41] For this Sephadex LH-20 SEC medium was swollen in buffer solution prior to use. 5 mL bed volume per mL vesicle suspension was transferred into a small plastic syringe with filter support and removed plunger and the solvent removed by centrifugation (Eppendorf bench top centrifuge, 15 sec @ 4400 rpm). Vesicle solutions were added onto the column and recovered by subsequent centrifugation.

Cu- and Zn-quantification via atomic emission spectroscopy (ICP-AES)

In order to verify the receptor concentration of prepared vesicles their total metal content was measured via ICP-AES on a Spectro Flame-EOP spectrometer. Standard curves were recorded in Millipore water to quantify Cu and Zn in stock solutions of **Cu3** and **$Zn_2$1**. Metal contents were again determined after receptor-embedding in vesicle membranes and purification of vesicular solutions via SEC.

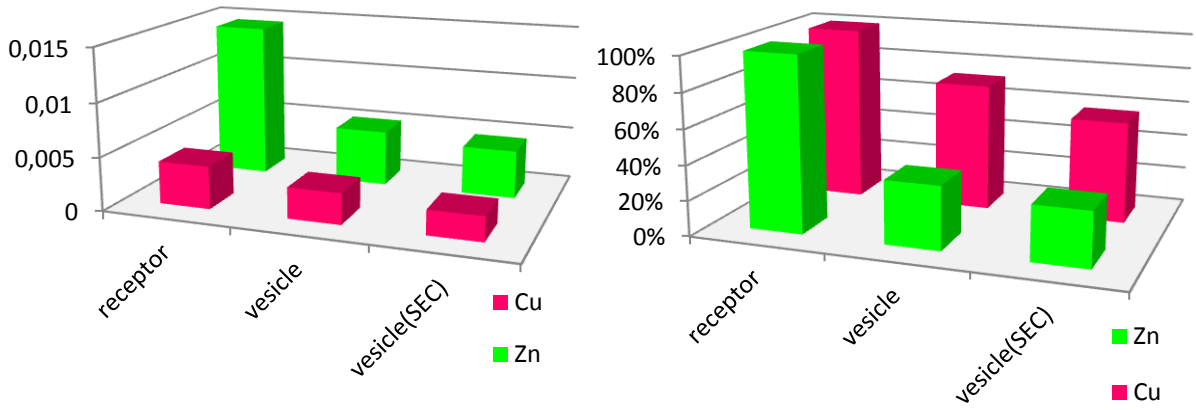

Figure S3. Absolute (left; in mM) and relative (right) concentrations of Cu and Zn in stock solutions of **Cu3** and **$Zn_2$1** and corresponding vesicle preparations before and after purification via SEC.

Supporting experimental data for $Zn_2$5-vesicles vs. P1

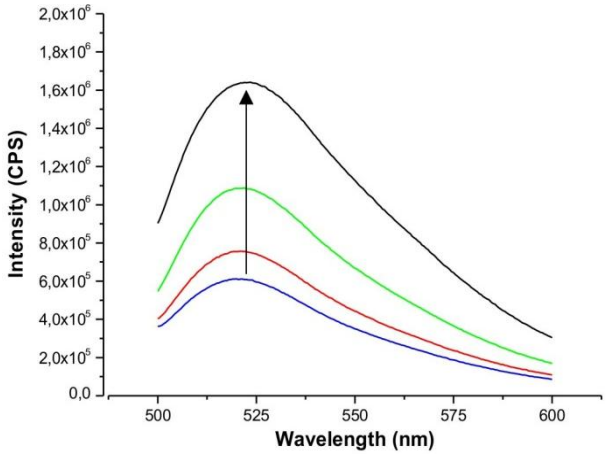

Figure S4. Raw **emission** spectra of **P1** in the presence of increasing amounts of receptor-vesicles.

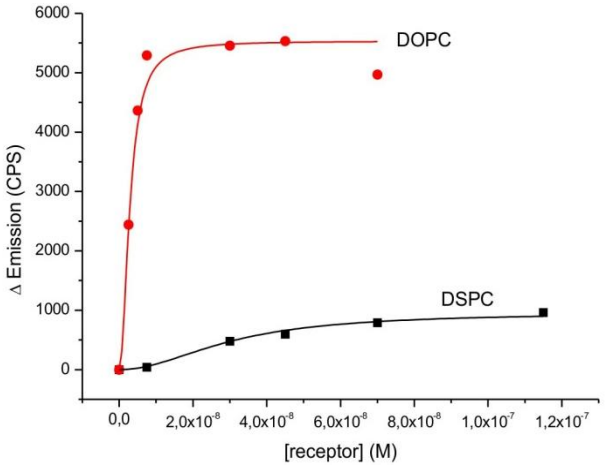

Figure S5. Emission response of **$Zn_2$5** doped (1 mol% each) DOPC and DSPC vesicle membranes.

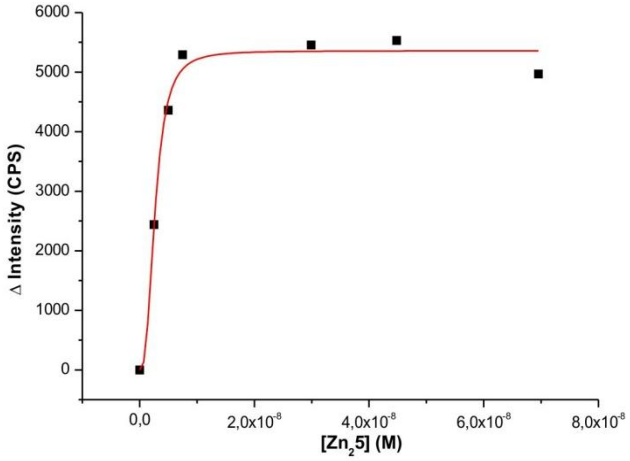

Figure S6. Non-linear curve fitting of DOPC-vesicles doped with 1 mol% **$Zn_2$5**.

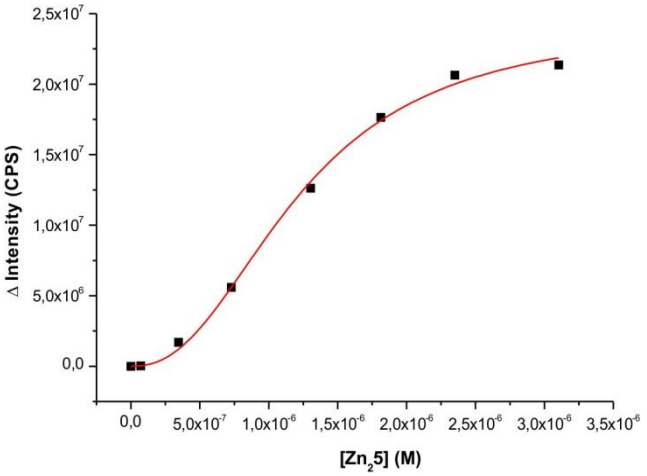

Figure S7. Non-linear curve fitting of DSPC-vesicles doped with 1 mol% **$Zn_2$5**.

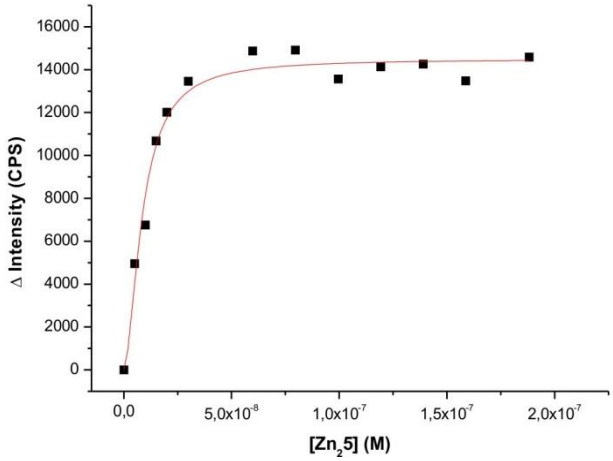

Figure S8. Non-linear curve fitting of DSPC-vesicles doped with 10 mol% **$Zn_2$5**.

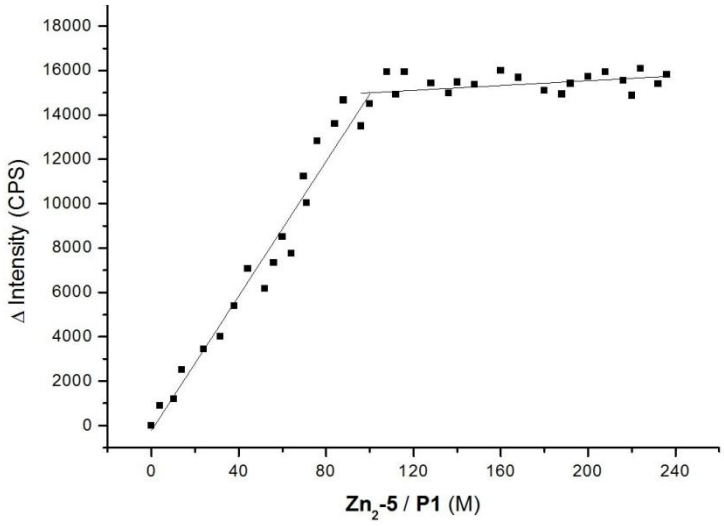

Figure S9. Job's Plot (limiting reagent method) of **P1** vs. DSPC-vesicles doped with 1 mol% **$Zn_2$5**.

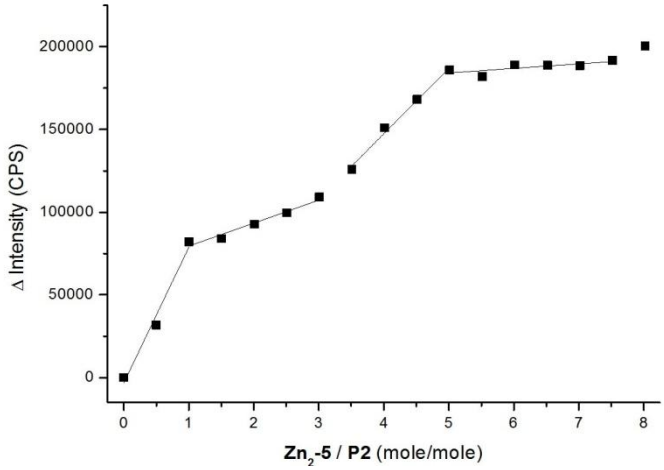

Figure S10. Job's Plot (limiting reagent method) of **P1** vs. DSPC-vesicles doped with 1 mol% **$Zn_2$5**.

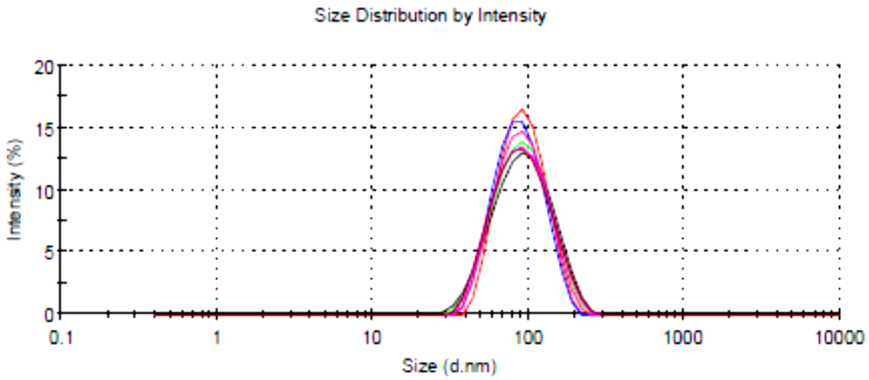

Figure S11. Size distributions of vesicles doped with 1 mol% **$Zn_2$5** in the presence of increasing amounts of **P1** (0.5 – 200 eq.) showing no apparent crosslinking of membranes.

Supporting experimental for $Zn_2$2/Cu4-vesicles vs. P1

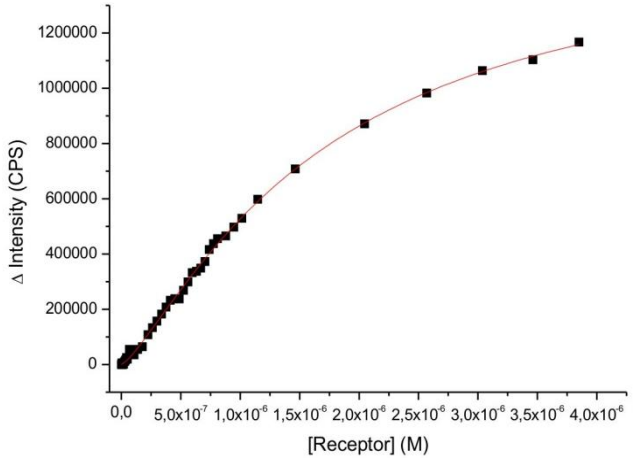

Figure S12. Non-linear curve fit for **$Zn_2$2** (1 mol%) in DOPC-vesicles.

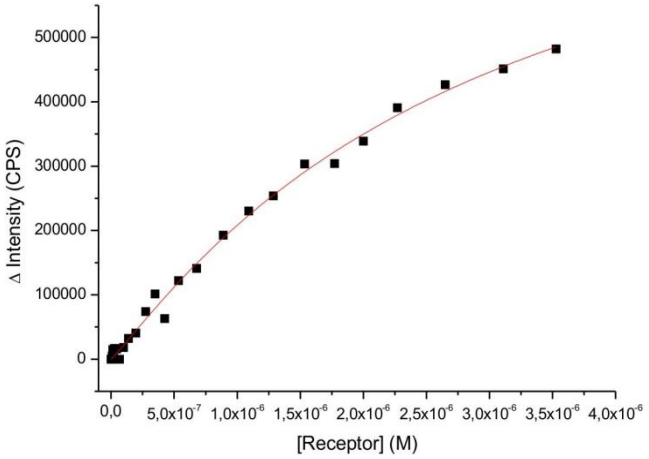

Figure S13. Non-linear curve fit for **Cu4** (1 mol%) in DOPC-vesicles.

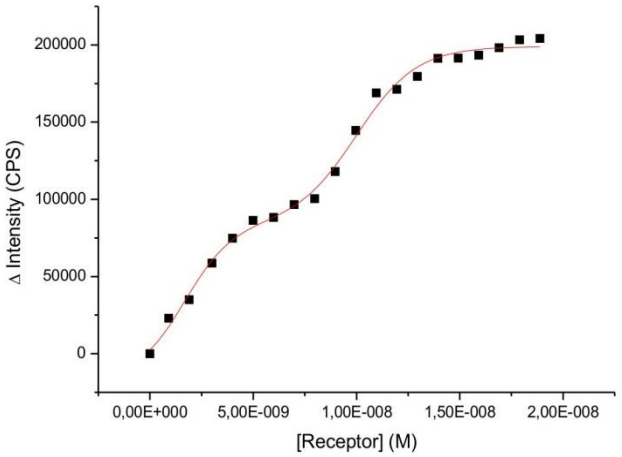

Figure S14. Non-linear curve fit for **$Zn_2$2** + **Cu4** (1 mol% each) in DOPC-vesicles.

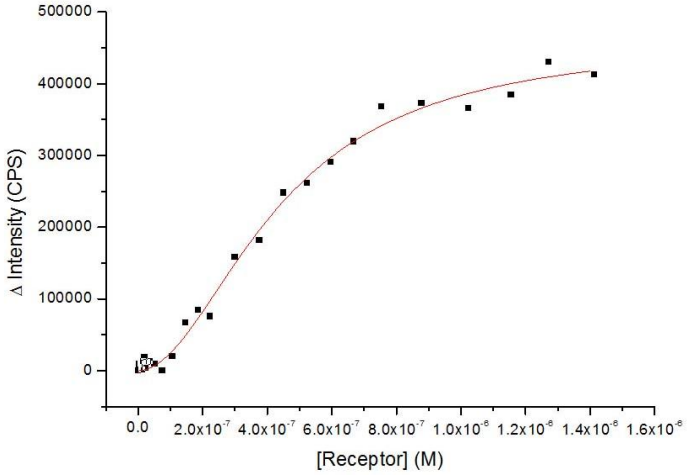

Figure S15. Non-linear curve fit for **$Zn_2$2** (1 mol% each) in DSPC-vesicles.

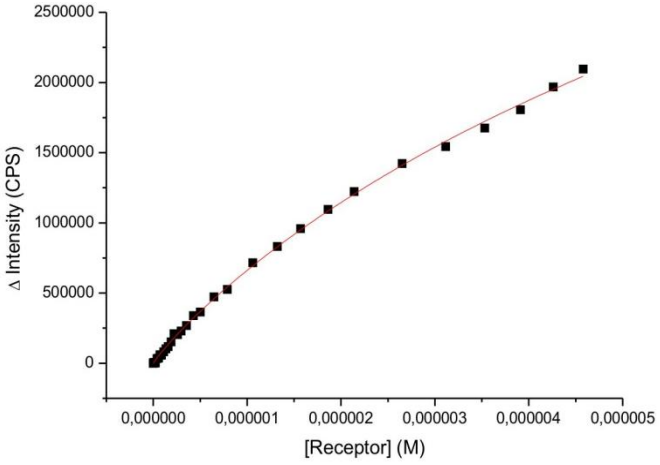

Figure S16. Non-linear curve fit for **Cu4** (1 mol% each) in DSPC-vesicles.

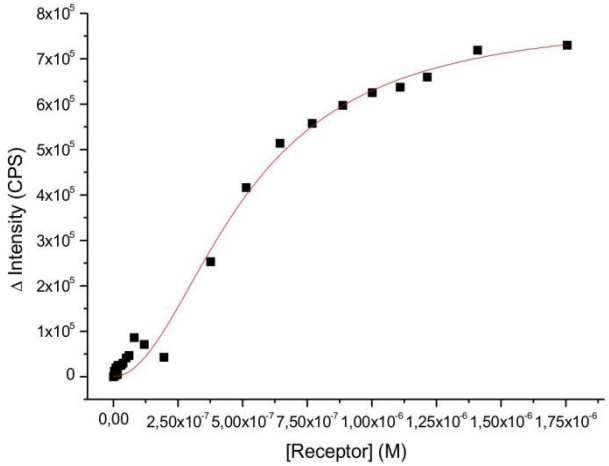

Figure S17. Non-linear curve fit for **$Zn_2$2** + **Cu4** (1 mol% each) in DSPC-vesicles.

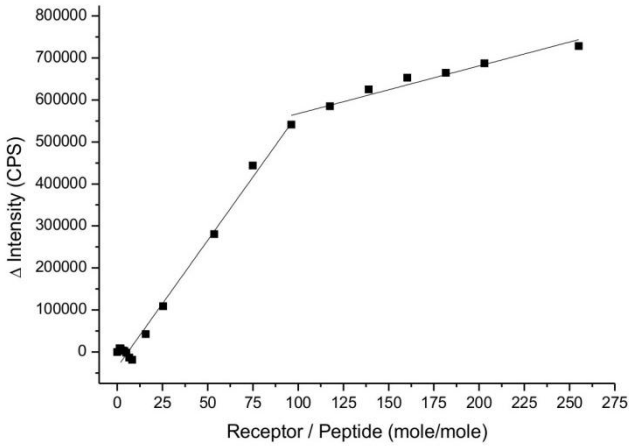

Figure S18. Job's Plot (limiting reagent method) of **P1** vs. DSPC-vesicles doped with **$Zn_2$2** + **Cu4** (1 mol% each).

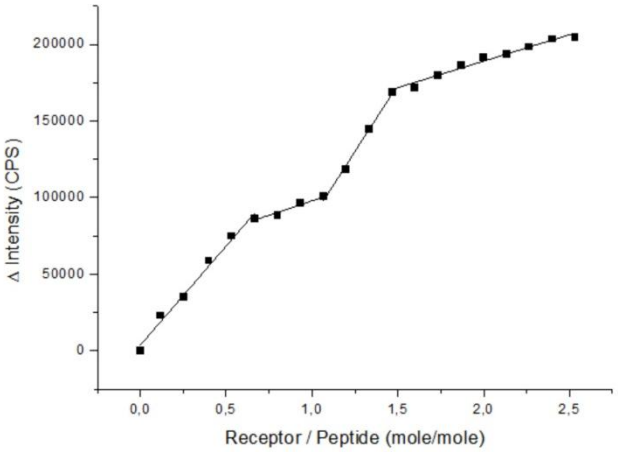

Figure S19. Job's Plot (limiting reagent method) of **P1** vs. DOPC-vesicles doped with **$Zn_2$2** + **Cu4** (1 mol% each).

Supporting experimental for $Zn_2$1/Cu3-vesicles vs. P2

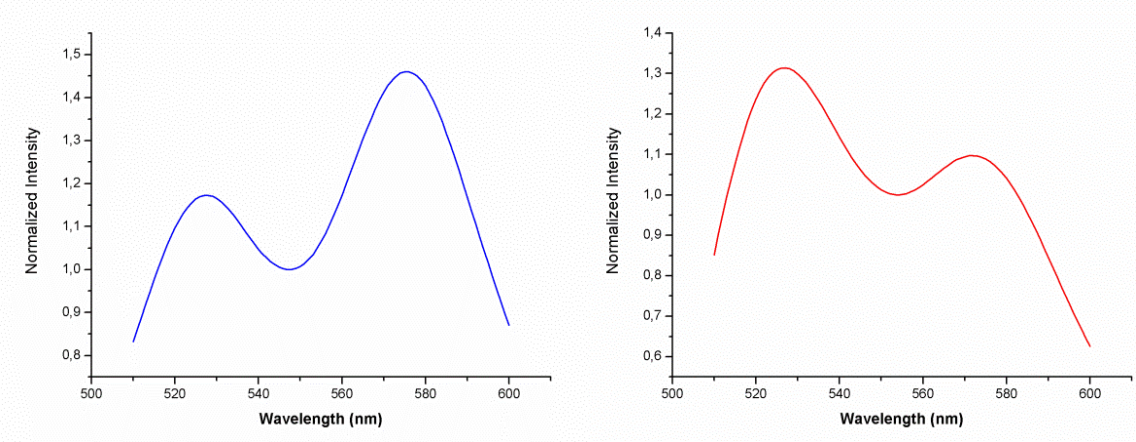

Figure S20. Fluorescence emission spectra of DSPC (left) and DOPC (right) vesicles equipped with **Cu3** and **$Zn_2$1** (0.5 mol% each).

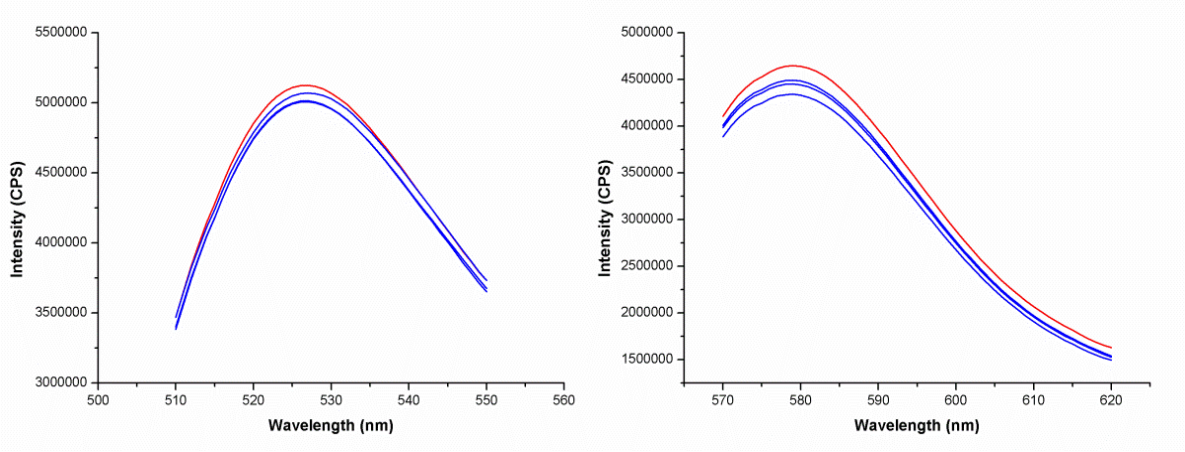

Figure S21. Raw emission spectra of DOPC vesicles functionalized with either 0.1 mol% of **$Zn_2$1** (left) or **Cu3** (right) in the presence of increasing amounts of mono- or divalent peptide ligands (**P_0**, **P_H**, **P_P** or **P2**, 0 – 100 eq.). Peptide binding towards these mono-receptor-vesicles does not produce a significant emission response.

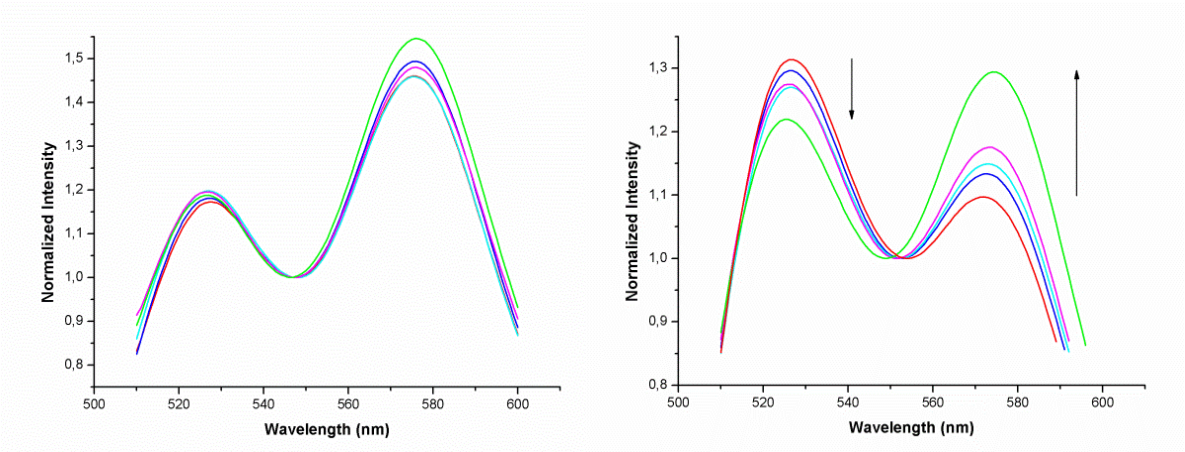

Figure S22. Emission spectra of DSPC vesicles (left) and DOPC vesicles (right) functionalized with 0.5 mol% **Cu3** and **$Zn_2$1** each in the presence of increasing amounts of **P2.**

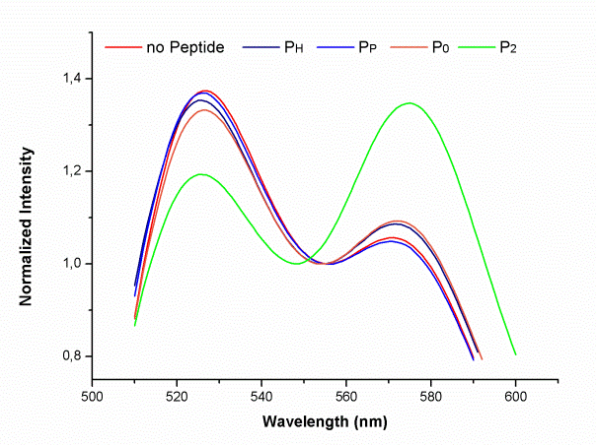

Figure S23. Emission spectra of DOPC vesicles (0.5 mol% **Cu3** and **$Zn_2$1**) in the presence of equivalent amounts of the control peptides **P_H**, **P_P** and **P_0** compared to **P2.**

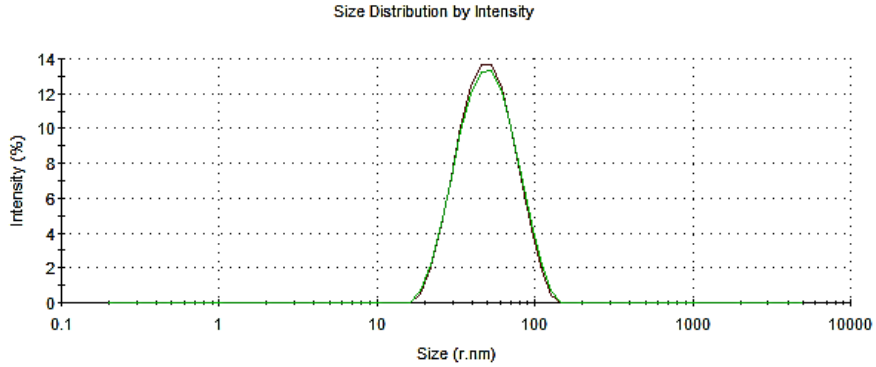

Figure S24. Observed particle size distribution for mixtures of DOPC/**Cu3**-vesicles (0.1 mol%) and DOPC/**$Zn_2$1**-vesicles (0.1mol%) before (red) and after (green) treatment with **P2** showing no apparent crosslinking and increase in vesicle size.

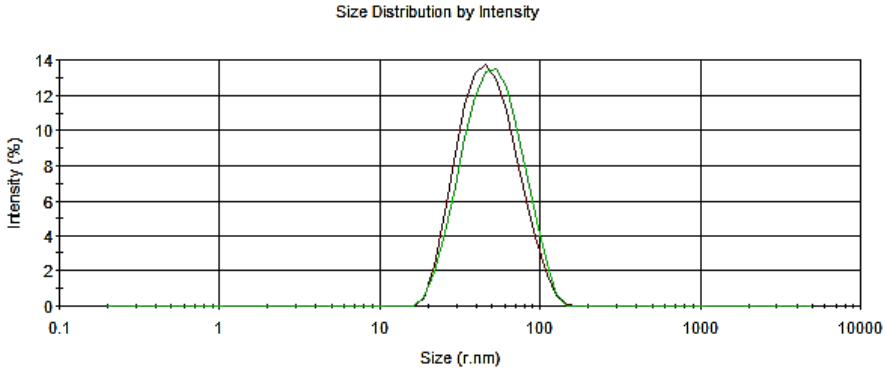

Figure S25. Observed particle size distribution for DOPC vesicles functionalized with **Cu3** and **$Zn_2$1** (0.1 mol% each) before (red) and after (after) treatment with **P2** showing no apparent crosslinking and increase in vesicle size.

Notes and References

1. B. Alberts, A. Johnson and J. Lewis, *Molecular Biology of the Cell. 4th edition*, Garland Science, New York, 2002.

2. M. Luckey, *Membrane Structural Biology*, Cambridge Univ. Press, 2008.

3. S. Singer, *Science*, 1992, **255**, 1671-1677.

4. A. Grakoui, S. K. Bromley, C. Sumen, M. M. Davis, A. S. Shaw, P. M. Allen and M. L. Dustin, *Science*, 1999, **285**, 221-227.

5. M. Renner, C. G. Specht and A. Triller, *Curr. Opin. Neurobiol.*, 2008, **18**, 532-540.

6. P. Tolar, J. Hanna, P. D. Krueger and S. K. Pierce, *Immunity*, 2009, **30**, 44-55.

7. S. Tomas and L. Milanesi, *Nat. Chem.*, 2010, **2**, 1077-1083.

8. X. Wang, R. J. Mart and S. J. Webb, *Org. Biomol. Chem.*, 2007, **5**, 2498-2505.

9. T. Schrader, M. Maue and M. Ellermann, *J. Recept. Signal Transduct. Res.*, 2006, **26**, 473-485.

10. K. Bernitzki and T. Schrader, *Angew. Chem. Int. Ed.*, 2009, **48**, 8001-8005.

11. A. I. Elegbede, M. K. Haldar, S. Manokaran, J. Kooren, B. C. Roy, S. Mallik and D. K. Srivastava, *Chem. Commun.*, 2007, 3377–3379.

12. A. Perl, A. Gomez-Casado, D. Thompson, H. H. Dam, P. Jonkheijm, D. N. Reinhoudt and J. Huskens, *Nat. Chem.*, 2011, **3**, 317-322.

13. P. Scrimin and P. Tecilla, *Curr. Opin. Chem. Biol.*, 1999, **3**, 730-735.

14. P. Tecilla, F. Mancin, P. Scrimin and U. Tonellato, *Coord. Chem. Rev.*, 2009, **253**, 2150-2165.

15. J. Voskuhl and B. J. Ravoo, *Chem. Soc. Rev.*, 2009, **38**.

16. B. Gruber, E. Kataev, J. Aschenbrenner, S. Stadlbauer and B. König, *J. Am. Chem. Soc.*, 2011, **133**, 20704-20707.

17. D. A. Jose, S. Stadlbauer and B. König, *Chem. Eur. J.*, 2009, **15**, 7404-7412.

18. E. Mahon, T. Aastrup and M. Barboiu, *Chem. Commun.*, 2010, **46**, 2441-2443.

19. L. Chen, S. Xu and J. Li, *Chem. Soc. Rev.*, 2011, **40**, 2922-2942.

20. M. Komiyama, T. Takeuchi, T. Mukawa and H. Asanuma, *Molecular Imprinting*, Wiley-VCH, 2004.

21. J. T. Groves, *Angew. Chem.*, 2005, **117**, 3590-3605.

22. S. Shinkai and M. Takeuchi, *Biosens. Bioelectron.*, 2004, **20**, 1250-1259.

23. N. W. Turner, B. E. Wright, V. Hlady and D. W. Britt, *J. Colloid Interface Sci.*, 2007, **308**, 71-80.

24. B. Gruber, S. Stadlbauer, A. Späth, S. Weiss, M. Kalinina and B. König, *Angew. Chem. Int. Ed.*, 2010, **49**, 7125-7128.

25. B. Gruber, S. Stadlbauer, K. Woinaroschy and B. König, *Org. Biomol. Chem.*, 2010, **8**, 3704-3714.

26. A. Grauer, A. Riechers, S. Ritter and B. König, *Chem. Eur. J.*, 2008, **14**, 8922-8927.

27. For phase transition temperatures and other physical properties of lipids see also LIPIDAT database (http://www.lipidat.tcd.ie/homeLIPIDAT.asp).

28. S.-i. Tamaru and I. Hamachi, ed. R. Vilar, Springer Berlin / Heidelberg, 2008, vol. 129, pp. 95-125.

29. The Zn-DPA complex will coordinate to the serine phosphate moiety, while complex Cu**4** coordinates the imidazoel moiety of histidine.

30. L. M. Loura and M. J. Prieto, *Frontiers in Physiology*, 2011, **2**.

31. Integrated DNA Technologies - Technical Bulletins, Fluorescence Resonance Energy Transfer, 2000, www.idtdna.com.

32. In the absence of the target analyte peptide no FRET-emission is detected, as the average distance of the two chromophores in the fluid membrane is too large (Figure S20).

33. As indicated by these measurements vesicle preparation and purification results in up to 25% loss of embedded amphiphiles. All apparent binding constants reported in here however were not corrected regarding this decreased receptor concentration. As a result all log K-values are considered "minimum" affinities.

34. S. Hünig, G. Märkl and J. Sauer, *Einführung in die apparativen Methoden in der Organischen Chemie, 2nd Edition*, Würzburg / Regensburg, 1994.

35. A. Ojida, K. Honda, D. Shinmi, S. Kiyonaka, Y. Mori and I. Hamachi, *J. Am. Chem. Soc.*, 2006, **128**, 10452-10459.

36. M. E. Jung and T. I. Lazarova, *The Journal of Organic Chemistry*, 1997, **62**, 1553-1555.

37. R. C. MacDonald, R. I. MacDonald, B. P. M. Menco, K. Takeshita, N. K. Subbarao and L.-r. Hu, *Biochim. Biophys. Acta*, 1991, **1061**, 297-303.

38. A. J. Jin, D. Huster, K. Gawrisch and R. Nossal, *Eur. Biophys. J.*, 1999, **28**, 187-199.

39. J. F. Nagle and S. Tristram-Nagle, *Biochim. Biophys. Acta*, 2000, **1469**, 159-195.

40. P. Balgavy, M. Dubnickova, N. Kucerka, M. A. Kiselev, S. P. Yaradaikin and D. Uhrikova, *Biochim. Biophys. Acta*, 2001, **1512**, 40-52.

41. D. W. Fry, J. C. White and I. D. Goldman, *Anal. Biochem.*, 1978, **90**, 809-815.

CHAPTER 2

THERMALLY INDUCED MOLECULAR IMPRINTING OF LUMINESCENT VESICLES

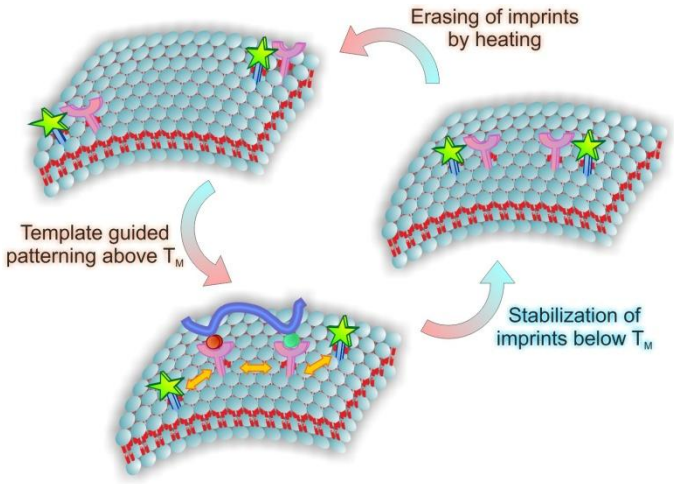

Thermal imprinting of the lipid-water interface of phospholipid vesicles is achieved by reversible non-covalent assembly of membrane embedded amphiphilic metal complexes. The complexes have affinity to phosphate and imidazole groups and are preorganized by a phosphorylated hexapeptide template above the phase transition temperature. The template induced patterning is transferred into the gel phase of the membrane by cooling below the transition temperature. This limits the lateral diffusion and stabilizes the metal complex receptor organization, as confirmed by FRET measurements with dye-labeled receptors. After template removal an enhanced rebinding affinity of one order of magnitude for the target peptide was observed for the imprinted membranes compared to identical non-imprinted interfaces.

This Chapter has been published:

S. Balk and B. König, *J. Incl. Phenom. Macrocycl. Chem.,* **2014**, DOI 10.1007/s10847-014-0442-2.

Author contributions:

SB synthesized vesicles, performed measurements and wrote the manuscript; BK supervised the project and is corresponding author.

Introduction

Template guided assembly and molecular imprinting are established strategies to improve ligand binding by creating specific receptors.[1-4] A multivalent target analyte binds reversible-covalently[2] or non-covalently[4] to molecules of complementary shape, charge and functional groups. Copolymerization of the assembly fixes the individual binding sites in the right spatial distance creating a specific receptor site that may provide a selective analyte rebinding after template removal. Such imprints have been applied in analyte sensing,[5-9] catalysis[10-12] or enzyme inhibition[13-16] and molecular imprinted polymers are already commercial products. However, the cross-linked bulk materials posses only a limited rebinding capacity, poor binding site accessibility and have long diffusion ways.[1] Surface imprinting can overcome these drawbacks and artificial binding sites have been attached to the surface of carbon nanotubes,[17, 18] silica beads,[19, 20] polymer microspheres,[21] magnetic nanoparticles[22] or nanogels.[23, 24] Another challenge is the use of molecular imprints in water for which e.g. hydrophilic surface functionalization[25, 26] and molecular imprinting of vesicles[27] have been developed.

The common strategy in imprinting is the irreversible covalent fixation of binding moieties by radical polymerization and crosslinking. Hence the optimized spatial arrangement of functional groups in the non-covalent assembly is altered during the covalent bond formation, which implies a loss of binding specificity that cannot be avoided. An alternative approach for crosslinking is changing the mobility of membrane embedded binding sites. Bayerl *et al*. demonstrated the molecular imprinting of a silica bead supported liposomal bilayer by thermal phase transition:[28] Cationic lipids in a phospholipid membrane were molded by non-specific attractive interactions using protein templates. Other examples have used temperature responsive conformation,[29] thermo-reversible swelling of hydrogels[30-32] or bond reorganization, so called “post imprinting”,[33, 34] altering the selectivity of an already molecular imprinted polymer. We report here the thermal non-covalent imprinting of amphiphilic metal complex receptors in the dynamic lipid-water interface of phospholipid vesicles.[35-37] Analyte binding to the phase segregated receptors[38, 39] induces their rearrangement and specific positioning in the fluid membrane.[40, 41] This analyte-induced arrangement is then non-covalently cross-linked by cooling the vesicles below their phase transition temperature from liquid-crystalline to gel phase suppressing lateral diffusion.[42-44]

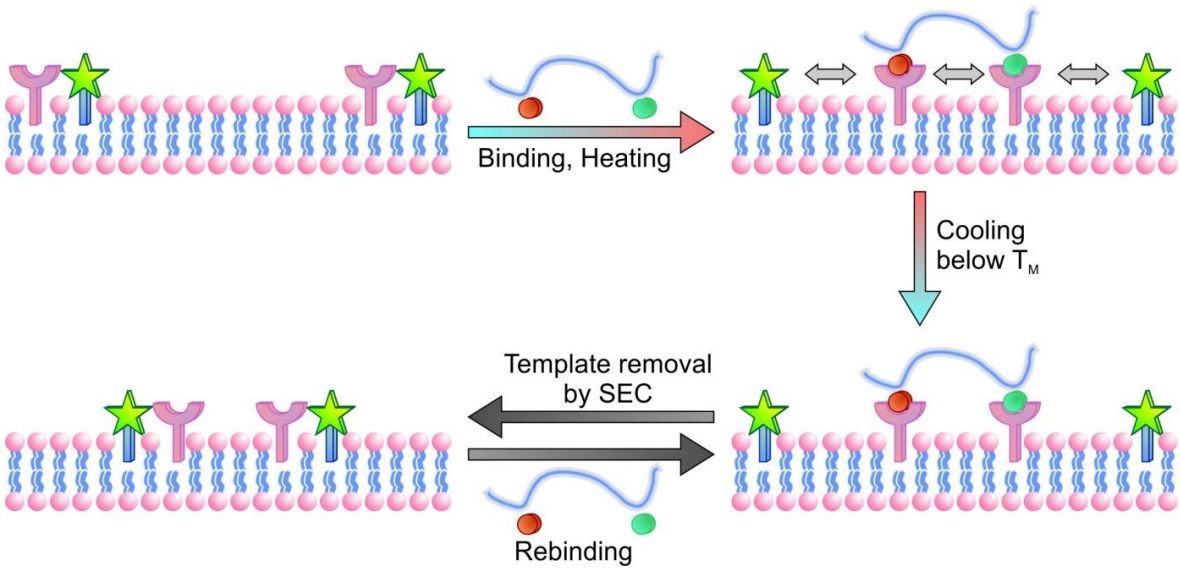

Scheme 1. Principle of thermal surface imprinting and analyte induced luminescent response (SEC: size exclusion chromatography).

Results and Discussion

We first monitored by fluorescence resonance energy transfer (FRET) the rearrangement of dye-labeled metal-complexes **Zn_2FAM** and **CuTMR** (Scheme 2) in a fluid membrane upon binding to a divalent peptide **P1** bearing phosphorylated serine and histidin moiety as ligands.[40] In order to show that the peptide-induced receptor assembly on the vesicle surface is transferred from the liquid-crystalline into gel phase, we prepared DPPC vesicles **V1** (T_M = 41 °C), functionalized with 0.75 mol% of **Zn_2FAM** and **CuTMR** in HEPES buffer (25 mM, pH = 7.4). **FAM-** and **TMR-**labels are established FRET pairs with a Förster-radius of 5.5 nm. The FRET emission of **V1**, with typical intensity maxima at 520 nm and 580 nm, was monitored in the presence and the absence of **P1** after donor-dye excitation at 494 nm.[i] No receptor rearrangement was detected upon analyte addition below the T_M at 10 °C, as the mobility of the embedded receptors is limited. A significant change of the FRET ratio was detected using the same solutions at 50 °C (Figure 1 gives the ΔFRET ratios). In the now fluid membrane the analyte-induced recruiting of the labeled receptors leads to a closer proximity and an increase of the FRET intensity. The receptor orientation is maintained when going back to the gel phase by fast cooling of **V1** from 50 °C to 10 °C as indicated by an unchanged FRET ratio (see SI for detailed

procedure). The FRET experiments show that template guided orientation of two receptors is stronger than the potential phase separation in vesicular DPPC membranes, which reorganize from liquid crystalline to gel phase.[ii]

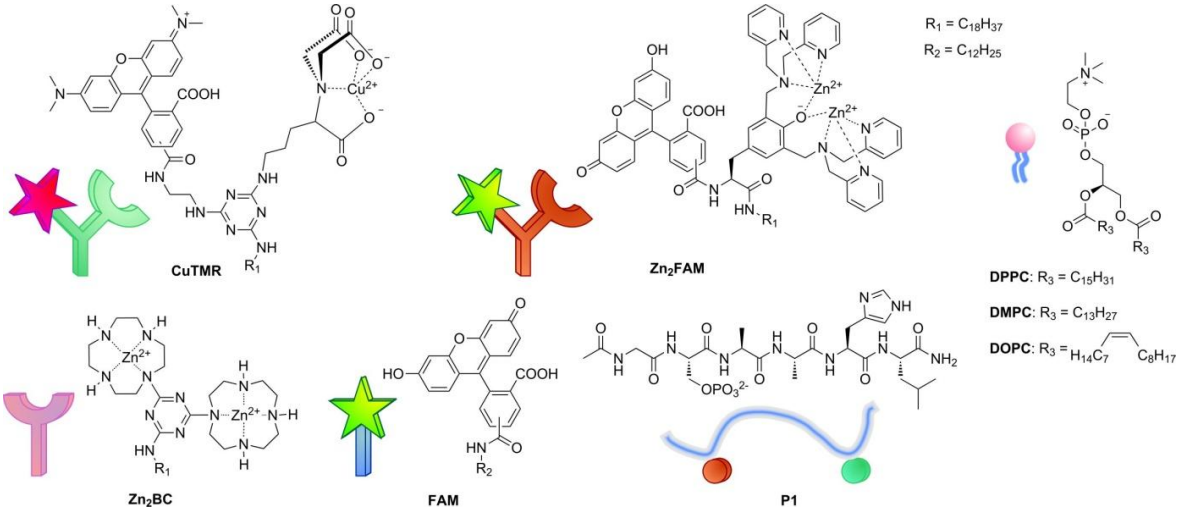

Scheme 2. Structures of functional amphiphiles and model peptide (counter ions omitted for clarity).

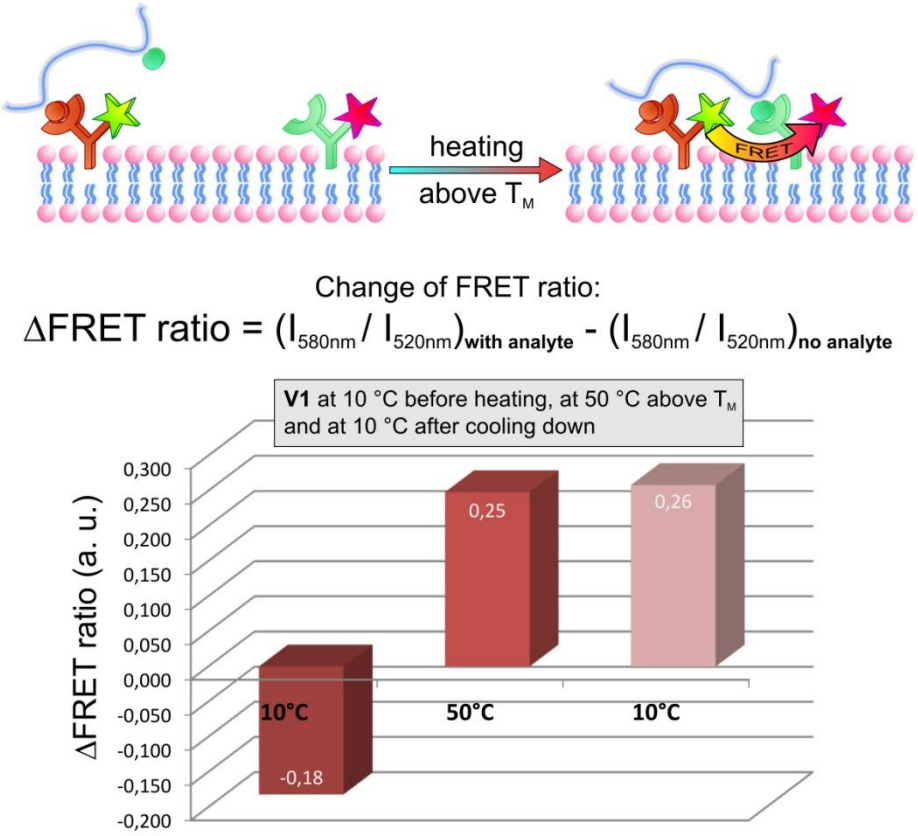

Figure 1. The peptide-induced arrangement of receptors in the bilayer above T_M can be transferred to the gel phase by cooling. The change of the FRET ratio (ΔFRET ratio) indicates different average distances between the receptors in the presence and the absence of **P1** after the heating/cooling cycle.

However, the use of FRET labeled receptors does not allow determining analyte binding constants, as the absolute fluorescence intensity and the energy transfer between the dyes changes in the binding process. Therefore, we co-embedded an amphiphilic reporter dye **FAM** (1 mol%) with **Zn_2BC** receptors (1 mol%) (molecules shown in scheme 2)[35] in 100 nm DMPC vesicles **V2** (T_M = 24 °C) in HEPES buffer (25 mM, pH = 7.4) (see SI for vesicle preparation). Differential scanning calorimetry (DSC) confirms no alteration of the phase transition temperature by the vesicle functionalization (see SI).[iii]

The binding of external added **P1** to vesicular attached **Zn_2BC** is monitored by a changing fluorescence intensity of the coembedded **FAM,** which is caused by an altered phase separation driven assembly of the dye and the receptor after analyte binding.[35] The changes in the local molecular environment of the dye molecule affect its emission properties. This receptor-dye co-embedding technique was recently used to monitor

analyte binding in covalently imprinted vesicles.[27] The buffered aqueous solution containing **V2** was warmed to 35 °C before template addition (for a detailed imprinting procedure, see SI). Stoichiometric template binding ([**Zn_2BC**] / [**P1**] 2:1) arranges the metal complex receptors in the liquid crystalline phase. Quick cooling of the solution below the phase transition temperature of **V2** imprints this arrangement into the bilayer by reducing the mobility of the embedded receptors. The template **P1** was removed by size exclusion chromatography (see SI) below T_M at 10°C and the rebinding of peptide **P1** to the thermally imprinted vesicle **V2** investigated. The fluorescence intensity change of **FAM** upon addition of **P1** was monitored at 520 nm (excitation at 485 nm) for the imprinted vesicles and compared to identically treated non-imprinted samples. The apparent binding constants were determined by non-linear fitting of the experimental data using the Hill equation (Figure 2).

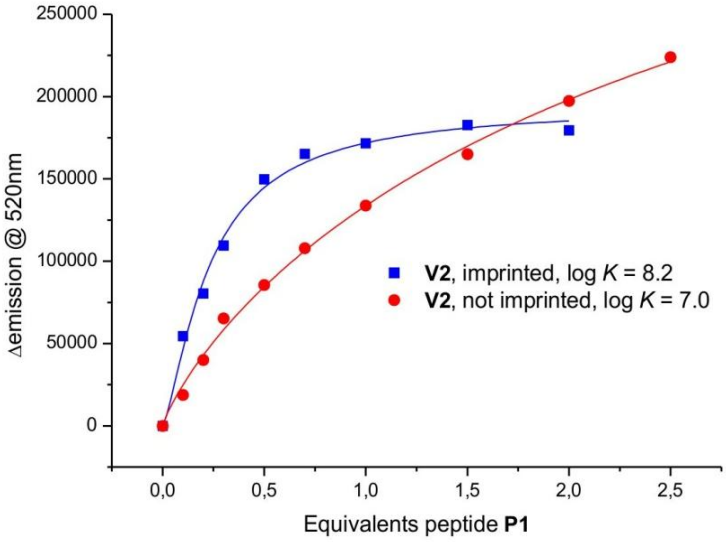

Figure 2. Changes in emission intensity (excitation at 485 nm, detection at 520 nm) of solutions of imprinted (blue) and non-imprinted (red) vesicles **V2** (DMPC 1 x 10^{-5} mol/L, **Zn_2BC** 1 x 10^{-7} mol/L and **FAM** 1 x 10^{-7} mol/L) upon titration with peptide **P1**.

The addition of one equivalent **P1** to the imprinted **V2** leads to a significant change in emission intensity reaching saturation. A binding affinity enhancement of one order of magnitude was observed for the rebinding of **P1** to imprinted vesicle with a log *K* = 8.2 (Figure 2). The positive cooperativity (n = 1.4) for imprinted vesicles and Job's plot analysis indicate a binding of preorganized **Zn_2BC** to **P1** with a ratio of 2:1 (see SI). In comparison, a binding affinity of log *K* = 7.0 was determined for non-imprinted vesicles.

We assume a reversible monovalent binding of **P1** to non-imprinted vesicles resulting in a peptide to receptor stoichiometry of 1:1. The Hill equation fit shows a slightly negative cooperativity (n = 0.8) (see SI). We expect that the low lateral diffusion in the membrane gel phase prevents a divalent binding.

A rebinding affinity enhancement of **P1** to thermally imprinted membranes is detected, compared to identical vesicles lacking a preorganizing template during the thermal cycle.[iv] The thermal imprinting of the surface is lost by heating: Imprinted vesicles were heated after template removal above their T_M, and the rebinding titrations after cooling resulted in a value of log *K* = 7.4 (see SI), which is comparable to the non-imprinted vesicles.

Previous studies showed an affinity enhancement of three orders of magnitude for covalently surface imprinted vesicles by photopolymerization with a value of log *K* = 7.4 in comparison to a log *K* = 4.6 for non-imprinted vesicles.[27] The much lower affinity enhancement for non-covalent surface imprinted vesicles may be explained by dynamic phase segregation,[38, 39] which competes with the imprinted assembling.

Conclusion

In conclusion, we have demonstrated the alteration of the binding behavior of functionalized vesicles to a peptide by preorganizing membrane embedded receptors in the fluid phase and transferring this arrangement to the gel phase by lowering the temperature. A hexapeptide, which is able to bind simultaneously to two metal complex receptors, was used to assemble the binding sites in the liquid-crystalline phase of DMPC and DPPC membranes. This template induced patterning was stabilized by phase transition to the gel phase of the liposomal membrane, as shown by FRET measurements. Specific rebinding of the target peptide to thermally imprinted vesicular receptors provides an enhancement of affinity of one order of magnitude after template removal.

Although the increase in binding affinity by the thermal imprint procedure is too small to be useful for a selective analyte detection, the immobilization of the membranes and applications e.g. in affinity chromatography[28] or other chromatographic separations may be envisaged.

Experimental Part and Supporting Information

General methods and material

Fluorescence measurements were performed in aqueous HEPES buffer (Sigma-Aldrich, sodium salt 99%, 25 mM, pH 7.4), using 0.2 cm or 0.4 cm quartz cuvettes (Hellma). Emission spectra were recorded on a Horiba "Fluoromax4" fluorescence spectrophotometer with temperature control for required temperatures (2 min equilibration time). DLS measurements were performed on a Malvern Zetasizer Nano at 20 °C using 1 cm disposable polystyrene cuvettes (VWR). DSC measurements were recorded with a Perkin Elmer DSC 8000. Starting materials were used without any further purification. Phospholipids were purchased from Avanti Polar Lipids Inc. Commercially available solvents of UV-grade quality (Merck) and water of millipor quality were used. Sephadex G25 "Coarse" from Sigma-Aldrich was used for size exclusion chromatography.

Receptors and Analyte

Zn_2FAM,[40] **CuTMR**,[40] **Zn_2BC**[35] and **FAM**[35] were synthesized by following synthetic procedures previously reported by us. Model Peptide **P1** was purchased from GL Biochem (Shanghai) Ltd. (purity > 95%).

Vesicles

Preparation

In small glass reaction vials the required volumes of solutions of DMPC or DPPC (20 mM in $CHCl_3$), **Zn_2FAM** (0.2 mM in MeOH), **CuTMR** (0.2 mM in $CHCl_3$), **Zn_2BC** (1 mM in MeOH) and **FAM** (1 mM in $CHCl_3$) were mixed. The solvent was completely removed under reduced pressure at 25 °C and an appropriate amount of buffer (HEPES 25 mM, pH 7.4) was added to obtain lipid concentrations of 1 mM. Vigorous shaking (900 min^{-1}) at 35 °C (DMPC) or 50 °C (DPPC) for 10 min yielded a turbid multi-lamellar vesicle suspension. Small uni-lamellar dispersions were obtained by extrusion through 100 nm-pore size polycarbonate membranes with a LiposoFast liposome extruder from Avestin.

Metal complex concentration

For all vesicles the receptor concentration refers to the outer surface exposed binding sites, as only these should be reactive, with the assumption that embedded compounds distribute equally in both layers of the vesicle membrane and the bilayer thickness for the prepared vesicles amounts to 5 nm.[45-48] This corresponds to a surface correction factor of 0.54 (only 54% of membrane embedded molecules is at the outer surface) to give surface accessible concentrations of **Zn_2FAM** (4×10^{-7} mol/L) and **CuTMR** (4×10^{-7} mol/L) in **V1** or **Zn_2BC** (5.4×10^{-8} mol/L) and **FAM** (5.4×10^{-8} mol/L) in **V2**. Assuming that one bivalent analyte (**P1**) is binding to two receptor molecules (**Zn_2BC**), one equivalent of **P1** is 2.7×10^{-8} mol/L in relation to **V2**.

Dynamic light scattering (DLS)

Vesicle size distributions were determined using dynamic light scattering (DLS). Vesicle **V2** (DMPC 1×10^{-5} mol/L, **Zn_2BC** 1×10^{-7} mol/L and **FAM** 1×10^{-7} mol/L) was incubated after addition of **P1** (2.7×10^{-8} mol/L) at 35 °C and cooled down to 10 °C before SEC. No significant change in size distribution was determined after imprinting compared with the typical size distribution of an extruded vesicle sample (Figure S1). Average size distribution of about 110 nm and monodispersity (polydispersity index = 0.16) were achieved.

		Size (d.nm):	% Intensity:	St Dev (d.nm):
Z-Average (d.nm): 114,1	Peak 1:	133,3	100,0	55,12
PdI: 0,161	Peak 2:	0,000	0,0	0,000
Intercept: 0,937	Peak 3:	0,000	0,0	0,000
Result quality : Good				

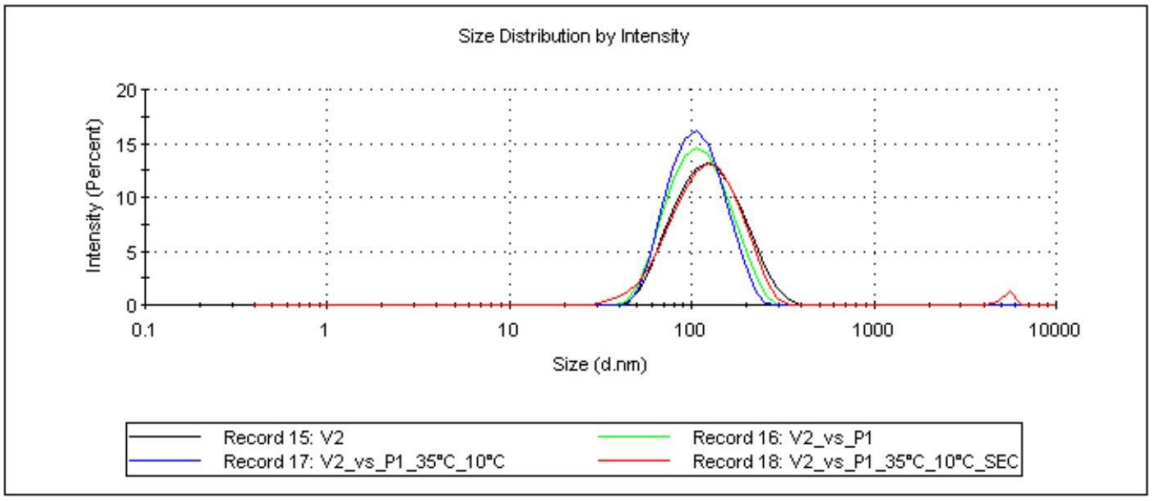

Figure S1. Size distribution of imprinted vesicles **V2** (red) is comparable with initial vesicle solutions (black). Analyte binding to **V2** (green) and temperature alteration changes size distribution only marginal. Average size of monodispers imprinted vesicles is about 110 nm (polydispersity index = 0.16).

FRET measurements

Receptor organization in the liquid-crystalline phase of DOPC membranes, which is induced by an external bivalent analyte and monitored by a significant change of the FRET emission, was previously established by us.[40] Based on these investigations it was shown that a template guided receptor orientation can be transferred from the liquid crystalline phase into the gel phase of a vesicular membrane by lowering the temperature below the phase transition temperature. This receptor assembly is stronger than phase separation in the gel phase of vesicles. Fluorescence intensity and therefore FRET emission is, next to the spatial distance of dyes, also dependent on the temperature. Hence it is not possible to compare FRET signals monitored at different temperatures. Therefore we detect FRET ratio (I_{580nm} / I_{520nm}) before and after analyte addition at different temperatures. The change of FRET ratio (ΔFRET ratio) is the difference between the FRET ratio in the presence of a binding partner and the FRET ratio without analyte. This

value is used to estimate the degree of analyte guided receptor arrangement below and above T_M.

A 1 x 0.2 cm^2 quartz cuvette was filled with 50 µL of a vesicles solution **V1** (T_M = 41 °C, DPPC 1.33 x 10^{-4} mol/L, **Zn_2FAM** 1 x 10^{-6} mol/L and **CuTMR** 1 x 10^{-6} mol/L in HEPES 25 mM, pH 7.4) and cooled to 10 °C with temperature control of the Horiba "Fluoromax4". Afterwards either 50 µL analyte **P1** (2 x 10^{-3} mol/L in water) or 50 µL water (as reference), both incubated at 10 °C, were added. Previous investigations showed that hexapeptides with only one or no binding moiety do not cause bivalent receptor rearrangement of **Zn_2FAM** and **CuTMR** in DOPC vesicles.[40] The **FAM**-label of **V1** was excited at 485 nm and FRET emission, with typical maxima at 520 nm and 580 nm, was monitored at 10 °C (Figure S2, Top). No receptor recruitment of **P1** was detected below T_M and FRET signaling of the analyte equipped sample is even weaker.[v]

The same vesicle solutions were heated up to 50 °C (in spectrometer with temperature control for 2 min). Analyte triggered receptor rearrangement is detected by a significant increase of the ΔFRET ratio observed for **V1** in the presence of suitable analytes, which is in accordance to previous investigations.[40] Subsequently the cuvettes were cooled for 1 min in an ice bath, before they were incubated for 2 min at 10 °C in the spectrometer. The orientation of FRET labeled receptors was transferred to the gel phase membrane of **V1**, as indicated by unchanged ΔFRET ratio values (Figure S2, Bottom). Cooling the vesicles from the liquid crystalline to the gel phase did not lead to a phase separation of the template arranged receptors in the membrane for at least 10 min.

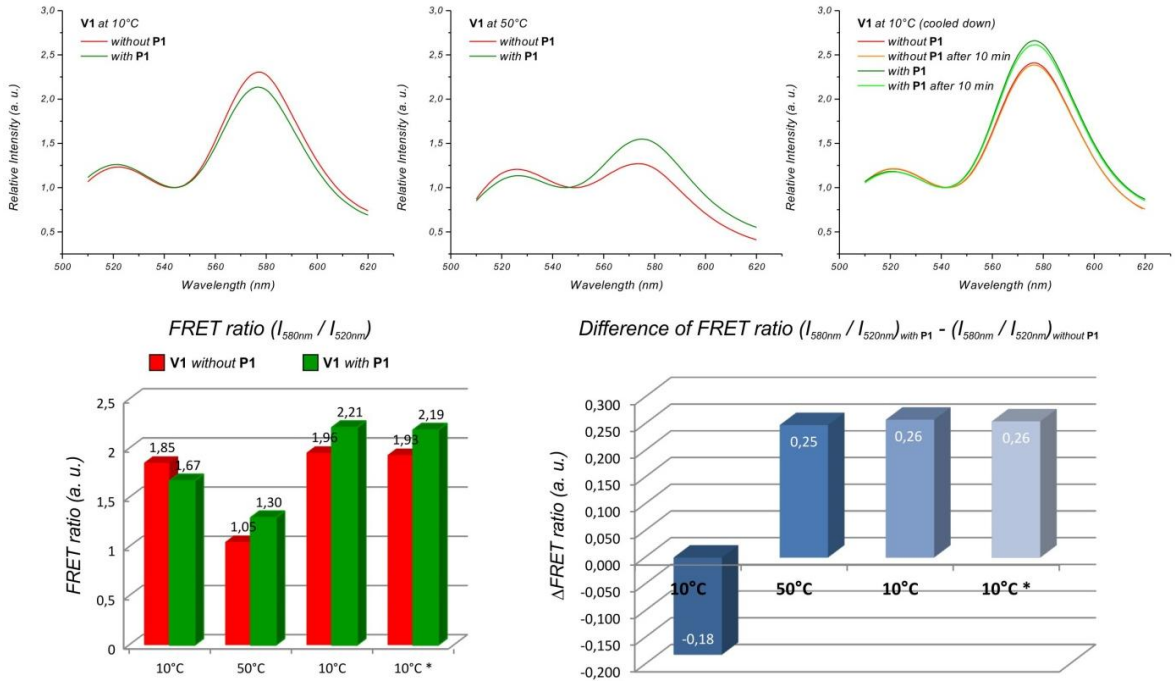

Figure S2. Top: FRET emission of **V1** in the presence and the absence of **P1** at 10 °C (left), 50 °C (middle) and 10 °C (right) after cooling. Bottom: The FRET ratio (left) was calculated from the emission spectra (see above). ΔFRET ratio (right) compares the spatial assembly of receptors in the presence and the absence of **P1** (*results recorded after 10 min).

Molecular imprinting procedure

A procedure for molecular imprinting on vesicular surfaces by photo crosslinking was recently published by us.[27] This technique was modified to investigate the imprinting by non-covalent thermal changes. DMPC vesicles (T_M = 24 °C) were functionalized with the amphiphilic receptor **Zn_2BC**, which binds to imidazole and phosphate moieties of **P1** and an amphiphilic fluorescent dye (**FAM**) monitoring the binding. Vesicle solutions **V2** (DMPC 1 x 10^{-5} mol/L, **Zn_2BC** 1 x 10^{-7} mol/L and **FAM** 1 x 10^{-7} mol/L) were filled in 1 x 0.4 cm^2 quartz cuvettes (1 mL) and incubated for 10 min at 35 °C, in order to prepare imprinted vesicles, or kept at 10 °C as reference sample. The template peptide **P1** (2.7 x 10^{-8} mol/L) was added to both solution and the temperature was maintained for additional 10 min. Both solutions were cooled in an ice bath for 1 min, followed by incubation at 10 °C for further 10 min. The vesicle solutions were passed through a SEC column at 10 °C to remove the template peptide **P1** below T_M. The obtained vesicle solutions were kept at 10 °C for 15 min before binding affinity was determined by titration.

Size exclusion chromatography (SEC)

Template peptides **P1** (2.7 x 10^{-8} mol/L) were removed from the vesicle solutions below T_M by size exclusion chromatography (SEC) using small spin columns.[49] Sephadex G-25 SEC medium was swollen in HEPES buffer (25 mM, pH 7.4) for 24 h prior to use. The sephadex solution (2.5 mL per mL vesicle solution) was transferred into a small plastic syringe with filter and the solvent was removed by centrifugation in an Eppendorf bench top centrifuge with temperature control (15 s @ 4400 rpm, 5 °C). Vesicles solutions were added onto the column and filtered by centrifugation (15 s @ 4400 rpm, 5 °C).

Differential scanning calorimetry (DSC)

DSC measurements confirmed that the phase transition temperature of **V2** was not changed by embedding 1 mol% of receptor and dye (each) in the DMPC membrane. T_M of DMPC vesicles is 24 °C.[42, 43] A sealed aluminum pan was filled with 11.2 mg **V2** (DMPC 1 x 10^{-3} mol/L, **Zn_2BC** 1 x 10^{-5} mol/L and **FAM** 1 x 10^{-5} mol/L) and DSC was measured in a Perkin Elmer DSC 8000 from 15 °C to 35 °C with a heat rate of 1 K min^{-1} under N_2-atmosphere in three reversible cycles (Figure S3). A phase transition temperature of 24 °C was found for functionalized vesicle **V2**. The value is identical to the T_M of DMPC vesicles.

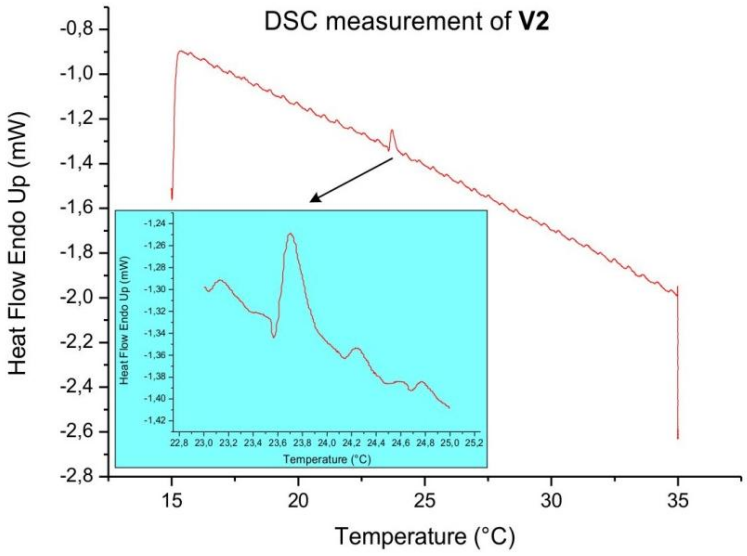

Figure S3. DSC measurement records a phase transition temperature of **V2** at 24 °C.

Rebinding studies

Vesicle solutions **V2** (DMPC 1 x 10^{-5} mol/L, **Zn_2BC** 1 x 10^{-7} mol/L and **FAM** 1 x 10^{-7} mol/L) obtained from the thermal imprinting procedure and removal of the template by SEC were titrated with **P1** under temperature control (10 °C). The change of fluorescence emission (excitation of **FAM** at 485 nm, emission maximum at 520 nm) was determined (Figure S4, Figure S5) and binding constants were calculated by non-linear fitting of the experimental data using the Hill equation (Figure 2, Results & Discussion). All measurements were repeated three times and the estimated error in determining the binding constant values is ± 0.2. Previous investigations proved that hexapeptides with only one or no binding moiety do not show bivalent binding to imprinted **Zn_2BC**, coembedded to **FAM**, in photocrosslinked DOPC vesicles.[27]

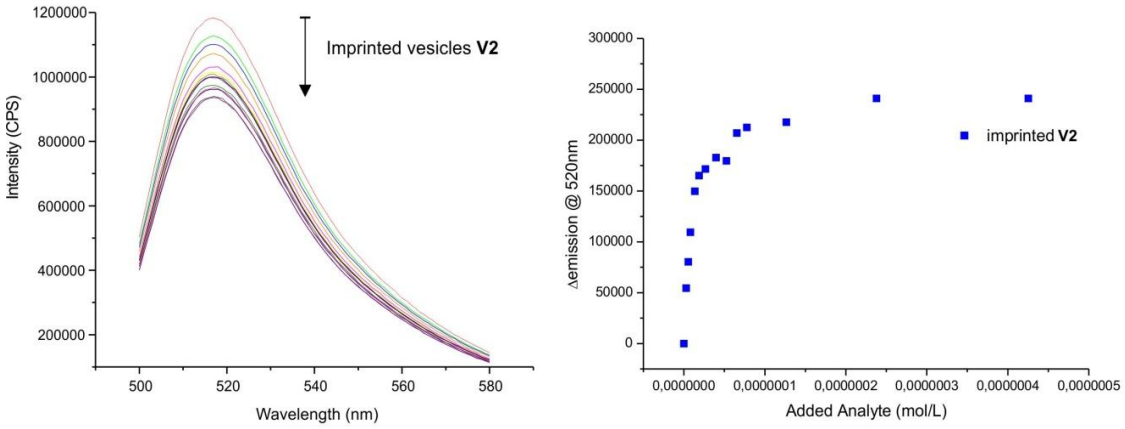

Figure S4. **FAM** emission (λ_{ex} = 485 nm, λ_{em} = 520 nm) upon **P1** addition to imprinted **V2**.

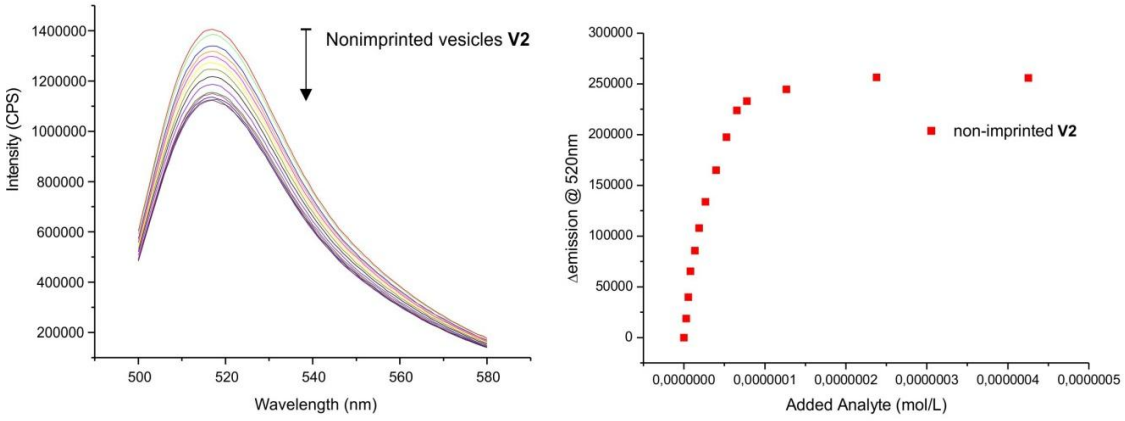

Figure S5. **FAM** emission (λ_{ex} = 485 nm, λ_{em} = 520 nm) upon **P1** addition to non-imprinted **V2**.

The observed binding of imprinted vesicles **V2** to **P1** is different in comparison to the non-imprinted vesicles of identical composition. A positive cooperativity (n = 1.4) is observed for imprinted **V2** in the Hill equation fitting of the spectroscopic data, whereas non-imprinted vesicles lead to a negative cooperativity (n = 0.8). The emission intensity change up to one equivalent of added **P1** is more pronounced for the imprinted vesicle indicating the preorganization (Figure S4). Upon addition of more than one equivalent of **P1** the difference in binding stoichiometry becomes visible. While **P1** binds to imprinted vesicles up to one equivalent in a 1:1 fashion, and only if an excess of **P1** is added a second saturation now with 2:1 stoichiometry is reached (Figure S6, left). Non-imprinted vesicles show no change in binding stoichiometry during the titration (Figure S6, right). A similar effect for DOPC vesicles was recently observed.[40]

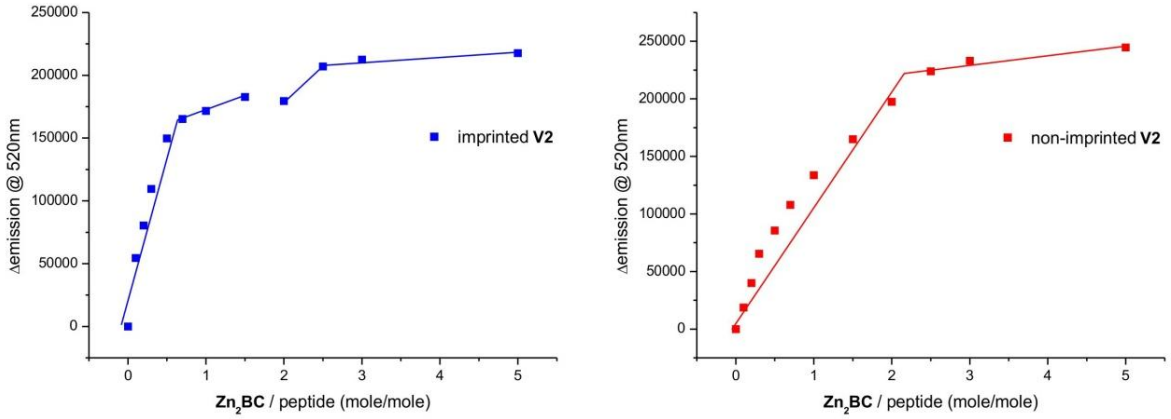

Figure S6. Job's Plot (limiting reagent method) of **P1** versus imprinted **V2** (left) and non-imprinted **V2** (right).

Erasing of imprinted surface patterns

Imprinted vesicle solutions **V2** (DMPC 1 x 10^{-5} mol/L, **Zn_2BC** 1 x 10^{-7} mol/L, **FAM** 1 x 10^{-7} mol/L) were heated above T_M (at 35°C) after template removal for 15 min, before they were used for rebinding studies with **P1** (Figure S7). Phase transition of imprinted vesicles will cause a deletion of template guided receptor patterning. Hence a loss of rebinding affinity is detected, leading to a log *K* = 7.4 (imprinted **V2**: log *K* = 8.2).

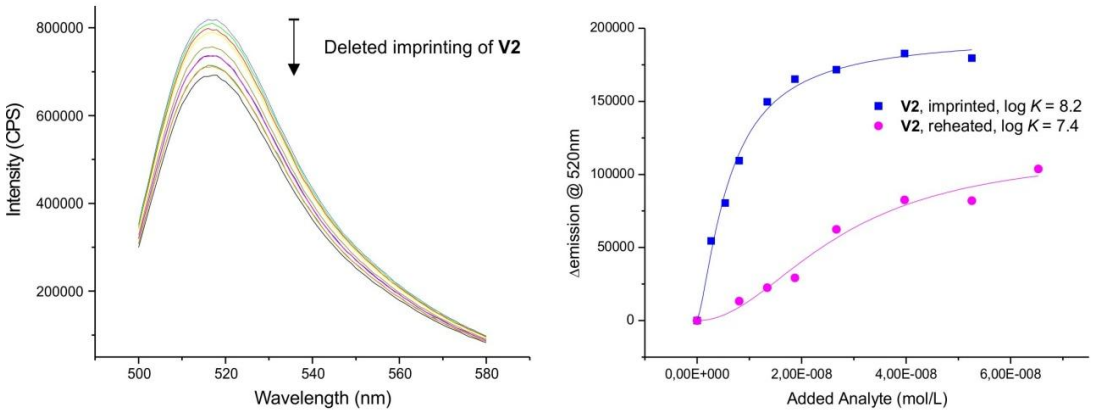

Figure S7. Hill equation fit of the binding data show a loss of the imprinting of **V2** after heating above T_M.

Imprinting of DPPC vesicles

Vesicle solutions **V3** (T_M = 41 °C, DPPC 1 x 10^{-5} mol/L, **Zn_2BC** 1 x 10^{-7} mol/L and **FAM** 1 x 10^{-7} mol/L) were prepared and incubated with peptide **P1** (2.7 x 10^{-8} mol/L) at either 65 °C (imprinted **V3**) or at 21 °C (non-imprinted **V3**) analogously to the above procedure. Solutions were cooled to 21 °C and the template **P1** removed by SEC.

Titration with **P1** in a rebinding study revealed by non-linear fitting a log *K* = 8.0 for imprinted **V3** and a log *K* = 7.3 for the non-imprinted sample. (Figure S8).

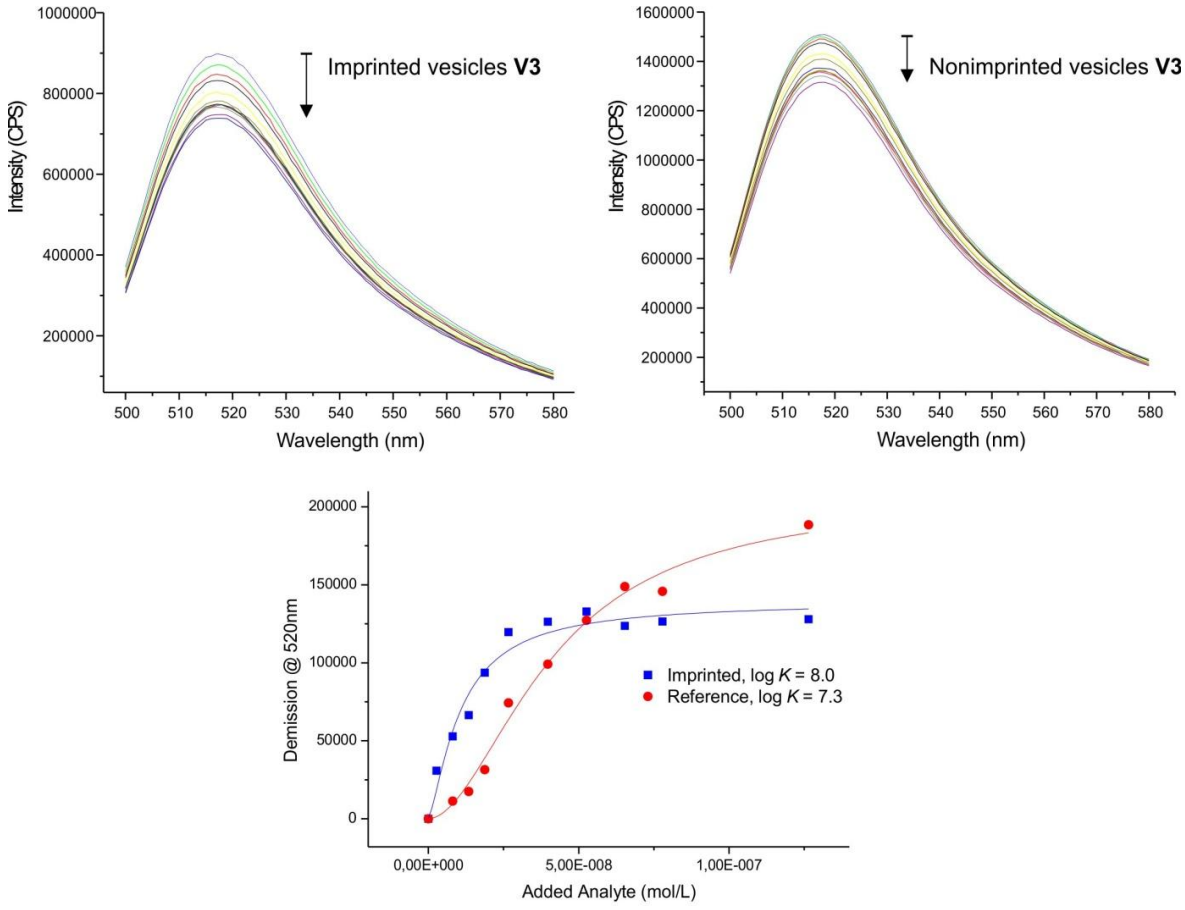

Figure S8. Top: **FAM** emission (λ_{ex} = 485 nm, λ_{em} = 520 nm) upon **P1** addition to imprinted DPPC vesicles **V3** (left) and non-imprinted **V3** (right). Bottom: Hill fit of binding curve for **V3.**

Notes and References

[i] Note: Fluorescence intensity and therefore FRET emission is temperature dependent. Hence it is not possible to compare FRET signals monitored at different temperatures. Therefore we determine the FRET ratio (I_{580nm} / I_{520nm}) before and after analyte addition at different temperatures. The change of FRET ratio (ΔFRET ratio) is the difference between FRET ratio in the presence of a binding partner and the FRET ratio without analyte. This value is used to estimate the degree of analyte guided receptor arrangement below and above T_M.

[ii] FRET emission intensities were not changing during 10 min after cooling **V1** to 10°C.

[iii] We previously reported the covalent molecular imprinting by photopolymerization using the same receptor – ligand pair (see ref. 27).

[iv] Rebinding of **P1** with a value of log *K* = 8.0 for imprinted and a value of log *K* = 7.3 for non-imprinted DPPC vesicles (T_M = 41°C) was determined analogously.

[v] This may be caused by a less strong clustering of analyte-bound receptors.

1. L. Chen, S. Xu and J. Li, *Chem. Soc. Rev.*, 2011, **40**, 2922-2942.

2. G. Wulff, *Angew. Chem. Int. Ed. Engl.*, 1995, **34**, 1812-1832.

3. K. Mosbach and O. Ramstrom, *Nat. Biotechnol.*, 1996, **14**, 163-170.

4. B. Sellergren, *TrAC, Trends Anal. Chem.*, 1997, **16**, 310-320.

5. K. Haupt and K. Mosbach, *Chem. Rev.*, 2000, **100**, 2495-2504.

6. G. Vlatakis, L. I. Andersson, R. Muller and K. Mosbach, *Nature*, 1993, **361**, 645-647.

7. M. Sibrian-Vazquez and D. A. Spivak, *J. Am. Chem. Soc.*, 2004, **126**, 7827-7833.

8. R.-N. Liang, D.-A. Song, R.-M. Zhang and W. Qin, *Angew. Chem. Int. Ed.*, 2010, **49**, 2556-2559.

9. P. Bures, Y. Huang, E. Oral and N. A. Peppas, *J. Controlled Release*, 2001, **72**, 25-33.

10. G. Wulff and J. Liu, *Acc. Chem. Res.*, 2011, **45**, 239-247.

11. G. Wulff, *Chem. Rev.*, 2002, **102**, 1-28.

12. S. Muratsugu and M. Tada, *Acc. Chem. Res.*, 2012, **46**, 300-311.

13. A. Cutivet, C. Schembri, J. Kovensky and K. Haupt, *J. Am. Chem. Soc.*, 2009, **131**, 14699-14702.

14. R. Manetsch, A. Krasiński, Z. Radić, J. Raushel, P. Taylor, K. B. Sharpless and H. C. Kolb, *J. Am. Chem. Soc.*, 2004, **126**, 12809-12818.

15. K. Mosbach, Y. Yu, J. Andersch and L. Ye, *J. Am. Chem. Soc.*, 2001, **123**, 12420-12421.

16. E. Meggers, *Angew. Chem. Int. Ed.*, 2011, **50**, 2442-2448.

17. D. Cai, L. Ren, H. Zhao, C. Xu, L. Zhang, Y. Yu, H. Wang, Y. Lan, M. F. Roberts, J. H. Chuang, M. J. Naughton, Z. Ren and T. C. Chiles, *Nat Nano*, 2010, **5**, 597-601.

18. C. Zheng, X.-L. Zhang, W. Liu, B. Liu, H.-H. Yang, Z.-A. Lin and G.-N. Chen, *Adv. Mater.*, 2013, **25**, 5922-5927.

19. C. D. Ki, C. Oh, S.-G. Oh and J. Y. Chang, *J. Am. Chem. Soc.*, 2002, **124**, 14838-14839.

20. J. Gauczinski, Z. Liu, X. Zhang and M. Schönhoff, *Langmuir*, 2012, **28**, 4267-4273.

21. H. Zhang, J. Jiang, H. Zhang, Y. Zhang and P. Sun, *ACS Macro Letters*, 2013, **2**, 566-570.

22. Y. Li, C. Dong, J. Chu, J. Qi and X. Li, *Nanoscale*, 2011, **3**, 280-287.

23. G. Wulff, B.-O. Chong and U. Kolb, *Angew. Chem. Int. Ed.*, 2006, **45**, 2955-2958.

24. M. Resmini, *Anal. Bioanal. Chem.*, 2012, **402**, 3021-3026.

25. G. Pan, Y. Zhang, Y. Ma, C. Li and H. Zhang, *Angew. Chem. Int. Ed.*, 2011, **50**, 11731-11734.

26. E. Benito-Peña, S. Martins, G. Orellana and M. C. Moreno-Bondi, *Anal. Bioanal. Chem.*, 2009, **393**, 235-245.

27. S. Banerjee and B. König, *J. Am. Chem. Soc.*, 2013, **135**, 2967-2970.

28. T. Bayerl, G. Decher and T. Braunschweig, US006051372A.

29. Y. Kondo, M. Yoshikawa and H. Okushita, *Polym. Bull.*, 2000, **44**, 517-524.

30. M. E. Byrne, K. Park and N. A. Peppas, *Adv. Drug Delivery Rev.*, 2002, **54**, 149-161.

31. G. Pan, Q. Guo, C. Cao, H. Yang and B. Li, *Soft Matter*, 2013, **9**, 3840-3850.

32. C. Alvarez-Lorenzo, O. Guney, T. Oya, Y. Sakai, M. Kobayashi, T. Enoki, Y. Takeoka, T. Ishibashi, K. Kuroda, K. Tanaka, G. Wang, A. Y. Grosberg, S. Masamune and T. Tanaka, *J. Chem. Phys.*, 2001, **114**, 2812-2816.

33. S. C. Zimmerman and N. G. Lemcoff, *Chem. Commun.*, 2004, 5-14.

34. H. Hiratani, C. Alvarez-Lorenzo, J. Chuang, O. Guney, A. Y. Grosberg and T. Tanaka, *Langmuir*, 2001, **17**, 4431-4436.

35. B. Gruber, S. Stadlbauer, A. Späth, S. Weiss, M. Kalinina and B. König, *Angew. Chem. Int. Ed.*, 2010, **49**, 7125-7128.

36. B. Gruber, S. Stadlbauer, K. Woinaroschy and B. König, *Org. Biomol. Chem.*, 2010, **8**, 3704-3714.

37. A. Grauer, A. Riechers, S. Ritter and B. König, *Chem. Eur. J.*, 2008, **14**, 8922-8927.

38. W. H. Binder, V. Barragan and F. M. Menger, *Angew. Chem. Int. Ed.*, 2003, **42**, 5802-5827.

39. A. Grochmal, E. Ferrero, L. Milanesi and S. Tomas, *J. Am. Chem. Soc.*, 2013, **135**, 10172-10177.

40. B. Gruber, S. Balk, S. Stadlbauer and B. König, *Angew. Chem. Int. Ed.*, 2012, **51**, 10060-10063.

41. B. Gruber and B. König, *Chem. Eur. J.*, 2013, **19**, 438-448.

42. L. K. Tamm and H. M. McConnell, *Biophys. J.*, 1985, **47**, 105-113.

43. B. R. Lentz, Y. Barenholz and T. E. Thompson, *Biochemistry*, 1976, **15**, 4521-4528.

44. A. Watts, D. Marsh and P. F. Knowles, *Biochemistry*, 1978, **17**, 1792-1801.

45. A. I. Elegbede, M. K. Haldar, S. Manokaran, J. Kooren, B. C. Roy, S. Mallik and D. K. Srivastava, *Chem. Commun.*, 2007, 3377–3379.

46. A. J. Jin, D. Huster, K. Gawrisch and R. Nossal, *Eur. Biophys. J.*, 1999, **28**, 187-199.

47. J. F. Nagle and S. Tristram-Nagle, *Biochim. Biophys. Acta*, 2000, **1469**, 159-195.

48. P. Balgavy, M. Dubnickova, N. Kucerka, M. A. Kiselev, S. P. Yaradaikin and D. Uhrikova, *Biochim. Biophys. Acta*, 2001, **1512**, 40-52.

49. D. W. Fry, J. C. White and I. D. Goldman, *Anal. Biochem.*, 1978, **90**, 809-815.

CHAPTER 3

TERBIUM(III)-CHOLATE FUNCTIONALIZED VESICLES AS LUMINESCENT INDICATORS FOR THE ENZYMATIC CONVERSION OF DIHYDROXYNAPHTHALENE DIESTERS

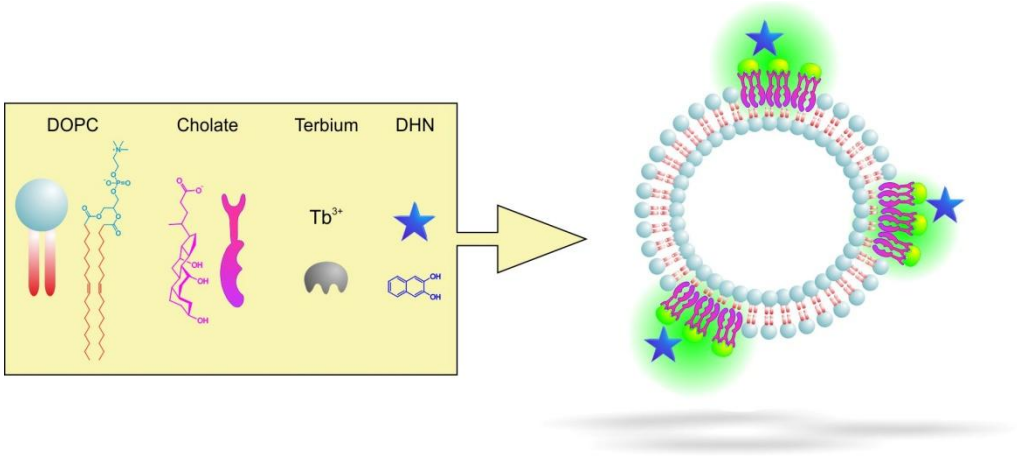

The phosphorescence intensity of unilamellar DOPC vesicles with embedded Tb^{3+}-cholate complexes depends on the concentration of dihydroxynaphthalene (DHN) as sensitizer in solution. This was used to monitor the enzymatic conversion of DHN esters or DHN glucosides by enzymes in aqueous buffered solution.

This Chapter has been published:

S. Balk, U. Maitra, B. König, *Chem. Commun.*, **2014**, 50, 7852–7854.

Author contributions:

SB synthesized vesicles, performed measurements and wrote the manuscript; UM and BK supervised the project and are corresponding authors.

Introduction

Cholic acids are known to aggregate in the presence of trivalent lanthanide ions resulting in three dimensional networks of hydrogels.[1-4] Such gels have found applications as optical materials,[1, 2, 5-7] in the preparation of nanoparticles,[3, 8] as confined reaction media[9, 10] and in the detection of analytes.[11-14] The lanthanide luminescence of hydrogels prepared from sodium cholate and terbium(III) salt is sensitized by 2,3-dihydroxynaphthalene (DHN). Only the dihydroxy compound coordinates to the Tb^{3+} ion and acts as sensitizer, but not DHN ester or acetal derivatives.[1] This observation has been used to monitor the enzymatic conversion of carboxy esters or the monoglucoside of DHN by changes in the phosphorescence intensity avoiding interference with background fluorescence.[15-19; 20-22] The luminescent gel indicator is prepared by self-assembly of all components in aqueous buffer, but the three dimensional gel limits the diffusion and the enzymes have to be added during gel preparation. Therefore we transferred this detection mechanism from hydrogels to the membrane of small unilamellar vesicles (Scheme 1). Functionalized lipid bilayers have been previously used in enzyme assays[23-25] or as luminescent indicators.[26-29]

Results and Discussion

A vesicular solution of 1,2-dioleoyl-sn-glycero-3-phosphatidylcholine (DOPC, 5 mM) in HEPES buffer (25 mM, pH 7.4), was prepared by extrusion in the presence of a submicellar concentration[‡] of cholic acid (0.75 mM). The cholic acid will phase separate in the DOPC membrane and added $TbCl_3$*6 H_2O (0.25 mM) coordinates to the membrane embedded bile salts. Alternatively, a post functionalization of DOPC vesicles by bile salts and Tb(III) is possible, when the components are added to buffered DOPC vesicle solutions. We assume the formation of membrane anchored terbium(III)-complex domains. The resulting vesicle solutions are homogeneous, stable and monodispers.

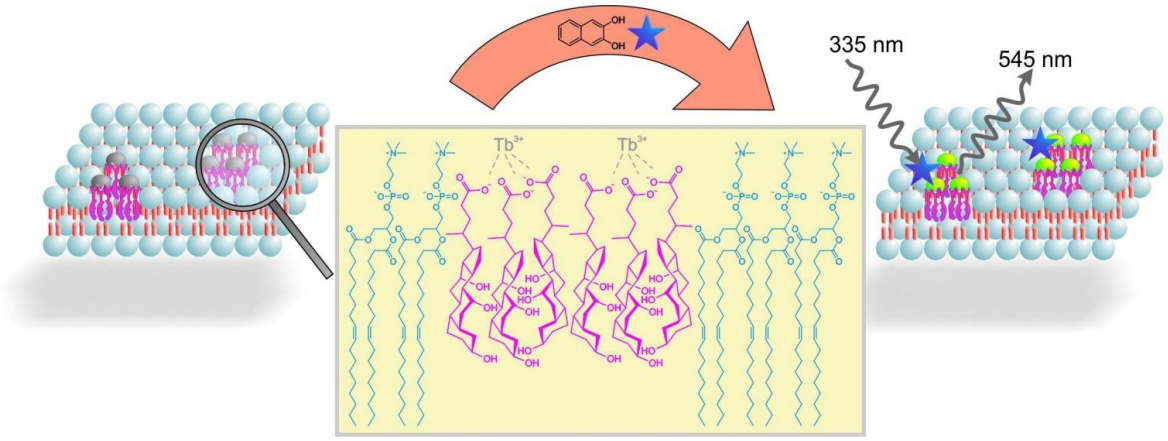

Scheme 1. Self assembly of amphiphiles (DOPC) and cholates in aqueous solution yields gel-functionalized small unilamellar vesicles after extrusion. The addition of dihydroxynaphthalene (DHN), which is coordinating to the metal complex, sensitizes the Tb^{3+}- luminescence.

Next, DHN (12.5 µM) was added to the aqueous vesicle solution **Vs1** ($c_{(DOPC)}$ = 5 mM, $c_{(Chol)}$ = 0.75 mM). Excitation of the mixture at 335 nm gave a significant terbium luminescence with an emission maximum at 545 nm (Scheme 2). Previous studies have shown that the DHN sensitization of the lanthanide emission requires a rigid gel matrix.[1, 11] The strong increase of terbium luminescence in the vesicle membrane therefore indicates that the Tb^{3+}-cholate patches might have gel like properties.

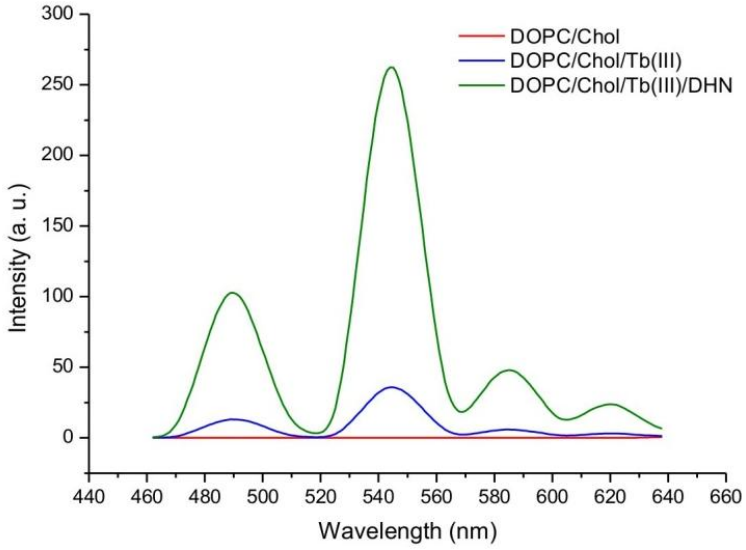

Scheme 2. Excitation of DHN at 335 nm in a cholate doped vesicle solution results in a strong Tb^{3+}- phosphorescence emission (green); without sensitizer (blue) the terbium luminescence is weak; no emission is detected for cholate-vesicles (red).

The presence of cholic acid, DHN and terbium (III) salts as membrane additives is essential to observe the lanthanide emission (Scheme 2), which was confirmed by different DOPC vesicle solutions (**Vs2**: $c_{(DOPC)}$ = 5 mM, **Vs1**: $c_{(DOPC)}$ = 5 mM, $c_{(Chol)}$ = 0.75 mM, **Vs3**: $c_{(DOPC)}$ = 5 mM, $c_{(Chol)}$ = 0.75 mM, $c_{(Tb^{3+})}$ = 0.25 mM, $c_{(DHN)}$ = 12.5 µM) and post functionalized DOPC vesicles (**Vs3p**: $c_{(DOPC)}$ = 5 mM, $c_{(Chol)}$ = 0.75 mM, $c_{(Tb^{3+})}$ = 0.25 mM, $c_{(DHN)}$ = 12.5 µM). Dynamic light scattering (DLS) confirmed a monodispers narrow size distribution around 110 nm for all samples. In contrast, solutions of cholate monomers (0.75 mM) in HEPES buffer (25 mM, pH 7.4) or $CHCl_3$ showed a broad size distribution and polydispersity (see SI for data). The embedding of the luminescent cholic acid – terbium complexes in the vesicle membrane was confirmed by fluorescence anisotropy: The terbium complex, excited by DHN (12.5 µM) at 335 nm, and bound to cholic acid doped vesicles **Vs4** ($c_{(DOPC)}$ = 5 mM, $c_{(Chol)}$ = 0.75 mM, $c_{(Tb^{3+})}$ = 0.25 mM) showed a fluorescence anisotropy, detected at 550 nm, which is about 8 times higher than for terbium in aqueous cholic acid solution ($c_{(Chol)}$ = 0.75 mM, $c_{(Tb^{3+})}$ = 0.25 mM, $c_{(DHN)}$ = 12.5 µM). Higher anisotropy values detected at 380 nm of DHN (12.5 µM) in the presence of **Vs4** compared to aqueous cholate solution indicated the coordination of DHN to terbium(III) ions at the surface of vesicle **Vs4** (see SI for data).

Since DHN derivatives lacking free hydroxy groups for metal coordination, do not sensitize the terbium(III) emission, reactions converting DHN derivatives into DHN can be easily monitored by the functionalized vesicles. Lipase (*Candida rugosa*, 2.5 U/mg, 50 mg/L) was added to the aqueous vesicle solution **Vs1** ($c_{(DOPC)}$ = 5 mM, $c_{(Chol)}$ = 0.75 mM) with added $TbCl_3$ * 6 H_2O (0.25 mM) and naphthalene- 2,3,-diyl dihexanoate (DHNdhn, 12.5 µM) or naphthalene-2,3-diyl diacetate (DHNdac, 12.5 µM). The enzymatic ester cleavage of DHNdhn into DHN leads to an increase of the vesicle luminescence intensity tracing the reaction (Scheme 3 and 4). 3-Hydroxynaphthalene-2-yl- β-glucoside (DHNglu, 12.5 µM) was likewise used to monitor the enzymatic activity of β-glucosidase (from almonds, 6.5 U/mg, 50 mg/L).

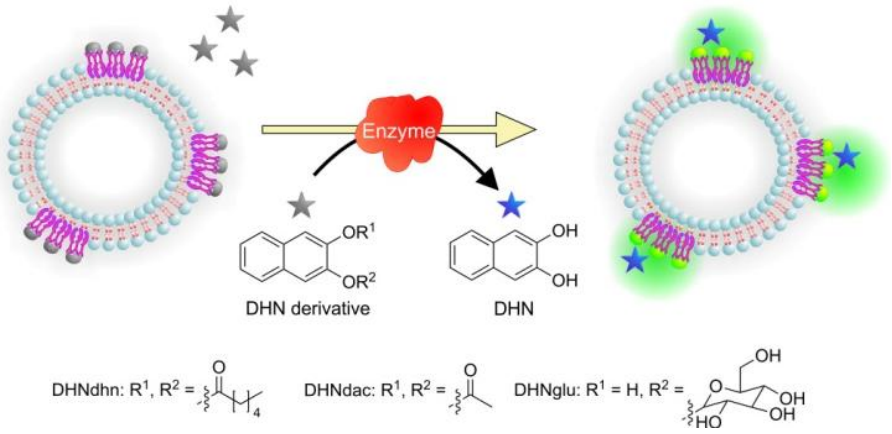

Scheme 3. Lipase conversion of naphthalene-2,3-dihydroxyesters (12.5 µM) into DHN leads to an increase of the terbium luminescence intensity.

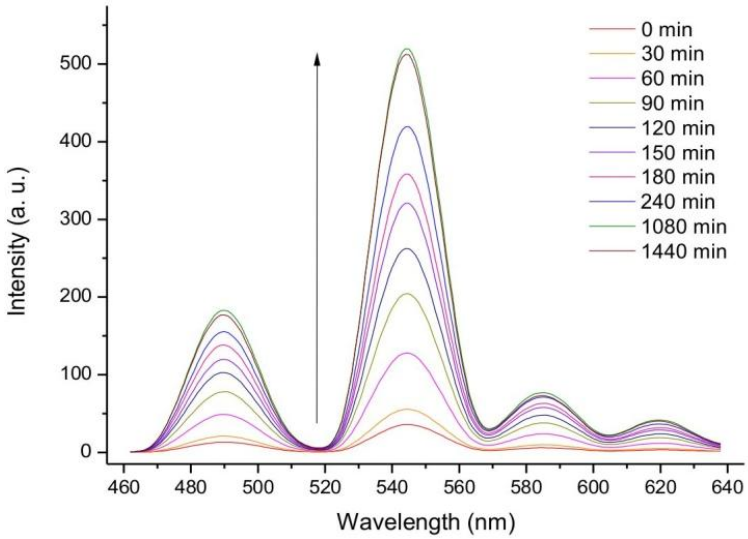

Scheme 4. Luminescence intensity of **Vs4** ($c_{(DOPC)}$ = 5 mM, $c_{(Chol)}$ = 0.75 mM, $c_{(Tb^{3+})}$ = 0.25 mM) is increasing in the presence of DHNdhn (12.5 µM) and lipase (50 mg/L) over 24h.

To confirm that the emission intensity change during the reaction correlates with the amount of produced DHN, we monitored the enzymatic conversion by HPLC in the absence of vesicles. The initial rate constants for the esterase activity of lipase derived from the emission intensity increase or the HPLC analysis of produced DHN were comparable with 1.3 x 10^{-8} and 1.9 x 10^{-8} mmol/min, respectively, (see SI for data).‡‡ A detection limit of 0.5 mg/L for lipase activity was determined for the assay using a 24 h incubation time, which significantly improved compared to the previously used hydrogels that required 900 mg/L.[5a]

Conclusion

In conclusion, we have embedded terbium – cholate aggregates into the membrane of 100 nm unilamellar DOPC vesicles. Dihydroxynaphthalene coordinates to the complexes at the membrane-water interface and sensitizes the terbium phosphorescence. As the concentration of free dihydroxynaphthalene in the aqueous solution correlates with the terbium phosphorescence intensity, enzymatic reactions of dihydroxynaphthalene esters and glycosides can be monitored in buffered aqueous solution. The phosphorescent vesicular indicator is easily prepared by self-assembly and many DHN derivatives as pro-sensitizers can be envisaged that are suitable substrates for a variety of enzymes. The detection principle may therefore find application as a facile luminescent on-line monitoring of enzymatic activity.

SB thanks the INDIGO network of the German Academic Exchange Service (DAAD) for travel support.

Experimental Part and Supporting Information

General methods and material

Fluorescence measurements were performed with UV-grade solvents (Baker or Merck) in 1.0 or 0.4 cm quartz cuvettes (Perkin Elmer / Hellma) and recorded on a Horiba Fluoromax4 spectrophotometer with temperature control at 20 °C. Phosphorescence measurements were recorded on a Varian ‘Cary Eclipse’ fluorescence spectrophotometer (total decay time: 0.020 s, delay time 0.1 ms, gate time 5.0 ms, slit 20 nm) with temperature control (20 °C) using 1 cm quartz cuvettes (Hellma). DLS measurements were performed on a Malvern Zetasizer Nano at 20 °C using 1 cm disposable polystyrene cuvettes (VWR). Starting materials were used without any further purification. Phospholipids were purchased from Avanti Polar Lipids Inc. Commercially available solvents of standard quality and water of millipore quality were used. Naphthalene- 2,3,-diyldihexanoate (DHNdhn) synthesis is described in the Ph.D. thesis of Mr. Sandip Bhowmik "Design and Applications of Bile-salt/Lanthanide based Hydrogels", Indian Institute of Science, Bangalore, February 2013. Naphthalene- 2,3,-diyl diacetate

(DHNdac) and 3-hydroxynaphthalene-2-yl- b-glucoside (DHNglu): synthesis is described in the supporting information of *Chem. Commun.*, 2012, **48**, 4624 (Sandip Bhowmik, Uday Maitra). *Candida rugosa* lipase was obtained from Sigma-Aldrich (2.5 Units/mg; catalogue no. 90860-5G and Batch no. 445584/1). Beta-glucosidase from almonds was obtained from Sigma-Aldrich (6.5 Units/mg; catalogue no. 49290-250 MG and Batch no. BCBD2305V). $TbCl_3$ * 6 H_2O was obtained from Sigma Aldrich (catalogue no. 212903-5G, batch no. MKBD6300V). Time dependent enzyme conversions were measured via HPLC analysis on a Agilent 1290 Series HPLC: Column: Phenomenex Luna C18, 3 µm, 150 x 2.00 mm, 100 Å; flow: 0.3 mL/min; solvent A: H_2O [0.059 Gew% TFA], solvent B: MeCN; gradient: 0-20 min: A/B 97/3, 20-30 min: A/B 2/98.

Vesicles

Preparation

In small glass reaction vessels 1 - 5 µmol of DOPC or DSPC were dissolved in chloroform and optionally 15 mol% of dissolved sodium cholate was added and mixed. The solvent was completely removed under reduced pressure at 25 °C (DOPC) or 75˚C (DSPC) and an appropriate amount of buffer (HEPES 25 mM, pH 7.4) was added to obtain lipid concentrations of 5 mM. Vigorous shaking at 25 °C (DOPC) or 75 °C (DSPC) for 10 min yielded a turbid multi-lamellar vesicle suspension. Small uni-lamellar dispersions were obtained by extrusion through 100 nm-pore size polycarbonate membranes with a LiposoFast liposome extruder from Avestin. DOPC- cholate vesicles were equipped with 5 mol% of aqueous $TbCl_3$ * $6H_2O$ and stored for 10 min to ensure cholate - terbium-complexation. Alternative pure DOPC vesicles were post functionalized with an appropriate amount of cholate and after 10 min $TbCl_3$ * 6 H_2O was added. In order to induce a luminescent response of Tb^{3+}- gel functionalized vesicle solutions 2,3-dihydroxynaphthalene (DHN) was added.

Dynamic light scattering (DLS)

Vesicle size distributions were determined using dynamic light scattering (DLS). Vesicle **Vs1** ($c_{(DOPC)}$ = 5 mM, $c_{(Chol)}$ = 0.75 mM) was functionalized with Tb^{3+} (0.25 mM) and DHN (12.5 µM), which induced no change in the size distribution. This indicates that no aggregates beside vesicles with an average size distribution of about 110 nm are present.

Results

			Size (d.nm):	% Intensity:	St Dev (d.nm):
Z-Average (d.nm):	109,2	Peak 1:	121,7	100,0	40,71
PdI:	0,101	Peak 2:	0,000	0,0	0,000
Intercept:	0,961	Peak 3:	0,000	0,0	0,000
Result quality :	Good				

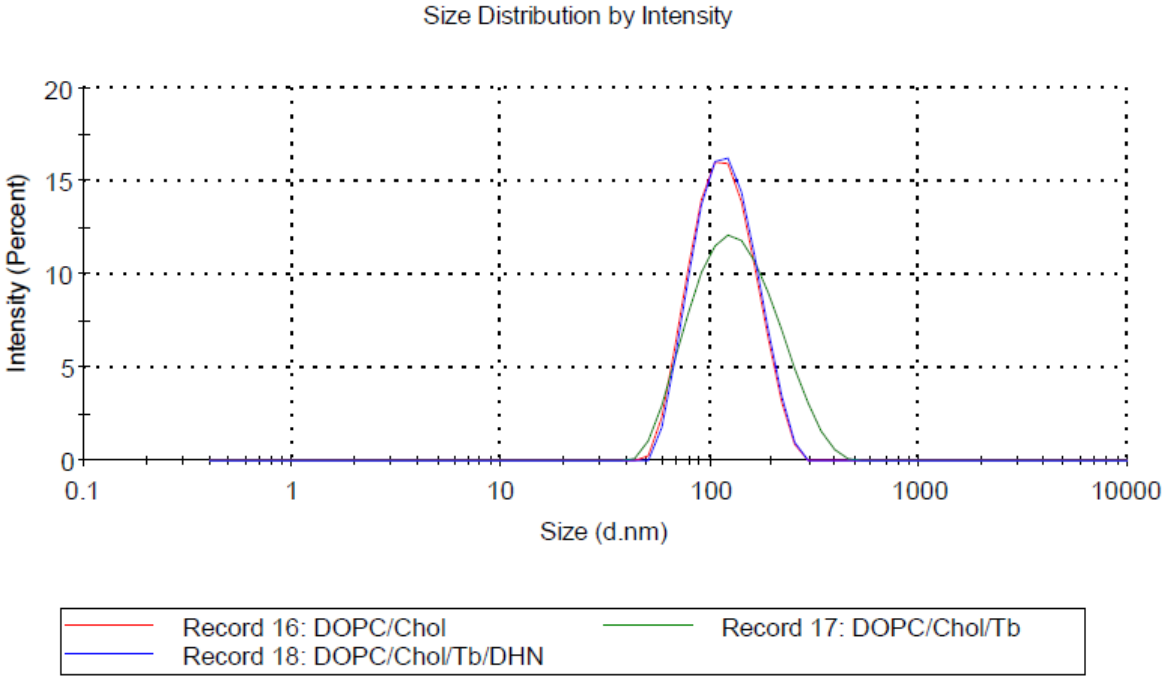

Scheme S1. Size distribution of **Vs1** ($c_{(DOPC)}$ = 5 mM, $c_{(Chol)}$ = 0.75 mM; red) before and after functionalization with Tb^{3+} (0.25 mM; blue) and additional DHN (12.5 µM; green).

For comparison, solutions of Chol (0.75 mM) in HEPES (25 mM, pH 7.4) and $CHCl_3$ have been prepared in the presence of DHN (12.5 µM) before treatment with Tb^{3+} (0.25 mM). The particle size distribution of these solutions is not reproducible, has a high polydispersity index and indicates agglomeration of bile salts in aqueous and organic solvents.

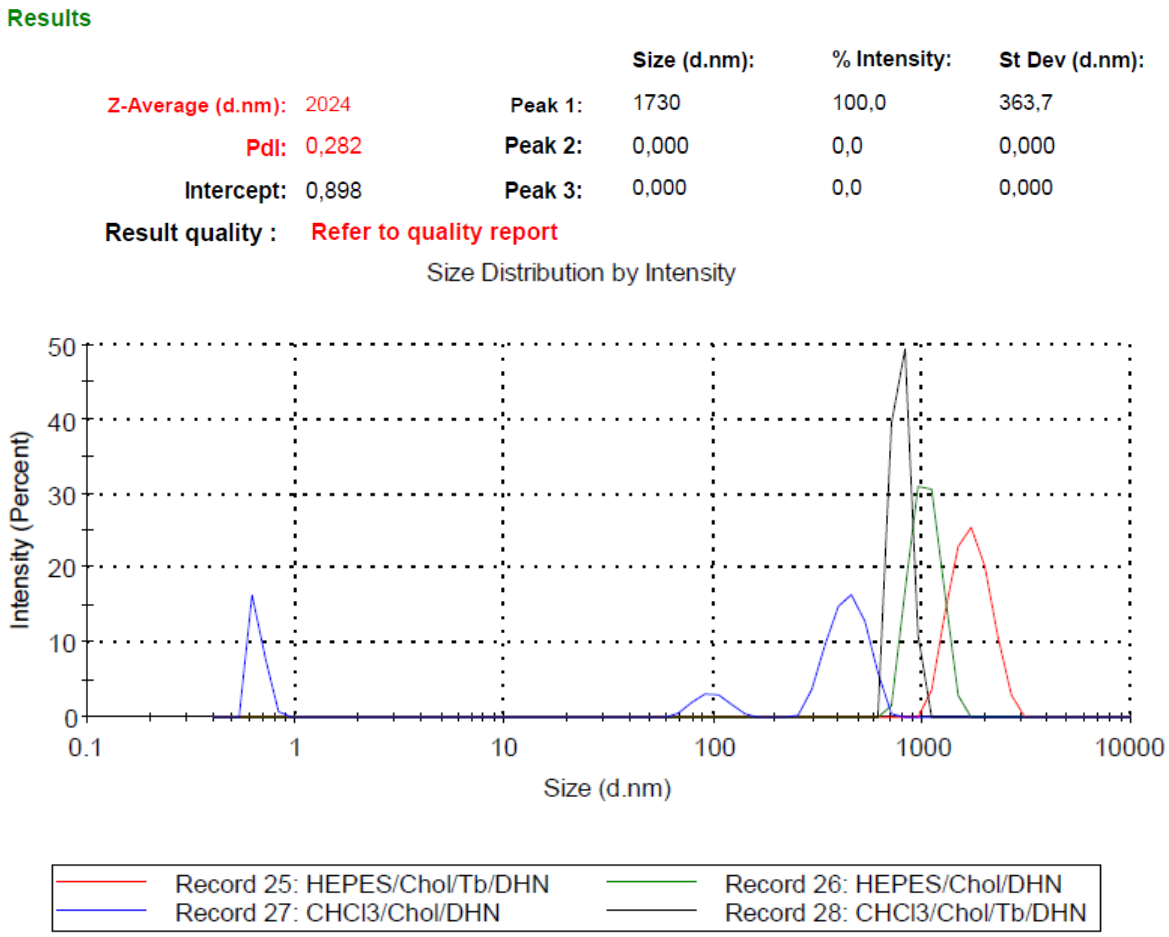

Scheme S2. Size distribution of Chol solutions ($c_{(Chol)}$ = 0.75 mM; red) with DHN (12.5 µM) in HEPES (green) and $CHCl_3$ (blue). After addition of Tb^{3+} (0.25 mM) to HEPES- Chol solution (red) and $CHCl_3$- Chol solution (black) an enlargement of aggregates is assumed.

The DOPC vesicle solution **Vs2** ($c_{(DOPC)}$ = 5 mM) was post functionalized with cholic acid (0.75 mM), Tb^{3+} (0.25 mM) and DHN (12.5 µM) giving a monodispers size distribution of vesicles.

Results

			Size (d.nm):	% Intensity:	St Dev (d.nm):
Z-Average (d.nm):	100,7	Peak 1:	116,1	100,0	39,62
PdI:	0,125	Peak 2:	0,000	0,0	0,000
Intercept:	0,947	Peak 3:	0,000	0,0	0,000
Result quality :	Good				

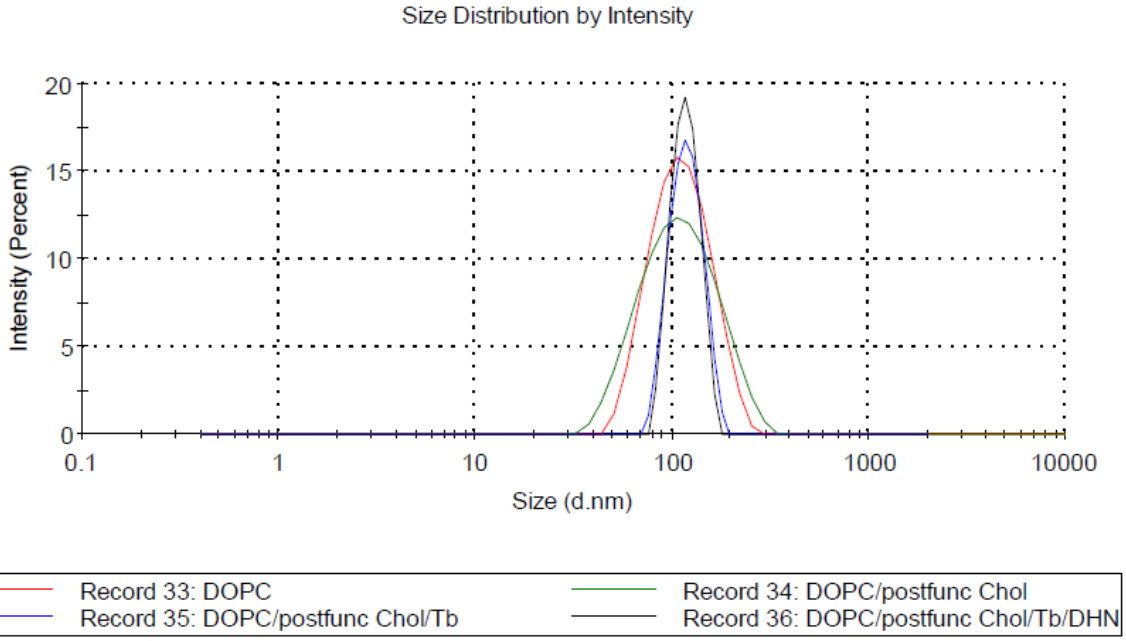

Scheme S3. Size distribution of **Vs2** ($c_{(DOPC)}$ = 5 mM; red) after addition of cholate (0.75 mM, green).

The aggregation of Chol (0.75 mM) in HEPES (25 mM, pH 7.4) or $CHCl_3$ after treatment with Tb^{3+} (0.25 mM) was obvious after a few minutes. In contrast, **Vs1** ($c_{(DOPC)}$ = 5 mM, $c_{(Chol)}$ = 0.75 mM) functionalized with Tb^{3+} (0.25 mM) remains a homogeneous monodispers solution.

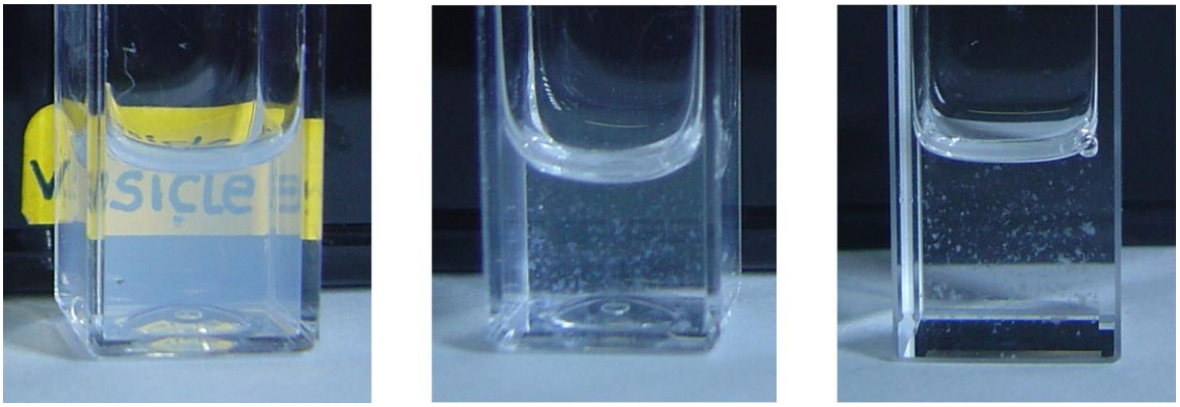

Figure S1. Solution of **Vs1** ($c_{(DOPC)}$ = 5 mM, $c_{(Chol)}$ = 0.75 mM; left) doped with Tb^{3+} (0.25 mM) yields a homogeneous monodispers solution. Chol- Tb^{3+} solutions in HEPES (25 mM, pH 7.4; middle) and $CHCl_3$ (right) indicate aggregate formation.

Fluorescence Anisotropy

The embedding of the luminescent cholic acid – terbium complexes in the vesicle membrane was confirmed by fluorescence anisotropy. The terbium complexes ($c_{(Tb^{3+})}$ = 0.25 mM) are excited by DHN (12.5 µM) at 335 nm and are bound to cholic acid doped vesicles **Vs4** ($c_{(DOPC)}$ = 5 mM, $c_{(Chol)}$ = 0.75 mM, $c_{(Tb^{3+})}$ = 0.25 mM) as they show a fluorescence anisotropy (Scheme S4, right; FA = 0.23), detected at 550 nm, which is about 8 times higher than for terbium in aqueous cholic acid solution (FA = 0.06; $c_{(Chol)}$ = 0.75 mM, $c_{(Tb^{3+})}$ = 0.25 mM, $c_{(DHN)}$ = 12.5 µM). Higher anisotropy values are detected at 380 nm for DHN (12.5 µM) with **Vs1** ($c_{(DOPC)}$ = 5 mM, $c_{(Chol)}$ = 0.75 mM) (Scheme S4, left; FA = 0.34) or in presence of 0.25 mM Tb^{3+} (Scheme S4, middle; FA = 0.33) than for aqueous cholate solutions (Scheme S4, left, $c_{(Chol)}$ = 0.75 mM, FA = 0.06 and middle $c_{(Chol)}$ = 0.75 mM, $c_{(Tb^{3+})}$ = 0.25 mM, FA = 0.03) indicate that DHN (12.5 µM) coordinates to the terbium(III)- cholate complex at the liposome membrane.

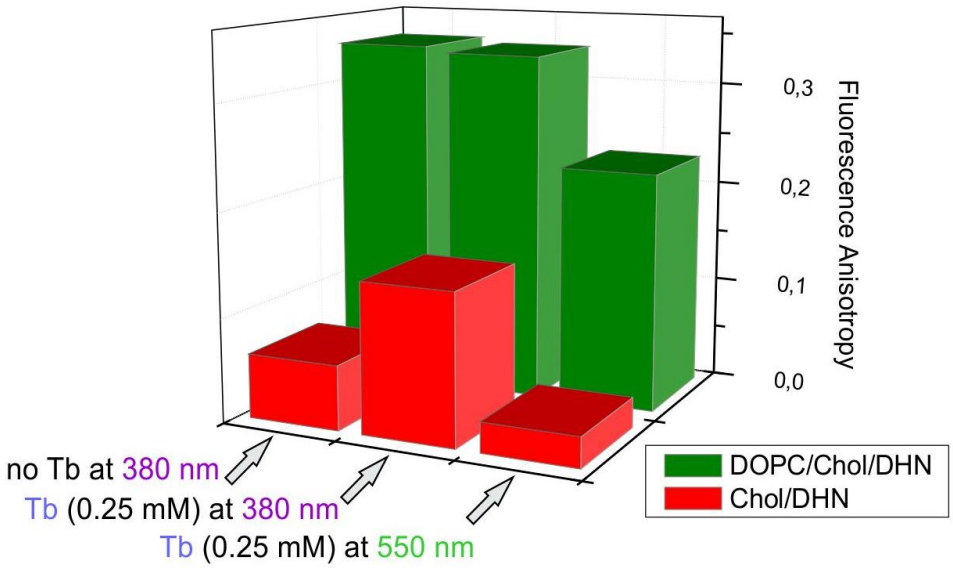

Scheme S4. Fluorescence anisotropy of DHN at 380 nm (left and middle) and Tb^{3+} at 550 nm (right) with cholate doped vesicles (green) is significant higher compared to aqueous solutions of Chol (red).

Phosphorescence measurements

Only terbium(III), which is complexed by cholate functionalized vesicles, shows intensive, significant terbium phosphorescence at 545 nm after excitation of coordinated DHN sensitizer at 335 nm.

A significant increase of terbium phosphorescence intensity at 545 nm of **Vs4** ($c_{(DOPC)}$ = 5 mM, $c_{(Chol)}$ = 0.75 mM, $c_{(Tb^{3+})}$ = 0.25 mM) was detected during the conversion of DHNdhn (12.5 µM) by lipase (50 mg/L) for 24 h. DHN is, in contrast to its ester derivative, coordinating with its dihydroxy moiety to the vesicular embedded, cholate complexed terbium, which provides an effective sensitization at 335 nm (see fluorescence anisotropy Scheme S4, left).

Enzyme activity assay

The emission intensity of **Vs4** ($c_{(DOPC)}$ = 5 mM, $c_{(Chol)}$ = 0.75 mM, $c_{(Tb^{3+})}$ = 0.25 mM) was monitored over 24 h in a cuvette (2 x 10 mm, 400 µL) at 545 nm in the presence of the respective DHN derivative ($c_{(DHN')}$ = 12.5 µM) and enzyme (50 mg/L lipase or glucosidase). (Scheme S5 and S7). Due to the higher sensitivity of the spectrometer, fluorescence emission intensity instead of phosphorescence intensity was used for the comparison with HPLC analysis of DHN.

The respective DHN derivative ($c_{(DHN')}$ = 12.5 µM) and enzyme (50 mg/L lipase or glucosidase) are incubated in a HEPES buffer solution (25 mM, pH 7.4), lacking any cholate doped vesicles or Tb^{3+}, over 24 h. Samples were analyzed by calibrated HPLC to monitor the evolving DHN amount over time.

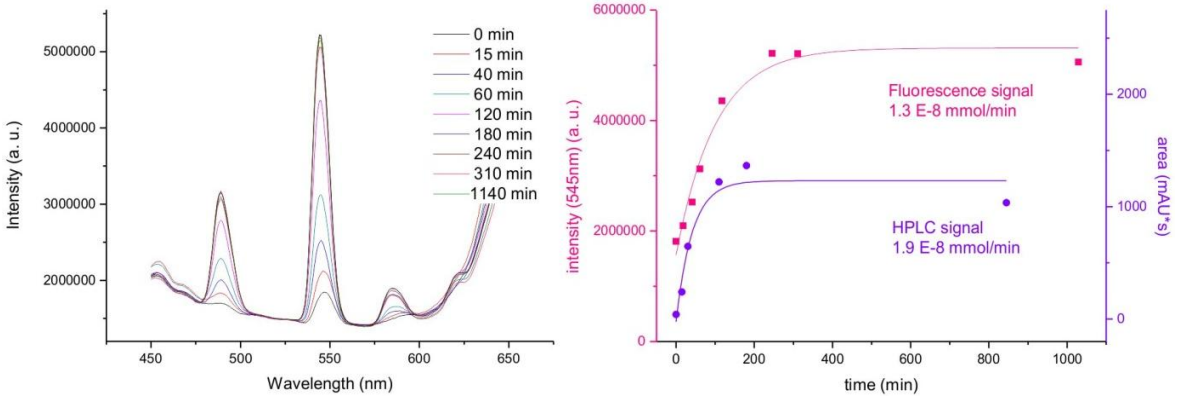

Scheme S5. Fluorescence intensity increase of **Vs4** ($c_{(DOPC)}$ = 5 mM, $c_{(Chol)}$ = 0.75 mM, $c_{(Tb^{3+})}$ = 0.25 mM) upon conversion of DHNdhn (12.5 µM) with lipase (50 mg/L) during 24h (left). DHNdhn conversion by lipase was monitored by fluorescence intensity changes of **Vs4** and HPLC analysis (right).

The initial rate constants for the lipase activity, derived from the fluorescent increase or the HPLC analysis of DHNdhn, are with 1.3 x 10^{-8} and 1.9 x 10^{-8} mmol/min, resp., comparable (Scheme S5). In order to correlate fluorescence intensity with the DHN concentration, increasing amounts of DHN were added to **Vs4** (Scheme S6). The slope of enzyme conversion (mmol/min) (Scheme S5, right) was detected during the first 60 min with an intensity increase from 1.8 x 10^6 to 3.1 x 10^6 cps. The value corresponds to the linear region of fluorescence intensity vs. sensitizer amount (Scheme S6, right).

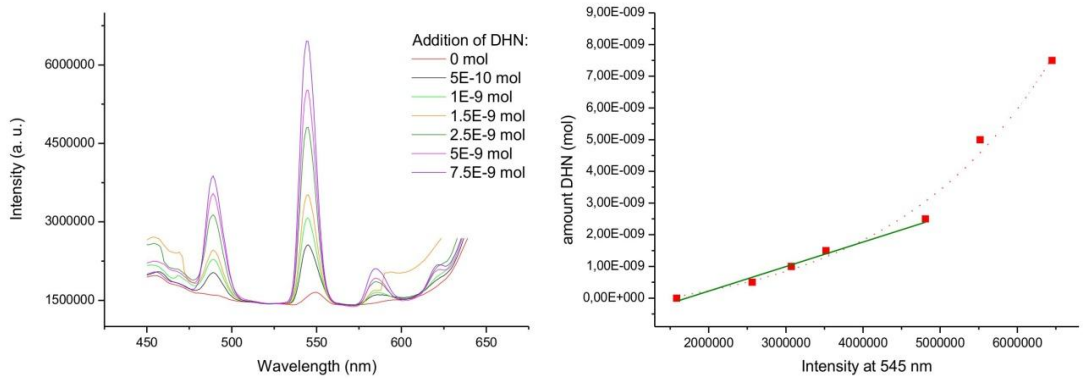

Scheme S6. Increasing fluorescence intensity of **Vs4** ($c_{(DOPC)}$ = 5 mM, $c_{(Chol)}$ = 0.75 mM, $c_{(Tb^{3+})}$ = 0.25 mM) upon addition of DHN (left). Fluorescence intensity increases linearly for small sensitizer concentrations (right), which were used to monitor enzyme activity.

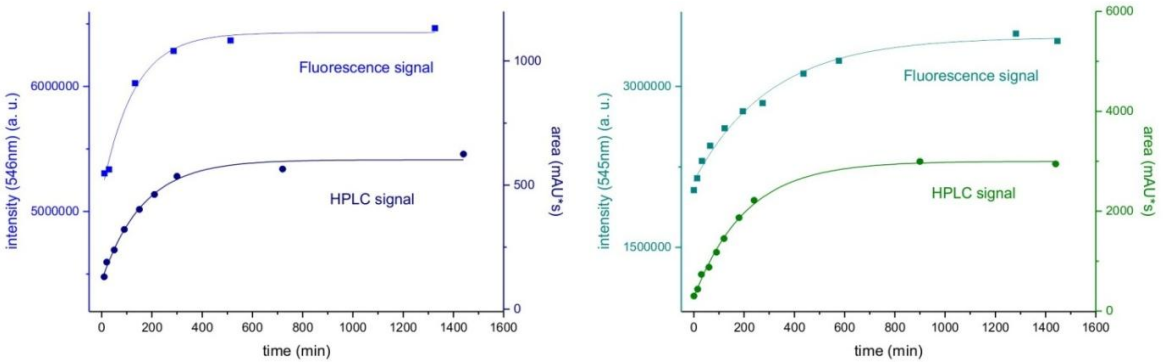

Scheme S7. Change of the terbium fluorescence intensity (left y-axis) of **Vs4** ($c_{(DOPC)}$ = 5 mM, $c_{(Chol)}$ = 0.75 mM, $c_{(Tb^{3+})}$ = 0.25 mM) during the conversion of DHNdac (12.5 µM) by lipase (50 mg/L) (left) and DHNglu (12.5 µM) by glucosidase (50 mg/L) (right). For comparison monitoring of the DHN conversion by HPLC is given on the right y-axis.

To exclude a potential inhibition of the enzyme activity in the presence of terbium ions,[30, 31] we monitored the DHNdhn (12.5 µM) conversion with lipase (50 mg/L) by HPLC in presence and absence of Tb^{3+} (0.25 mM). The conversion of the DHNdhn is comparable in both cases, though the amount of free DHN in solution detected by HPLC is little lower in the presence of Tb^{3+} (Scheme S8). However, this is not caused by inhibition of the lipase activity, but by the coordination of DHN to the lanthanide cation. The complex is not detected by HPLC. Moreover the measured amount of DHN is even lower for an equal DHNdhn lipase sample which was treated with Tb^{3+} (0.25 mM) only shortly before HPLC or for a sample, equipped with Tb^{3+} (0.25 mM) and cholate (0.75 mM), showing precipitation (Scheme S8, inset). The coordination of DHN towards Tb^{3+} was also observed with fluorescence anisotropy measurements of DHN (Scheme S4, red columns left and middle). Hence the presence of Tb^{3+} does not affect the enzymatic conversion and provides unambiguous enzyme activity detection with fluorescence emission and HPLC (Scheme S5, right and S7).

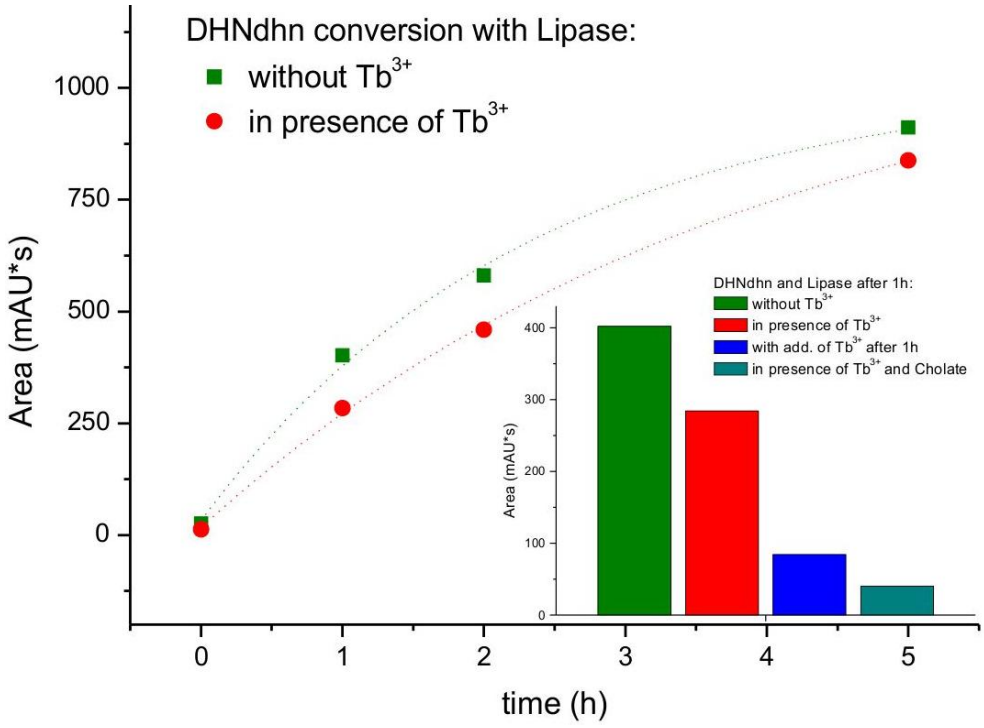

Scheme S8. HPLC analysis confirms that the enzymatic conversion of DHNdhn (12.5 µM) is not inhibited by the presence of terbium ions (0.25 mM). Changing concentrations of HPLC detectable DHN in solution in presence of terbium is a result of complex formation, which masks the DHN for HPLC analysis.

Control experiments (Scheme S9) show no significant fluorescence intensity increase of **Vs4** ($c_{(DOPC)}$ = 5 mM, $c_{(Chol)}$ = 0.75 mM, $c_{(Tb^{3+})}$ = 0.25 mM) in the presence of a DHN derivate (12.5 µM) without enzymes after 24 h.

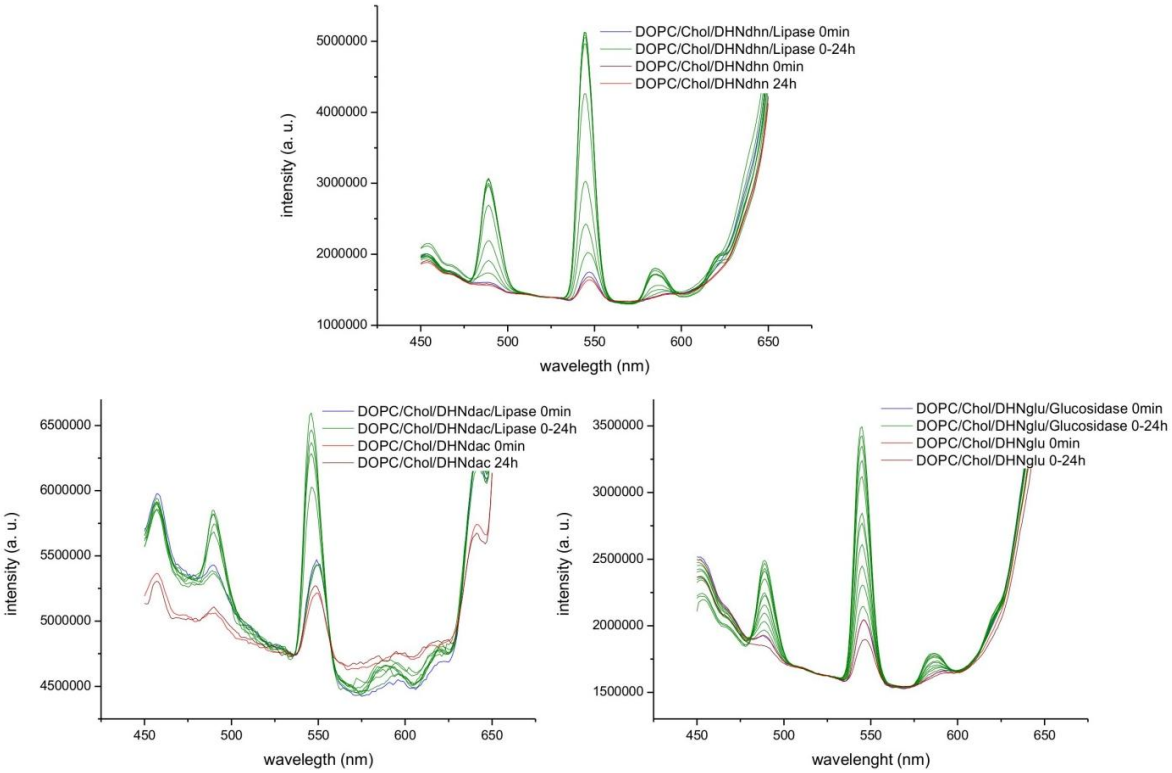

Scheme S9. Increase of emission intensity of **Vs4** over time in the presence of DHN esters in the presence and in the absence of enzymes.

A detection limit of 0.5 mg/L for lipase enzymatic activity was determined with **Vs4** ($c_{(DOPC)}$ = 5 mM, $c_{(Chol)}$ = 0.75 mM, $c_{(Tb^{3+})}$ = 0.25 mM) for the previous described assay (lipase 50 mg/L) with reduced amounts of enzyme using 24 h incubation time.

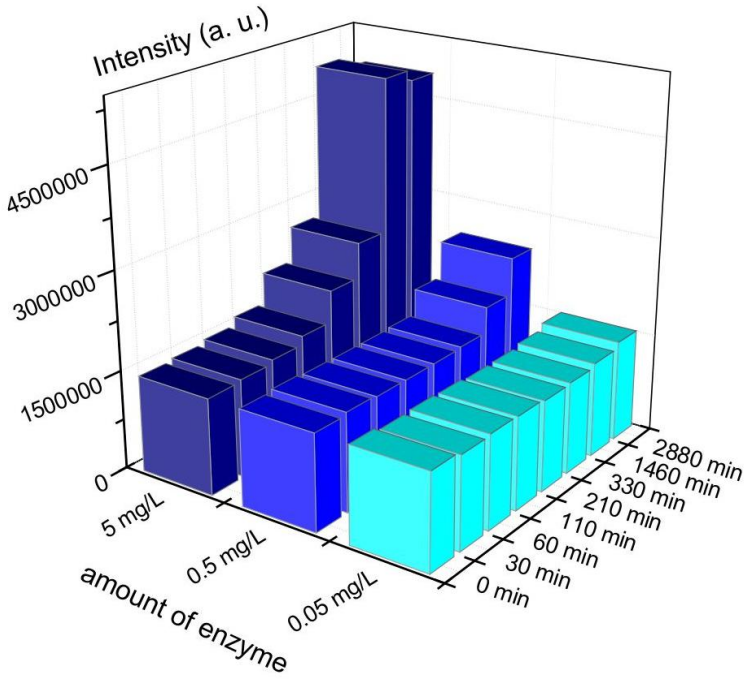

Scheme S10. The limit of detection of lipase activity assay with DHNdhn and **Vs4** is 0.5 mg/L; 1 % of the enzyme standard solution (50 mg/L).

Notes and References

‡ Critical micellar concentration (cmc) for sodium cholate is 9 – 14 mM.

‡‡ Non-enzymatic spontaneous hydrolysis of DHN esters over 24 h is negligible.

1. S. Banerjee, R. Kandanelli, S. Bhowmik and U. Maitra, *Soft Matter*, 2011, **7**, 8207-8215.

2. S. Bhowmik, S. Banerjee and U. Maitra, *Chem. Commun.*, 2010, **46**, 8642-8644.

3. A. Chakrabarty, U. Maitra and A. D. Das, *J. Mater. Chem.*, 2012, **22**, 18268-18274.

4. H. Svobodová, V. Noponen, E. Kolehmainen and E. Sievänen, *RSC Advances*, 2012, **2**, 4985-5007.

5. Y. Qiao, Y. Lin, S. Zhang and J. Huang, *Chem. Eur. J.*, 2011, **17**, 5180-5187.

6. N. Tang and J. Wu, *Dalton Transactions*, 2014.

7. D. I. Alexandropoulos, A. Fournet, L. Cunha-Silva, A. M. Mowson, V. Bekiari, G. Christou and T. C. Stamatatos, *Inorg. Chem.*, 2014, **53**, 5420-5422.

8. Y. Qiao, H. Chen, Y. Lin, Z. Yang, X. Cheng and J. Huang, *J. Phys. Chem. C*, 2011, **115**, 7323-7330.

9. S. Bhat and U. Maitra, *Molecules*, 2007, **12**, 2181-2189.

10. J. Bachl, A. Hohenleutner, B. B. Dhar, C. Cativiela, U. Maitra, B. Konig and D. D. Diaz, *J. Mater. Chem. A*, 2013, **1**, 4577-4588.

11. S. Bhowmik and U. Maitra, *Chem. Commun.*, 2012, **48**, 4624-4626.

12. S. Mizukami, K. Tonai, M. Kaneko and K. Kikuchi, *J. Am. Chem. Soc.*, 2008, **130**, 14376-14377.

13. T. Terai, K. Kikuchi, Y. Urano, H. Kojima and T. Nagano, *Chem. Commun.*, 2012, **48**, 2234-2236.

14. T. Terai, H. Ito, K. Kikuchi and T. Nagano, *Chem. Eur. J.*, 2012, **18**, 7377-7381.

15. T. Steinkamp, F. Schweppe, B. Krebs and U. Karst, *Analyst*, 2003, **128**, 29-31.

16. K.-H. Leung, H.-Z. He, V. P.-Y. Ma, H.-J. Zhong, D. S.-H. Chan, J. Zhou, J.-L. Mergny, C.-H. Leung and D.-L. Ma, *Chem. Commun.*, 2013, **49**, 5630-5632.

17. B. K. McMahon and T. Gunnlaugsson, *J. Am. Chem. Soc.*, 2012, **134**, 10725-10728.

18. U. Reddy G, P. Das, S. Saha, M. Baidya, S. K. Ghosh and A. Das, *Chem. Commun.*, 2013, **49**, 255-257.

19. J. Hu, G. Zhang and S. Liu, *Chem. Soc. Rev.*, 2012, **41**, 5933-5949.

20. C. M. Spangler, C. Spangler and M. Schäerling, *Ann. N.Y. Acad. Sci.*, 2008, **1130**, 138-148.

21. E. F. Gudgin Dickson, A. Pollak and E. P. Diamandis, *J. Photochem. Photobiol., B*, 1995, **27**, 3-19.

22. R. A. Evangelista, A. Pollak and E. F. Gudgin Templeton, *Anal. Biochem.*, 1991, **197**, 213-224.

23. G. Das, P. Talukdar and S. Matile, *Science*, 2002, **298**, 1600-1602.

24. T. Takeuchi and S. Matile, *Chem. Commun.*, 2013, **49**, 19-29.

25. P. Walde and S. Ichikawa, *Biomol. Eng*, 2001, **18**, 143-177.

26. B. Gruber and B. König, *Chem. Eur. J.*, 2013, **19**, 438-448.

27. B. Gruber, S. Balk, S. Stadlbauer and B. König, *Angew. Chem. Int. Ed.*, 2012, **51**, 10060-10063.

28. S. Banerjee and B. König, *J. Am. Chem. Soc.*, 2013, **135**, 2967-2970.

29. B. Gruber, S. Stadlbauer, A. Späth, S. Weiss, M. Kalinina and B. König, *Angew. Chem. Int. Ed.*, 2010, **49**, 7125-7128.

30. W. K. Xin and X. X. Gao, *Analyst*, 1996, **121**, 687-690.

31. Y. Wu, *Biometals*, 2000, **13**, 195-201.

SUMMARY

This work describes the membrane functionalization of small unilamellar phospholipid vesicles by incorporation of artificial amphiphiles. The presented investigations demonstrate a fast and simple approach for sensing molecular recognition events at the membrane-water interface.

Chapter 1 describes the dynamic recognition of multivalent ligands by receptor recruiting in fluid vesicle membranes. Two amphiphilic metal-complexes with attached FRET-pair labels were prepared and embedded into DOPC vesicles. Simultaneous binding of a model peptide enables receptor recruiting at the liquid-crystalline liposome membrane and a significant increase in energy transfer was observed as the two fluorescence labels come into close proximity.

Chapter 2 presents the approach of thermal imprinting by non-covalent assembly of metal-complexes embedded in DMPC vesicles. Template induced patterning in the liquid-crystalline phase was reversibly stabilized by phase transition of the liposomal membrane to the gel phase as shown by FRET measurements. Specific rebinding of thermally imprinted vesicular receptors to the bivalent target peptide provides an affinity enhancement after template removal.

In Chapter 3, terbium-cholate aggregates were used to functionalize DOPC vesicles. The phosphorescence intensity of these gel-like liposomal Tb^{3+}-patches depends on the concentration of DHN as sensitizer in solution. Based on this result a novel enzymatic assay was established to monitor the conversion of DHN esters or DHN glucosides by enzymes in aqueous solutions.

ZUSAMMENFASSUNG

In der vorliegenden Arbeit wurden selbstorganisierte Membranen von unilamellaren Phospholipid-Vesikeln durch Einlagerung synthetischer Amphiphile funktionalisiert. Die aufgezeigten Untersuchungen demonstrieren eine schnelle und einfache Methode zur Detektion molekularer Erkennungsvorgänge an der Grenzfläche von Membran und Wasser.

Kapitel 1 beschreibt die Erkennung multivalenter Liganden mittels dynamischer Strukturierung von Bindungsstellen in fluiden Vesikelmembranen. Dazu wurden zwei amphiphile Metallkomplexe mit FRET-komplementären Fluoreszenzlabeln synthetisiert und in DOPC-Vesikel eingebaut. Die gleichzeitige spezifische Koordination eines Modellproteins an beide Bindungsstellen ermöglicht die Umstrukturierung der Rezeptoren in der flüssig-kristallinen Phase der Liposomen. Dabei wurde ein signifikanter Anstieg des Energietransfers aufgrund der geschaffenen räumlichen Nähe der Fluoreszenzlabel festgestellt.

Kapitel 2 demonstriert die Methode des thermischen Imprintings durch nicht-kovalentes Anordnen von Metallkomplexen in DMPC-Vesikel. Die Templat-induzierte Strukturierung in der flüssig-kristallinen Phase wurde durch Phasenumwandlung der Vesikelmembran reversibel fixiert und durch FRET-Messungen nachgewiesen. Die spezifische erneute Bindung des bivalenten Zielpeptids durch Vesikel mit thermisch geprägten Rezeptoren erzielt nach Abtrennung des Templats eine höhere Affinität.

In Kapitel 3 wurden Terbium-Cholat-Komplexe für die Funktionalisierung von DOPC-Vesikel benutzt. Die Phosphoreszenzintensität dieser gelähnlichen Tb^{3+}-Strukturen ist abhängig von der DHN-Konzentration welche zur photochemischen Anregung in der Lösung verwendet wird. Dies bildet die Grundlage für einen neuen Enzymassay, welcher den Umsatz von DHN Estern oder DHN Glucosiden durch Enzyme in wässriger Lösung nachverfolgt.

ABBREVIATIONS

AES	Atomic emission spectroscopy
AFM	Atomic force microscopy
Aq	Aqueous
Ar	Aryl
Bipy	Bipyridine
Boc	*tert*-Butyloxycarbonyl
BSA	Bovine serum albumin
c	Concentration
calcd	Calculated
Cbz	Benzyloxycarbonyl
CF	Carboxyfluorescein
Chol	Cholic acid
CI	Chemical ionization
COSY	Correlated spectroscopy
cyclen	1,4,7,10-tetraazacyclododecane
d	Day(s)
DAD	Diode array detector
DCC	Dicyclohexylcarbodiimide
DCM	Dichloromethane
DEA	Diethylamine
DET	Diethylenetriammonium
DHN	2,3-dihydroxynaphthalene
DHNdac	Naphthalene-2,3-diyl diacetate
DHNdhn	Naphthalene- 2,3,-diyl dihexanoate
DHNglu	3-hydroxynaphthalene-2-yl- β-glucoside
DIPEA	Diisopropylethylamine
DLS	Dynamic light scattering
DMAP	4-(dimethylamino)-pyridine
DMF	Dimethylformamide
DMPC	1, 2-dimyristoyl-sn-glycero-3-phosphocholine
DMSO	Dimethylsulfoxide

DOPC	1,2-dioleoyl-sn-glycero-3-phosphocholine
DP	Di-picolyl
Dpa	Di-(2-picolyl)amine
DPPC	1,2-dipalmitoyl-sn-glycero-3-phosphocholine
DSC	Differential scanning calorimetry
DSPC	1,2-distearoyl-sn-glycero-3-phosphocholine
EA	Ethylacetate
EDC	N-(3-Dimethylamino-propyl)-N'-ethylcarbo-diimide
EI-MS	Electron-impact ionization mass spectrometry
eq	Equivalents
ES-MS	Electrospray ionization mass spectrometry
Et	Ethyl
EtOAc	Ethylacetate
EtOH	Ethanol
FA	Fluorescence Anisotropy
FAB	Fast-Atom-Bombardment
FAM	Carboxyfluorescein
FRET	Fluorescence resonance energy transfer
h	Hour
HBTU	2-(1H-Benzotriazole-1-yl)-1,1,3,3-tetramethyl-uronium hexafluorophosphate
HEPES	N-2-Hydroxy-ethylpiperazine-N'-2-ethansulfonic acid
His	Histidine
HOBt	Hydroxybenzotriazole
HPLC	High pressure liquid
HRMS	High resolution mass spectrometry
HSQC	Heteronuclear single quantum coherence
ICP	Inductively coupled plasma
IR	Infrared
ITC	Isothermal titration calorimetry
J	Coupling Constant
LB	Langmuir Blodgett
Me	Methyl

MeCN	Acetonitrile
MeOH	Methanol
MF	Molecular formula
min	Minutes
MLV	Multilamellar vesicles
MP	Melting point
MW	Molecular weight
NEt_3	Triethylamine
NMR	Nuclear magnetic resonance
NOESY	Nuclear overhauser enhancement spectroscopy
NTA	Nitrilotriacetic acid
PE	Petrol Ether (Hexanes)
Ph	Phenyl
PMT	Photo multiplier tube
PPi	Pyrophosphate
pSer	Phosphorylated serine
R_f	Retention factor
ROESY	Rotating frame NOE spectroscopy
rpm	Rounds per minute
RT	Room temperature
SAM	Self assembled monolayer
SEC	Size exclusion chromatography
SUV	Small unilamellar vesicles
TAMRA	Tetramethylrhodamine
TBTU	O-(benzotriazol-1-yl)-*N*,*N*,*N*',*N*'-tetramethyluronium tetrafluoroborate
TEM	Transmission electron microscopy
Terpy	Terpyridine
TFA	Trifluoroacetic acid
THF	Tetrahydrofuran
TLC	Thin layer chromatography
T_M	Phase transition temperature
TMR	Tetramethylrhodamine
TRIS	Tris(hydroxymethyl)-aminomethane

UV	Ultraviolett
Vis	Visible
x	Mole Fraction

CURRICULUM VITAE

Personal Data

Name	Stefan BALK
Date of birth	24. 01. 1985
Place of birth	Roding (Germany)
Nationality	German

Education

10 / 2010 – 08 / 2014	**PhD Thesis** *"Luminescent Functionalized Vesicles: Synthesis, Characterization and Analytical Applications"* Group of Prof. Dr. Burkhard König, Institute of Organic Chemistry, University of Regensburg
01 / 2010 – 09 / 2010	**Master Thesis** *"Synthesis of functionalized vesicles for FRET based distance measurements"* Group of Prof. Dr. Burkhard König, Institute of Organic Chemistry, University of Regensburg
10 / 2005 – 12 / 2009	**Studies of Chemistry** University of Regensburg
07 / 2004 – 04 / 2005	**Military service** Sanitätslehrregiment 7, Gäubodenkaserne Feldkirchen
09 / 1995 – 06 / 2004	**Abitur (university-entrance diploma)** Joseph von Fraunhofer Gymnasium, Cham

Research and teaching experience

11 / 2010 – 06 / 2014 **Scientific Co-worker**

Research:

- Synthesis and characterization of luminescent functional vesicles
- Development of artificial membrane based analytical applications

Teaching:

- Supervision of practical lab courses in organic chemistry
- Supervision of Bachelor theses and research internships
- Assistance with the organization of exams and conferences

Internships

02 / 2013 – 05 / 2013 **PhD research internship**

Exchange program of the INDIGO network of the German Academic Exchange Service (DAAD), Indian Institute of Science, Bangalore, Organic Institute, Group of Prof. Dr. Uday Maitra

08 / 2002 **Scholar internship**

Forschungs und Technologie Zentrum Deutsche Bahn AG, Munich

Memberships

since 01 / 2013	INDIGO network of the German Academic Exchange Service (DAAD): Indian-German Graduate School of Advanced Organic Synthesis for a Sustainable Future
since 07 / 2012	Gesellschaft Deutscher Chemiker (GDCh)
since 07 / 2012	Verband angestellter Akademiker und leitender Angestellter der chemischen Industrie e.V. (VAA)

Awards and scholarships

11 / 2010 – 06 / 2014	Travel grants from INDIGO network (DAAD), GDCh, Liebig-Vereinigung, Freunde der Universität Regensburg e.V.
04 / 2004	1st price of the local “Jugend Forscht“ competition in chemistry (Oberpfalz)

Publications

- S. Balk and B. König, *J. Incl. Phenom. Macrocycl. Chem.,* **2014**, DOI 10.1007/ s10847-014-0442-2.
- S. Balk, U. Maitra, B. König, *Chem. Commun.*, **2014**, 50, 7852–7854.
- B. Gruber, S. Balk, S. Stadlbauer, B. König, *Angew. Chem. Int. Ed.*, **2012**, 51, 10060–10063 (Hot paper).

Presentations

- S. Balk, B. König, *4th INDIGO PhD Research Conference and Intensive Course*, Regensburg / Ludwigshafen (Germany), 10 / **2013**, Presentation.
- S. Balk, B. König, *ACS 246th National Meeting & Exposition*, Indianapolis (US), 09 / **2013**, Presentation.
- S. Balk, B. König, *GDCh Wissenschaftsforum 2013*; Darmstadt (Germany), 09 / **2013**, Poster.
- S. Balk, B. König, *IPID, PhD student meeting of DAAD*, Cologne (Germany), 05 / **2013**, Workshop.
- S. Balk, B. König, *Christmas Colloquium of the Institute of Organic Chemistry*, Regensburg (Germany), 12 / **2012**, Presentation.
- S. Balk, B. König, *7th European Summer School on Supramolecular, Intermolecular, Interaggregate Interactions and Separation Chemistry*, Moscow (Russia), 07 / **2012**, Presentation.
- S. Balk, B. Gruber, S. Stadlbauer, B. König, *6th International "Supramolecular Systems in Chemistry and Biology"*, Strasbourg (France), 09 / **2012**, Poster.
- S. Balk, B. Gruber, S. Stadlbauer, B. König, *4th EuCheMS Chemistry Congress*, Prag (Czech Republic), 08 / **2012**, Poster.
- S. Balk, T. Lang, B. Gruber, B. König, *Suprachem - 4th International Summer School*, Regensburg (Germany), 09 / **2011**, Poster.
- S. Balk, T. Lang, B. Gruber, B. König, *Symposium in Supramolecular Chemistry*, Duisburg-Essen (Germany), 02 / **2011**, Poster.